A Practical Method to Estimate the Effective Thermal Resistance of Exterior Masonry Walls

By

Maysoun Ismaiel

A thesis submitted in partial fulfillment of the requirements for the degree of

Doctor of Philosophy

in Civil (Cross-disciplinary)

Department of Civil and Environmental Engineering
University of Alberta

Abstract

Evaluation of the thermal resistance of building envelope elements is essential for a reliable assessment of the thermal behaviour and energy efficiency of buildings. Energy codes continue to drive the building construction industry toward more stringent thermal performance standards. To reduce energy consumption in buildings and comply with newer, more stringent energy code requirements, evaluation of the thermal resistance of above-grade wall assemblies is becoming essential. Masonry veneer cladding is typically supported by the building structure using intermittent anchors and shelf angle bearing supports. However, elements with high thermal conductivity, such as floor intersections and cladding attachment systems, often penetrate the insulation and cause thermal bridging. Thermal bridges have a significant reduction effect on the elements' thermal resistance. Moreover, condensation on thermal bridging elements is expected. As a result, damage to building elements occurs. In terms of calculating the effective thermal resistance (R-value), the lateral heat flows caused by these highly conductive elements allow heat to be transferred in multiple directions, which is considered a challenge in the R-value estimations and causes the inability of a quick estimate of the effective thermal resistance of masonry components with sufficient precision due to the complexity of masonry construction. Currently, an accurate estimation of the R-value of masonry walls is a time-consuming task, which lengthens the design process, especially in the early design stage. Therefore, this study aims to provide efficient approaches for estimating the R-values of common concrete masonry cavity walls. Two estimation approaches are presented. First, the estimation of the R-value of common concrete masonry veneer wall configurations is presented in the form of simple design charts and R-value multipliers. Parameters such as the concrete block density, thermal insulation

value, as well as the types of ties and shelf angles are addressed. The approach provides simultaneously the mechanical (the masonry compressive strength, fm′) and thermal (R-value) properties of different veneer wall configurations, allowing designers to obtain appropriate structural and thermal properties during the preliminary design phase. In addition, the design charts and R-value multipliers help designers evaluate and compare the impacts of changes in different parameters on R-values, thereby facilitating their design development. A comparison of the impacts of different parameters on the thermal resistance of masonry walls was presented. The results showed that the thermal resistance of masonry cavity walls was improved by using different tie types and materials. In the case of using galvanized, stainless-steel and Glass Fiber Reinforced Polymers (GFRP) perforated fastened on block's surface ties, the thermal resistance improved by 25%, 43% and 60%, respectively, compared to the traditional galvanized solid block ties. Using knife plate galvanized and stainless-steel shelf angles in the intermediate floor intersection assemblies improved the overall average R-values by 30% and 63%, respectively, compared to the traditional galvanized steel directly attached shelf angle. Moreover, the results showed that the shape and material of the ties and shelf angles are more effective in the masonry wall assemblies with higher insulation R-values. Also, the effect of the concrete block density was addressed, and the results showed that, on average, the reduction of the concrete block density by 10% showed an improvement in the effective R-value of 3.5%. In addition, configurations with an expected lower effective thermal resistance are more sensitive to the concrete block density. Also, cases using solid ties are more sensitive to block density reduction than cases using perforated ties.

The second approach provides adjustments to current analytical methods of thermal resistance estimation (i.e., isothermal plane and parallel path methods) to include the effect of the thermal

bridge resulting from veneer ties and slab intersections. The R- values obtained from the suggested adjustments were compared with numerical simulations using a 3D steady-state finite element method (FEM) in addition to experimental validation obtained from the literature. The clear wall adjustment factors result showed an average accuracy of 2% in the case of using the suggested adjustments, compared to 19% and 25% for isothermal plane and parallel path methods, respectively. With the presented approaches, designers can choose the optimum wall components' material properties in the early design phase to meet structural and thermal requirements without using computer simulations or experimental investigations.

Preface

Chapter 2 of this thesis has been published by Ismaiel, M., Chen, Y., Cruz-Noguez C. and Hagel, M. (2021). "Thermal resistance of masonry walls: a literature review on influence factors, evaluation, and improvement". Journal of Building Physics. Vol 45, Issue 4, 2022, journal article. https://doi.org/10.1177/17442591211009549. In addition to a conference paper, Ismaiel, M., and Chen, Y. (2020). "STATE OF ART: EVALUATING THERMAL RESISTANCE OF MASONRY WALLS". Proceedings of the 17th International Brick and Block Masonry Conference 2020, Krakow, Poland. https://doi.org/10.1201/9781003098508.

Chapter 3 of this thesis has been published as Ismaiel, M., Westover, L., and Chen, Y. (2022) "An Efficient Approach for Thermal Design of Masonry Walls Using Design Charts and R-value Multipliers" Journal of Building Performance Simulation. https://doi.org/10.1080/19401493.2022.2095032. In addition to a conference paper, Ismaiel, M., Chen, Y., Cruz-Noguez, C. (2021)." Design Charts for Estimating Overall Thermal Resistance of Typical Concrete Masonry Cavity Walls". (14th CMS) 14th Canadian masonry symposium. Montreal, Quebec, Canada. 16-20 May 2021. https://www.canadamasonrydesigncentre.com/research/design-charts-for-estimating-overall-thermal-resistance-of-typical-concrete-masonry-cavity-walls/

Selected sections from chapter 4 of this thesis have been published as a conference paper: Ismaiel, M., and Chen, Y. (2022). "Adjustments of Analytical Simplified Methods to Estimate the Effective Thermal Resistance of Masonry Walls" the 12th eSim Building Simulation Conference -June 22-23, 2022 at Carleton University in Ottawa, Canada.

I was responsible for the data collection and analysis as well as the manuscript composition. All the co-authors contributed to manuscript edits. Dr. Yuxiang Chen was the supervisory author and was involved with the concept formation and manuscript composition of all publications.

Dedication

This research is dedicated to my beloved parents and sister. Their emotional support and prayers consistently provided me with motivation and inspiration to achieve this goal.

Acknowledgments

May all praise and thanks (first and last) are to ALLAH, the Almighty, with whose gracious help it was possible to accomplish this work.

I want to express my deepest thanks and gratitude to my supervisor Dr. Yuxiang Chen, Associate Professor, Department of Civil and Environmental Engineering, University of Alberta, for his consistent guidance, interest, valuable suggestions continuous support during the research program as well as his time and effort spent in discussion of the results. Also, I am extremely grateful to my annual supervisory committee: Dr. Carlos Cruz Noguez, Associate Professor, Department of Civil and Environmental Engineering, University of Alberta and Dr. Lindsey Westover, Assistant Professor, Faculty of Engineering - Mechanical Engineering Department, University of Alberta, for their continuous following up, guidance and support. I would like to thank and acknowledge the efforts and guidance provided by Dr. Mark D. Hagel, the executive director of the Alberta Masonry Council, for help in providing innovative and comprehensive information on the masonry industry. My sincere thanks and appreciation to my Ph.D. thesis defence committee members, Dr. Yong Li (Chair), Dr. Yuxiang Chen (Examiner and Supervisor), Dr. Carlos Cruz Noguez (Examiner), Dr. Lindsey Westover (Examiner), Dr. Douglas Tomlinson (Examiner), and Dr. Caroline Hachem-Vermette (External Examiner-University of Calgary), for their time and helpful suggestions.

I wish to extend my thanks to my groupmate Charlie Shields and all my groupmate colleagues for their help and discussions in some FEM modelling. Also, I would like to thank Dr. Tooba N. Shamsi for her technical writing suggestions.

Additionally, this endeavour would not have been possible without the generous support from the National Sciences and Engineering Research Council of Canada (NSERC), the Canadian Concrete Masonry Producers Association (CCMPA), and the Masonry Contractors Association of Alberta-Northern Region (MCAA), who financed my research.

Words cannot express my gratitude to my lovely parents and sister whose continuous encouragement, patience, support and love made this work possible.

Table of Contents

Abstract ii
Acknowledgments v
Dedication vi
Preface v
Table of Contents viii
List of Tables xi
List of Figures xii
List of Symbols xiv
1. Introduction 1
1.1. Background 1
1.2. Research Objectives 3
1.3. Thesis layout 5
2. Literature Review 7
2.1. Introduction 7
2.2. Influence and Improvement measures of different components 9
2.2.1. Concrete Blocks and Clay Bricks 10
2.2.2. Grout and Mortar 11
2.2.3. Ties and Shelf Angles 13
2.2.4. Insulation for Concrete Masonry Walls 16
2.2.5. Masonry Veneer and Air Cavity 19
2.3. Overall Design Considerations 20
2.3.1. Loading Effect of Cavity Walls 21
2.3.2. Contact Resistance 21
2.3.3. Moisture Accumulation 22
2.3.4. Temperature Dependency of Material Properties 22
2.3.5. Insulation and Materials Aging Effect 24
2.3.6. Energy Efficient Wall Systems, Insulation Schemes, Materials and Block Design 25
2.3.7. Whole Building Thermal Analysis and Energy Consumption 26
2.3.8. Construction and Design Recommendations 27
2.4. Estimation of Thermal Resistance 28
2.4.1. Simplified Analytical Approach 29

2.4.1.1. Thermal Resistance of Concrete Masonry Units 29
2.4.1.2. Series and Parallel Heat Flow Paths 30
2.4.1.3. ISO 6946 Combined Method 32
2.4.1.4. ASHRAE Method 33
2.4.1.5. Point and Linear Transmittances 33
2.4.2. Experimental Testing for R-value 34
2.4.2.1. Laboratory Testing Using Hot Box Apparatus 35
2.4.2.2. R-Value Measurements Using Thermal Imaging 37
2.4.2.3. On-Site Overall R-Value Measurements for Masonry Walls 37
2.4.3. Numerical Simulation 39
2.5. Research Gap and Recommendations 39
2.6. Summary of Influence and Improvement measures of different components 41
3. R-value Estimation Using Design Charts 46
3.1. Introduction 46
3.2. Methodology 50
3.2.1. Configurations Types and Parameters 51
3.2.2. Model Setup and Validation 55
3.2.3. Design Charts and R-value Multipliers 60
3.3. Results Discussion 64
3.3.1. Clear Walls (Type A) 64
3.3.2. Intermediate Floor Intersection (Type B) 69
3.4. Summary of Results 72
3.5. Conclusion 75
3.6. Appendix 77
3.6.1. Examples 77
3.6.2. Figures 80
4. Adjustments of Existing Methods for Estimating the Thermal Resistance of Masonry Veneer Clear Walls 83
4.1. Introduction 83
4.2. Current Analytical Methods 87
4.2.1. Isothermal plane and parallel path methods 87
4.2.2. ISO 6946 Combined Method 88
4.2.3. The Zone Method 88

4.3. Methodology 89
4.3.1. Models Description 90
4.3.1.1. Simplified Clear Wall Assemblies (Type A) 91
4.3.1.2. Detailed Clear Wall Assemblies (Type B) 93
4.3.2. Finite Element Analysis Simulations 95
4.4. Discussion and Results 98
4.4.1. Results for Type A 98
4.4.2. Results for Type B 102
4.5. Conclusion 105
4.6. Appendix 106
5. Adjustments of Existing Methods for Estimating the Thermal Resistance of Masonry Walls with Intermediate Floor Intersections 108
5.1. Introduction 108
5.2. The Point and Linear Transmittance method 111
5.3. Methodology 112
5.3.1. Finite Element Analysis Simulations 112
5.3.2. Models Description 116
5.3.3. Adjustment Description 118
5.4. Results 122
5.5. Conclusion 127
6. Conclusions 128
7. Research Contribution and Future Recommendation 131
References 133

List of Tables

Table 2-1: R-value reduction percentage caused by grout (Kosny, 1995) 12
Table 2-2: The percentage of thermal degradation results compared to the no-tie case 14
Table 2-3: R-values of different shelf angles (Wilson and Higgins, 2019) 15
Table 2-4: R-values for different shelf angles (Hershfield, 2016a) 16
Table 2-5: Differences between various insulation strategies (NCMA, 2010) 17
Table 2-6: Comparison between guarded hot box and calibrated hot box 35
Table 2-7: Summary of the effect of different variables on thermal resistance 41
Table 3-1: Common material thicknesses and properties used in the studied configurations 54
Table 3-2: The parameters considered in each studied scheme 54
Table 3-3: Percentages of R-value improvements for each group when compared to the solid block galvanized steel tie 66
Table 3-4: R-values design multipliers for clear wall configurations compared to the reference group 66
Table 3-5: Average range increase percentage in effective R-value that corresponds to an average of 10% decrease in the concrete block density 68
Table 3-6: Percentages of R-values improvements for each group when compared to the directly attached galvanized steel shelf angle 69
Table 3-7: R-value multipliers for intermediate floor intersection configurations with different shelf angle types and materials (all configurations have solid galvanized steel block ties) 70
Table 3-8: Average increase percentage in effective R-value that corresponds to an average of 10% decrease in the concrete block's density for the intermediate floor intersection configurations 71
Table 3-9: R-value multipliers summary and relations obtained by comparing all the addressed configurations 72
Table 3-10: Calculations for clear wall configurations (Example 2) 79
Table 3-11: Calculations for the Intermediate floor intersection configurations (Example 2) 80
Table 4-1: The range of dimensions and thermal conductivity used for each layer 91
Table 4-2: Material thickness and properties used in the studied schemes for Type B models 93
Table 4-3: The variables considered in each studied scheme 93
Table 4-4: Correlation matrix between significant variables and the R-values obtained from the FE simulation 99
Table 4-5: Adjustment factors 102
Table 5-1: Common material thickness and properties used in the studied scheme 117
Table 5-2: The variables considered in each studied scheme 117
Table 5-3: Adjustment factors 123

List of Figures

Figure 1-1: Research phases 4
Figure 2-1: Two common concrete masonry cavity wall configurations and their typical components (clear wall and intermediate floor intersections, respectively) 10
Figure 2-2: Shape of concrete masonry units. 12
Figure 2-3: (a) Slotted ties and (b) block shear connector. 14
Figure 2-4 : Common shelf angle types 15
Figure 2-5: Arrangement of thermal insulation inside different block cavities. 18
Figure 2-6: Types of cavity walls. 20
Figure 2-7: Horizontal schematic of a Composite block wall (Su et al., 2019). 26
Figure 2-8: a-Typical guarded hot box; b- Typical calibrated hot box (ASTM, 2011) 35
Figure 3-1: Two common concrete masonry cavity wall configurations and their typical components (clear wall and intermediate floor intersection respectively) 50
Figure 3-2: Type and dimensions of the 3D FE studied clear wall configurations (Type A) 51
Figure 3-3: Type and dimensions of the 3D FE studied intermediate floor intersection configurations (Type B) 52
Figure 3-4:Three-dimensional heat conduction through a rectangular volume element 56
Figure 3-5: Convergence of the average RMSE of the addressed configurations versus the number of nodes used in the mesh for the clear wall and the intermediate floor configuration, respectively 59
Figure 3-6: A flowchart used for determining the R-value multipliers of the studied groups. Note: these steps are repeated for all the studied groups to obtain the required multiplier for each group 62
Figure 3-7: Masonry walls' R-value, density and f_m' for both grouted and hollow units clear wall configurations with different insulation and using galvanized steel solid block tie 65
Figure 3-8: R-value, block density, and f_m' for both grouted and hollow units (un-grouted) intermediate floor intersections with different insulation and using galvanized steel solid block 69
Figure 3-9: Thermal distribution and the heat flux for cases with insulation R-20 and concrete blocks' density of 1550Kg/m^3 81
Figure 3-10: Thermal distribution for intermediate floor intersections using insulation R-20 and concrete block density of 2100 kg/m^3 82
Figure 4-1: Components of a concrete-block clear masonry cavity walls 85
Figure 4-2: Shape of tie types used in detailed models (Type B) 91
Figure 4-3: Simplified assemblies, Type $A_{(s)}$ representing fastened on-surface ties 92
Figure 4-4: Simplified assemblies, Type $A_{(B)}$ representing block tie type. 92
Figure 4-5: Detailed clear wall assemblies (Type B) 94
Figure 4-6: Convergence of the heat flux versus the number of nodes used in the mesh for the clear wall Type A and B, respectively. 96
Figure 4-7: Model $A_{(S)}$, $A_{(B)}$ equivalent isothermal and parallel thermal circuit 98
Figure 4-8: R-value results using isothermal, parallel path and ANSYS with respect to the Ratio 100
Figure 4-9: Equivalent isothermal and parallel thermal circuits for B_{SB} assemblies 103
Figure 4-10: Equivalent isothermal and parallel thermal circuits for B_{SS} assemblies. 103
Figure 4-11: Adjusted method with respect to the Finite Element modelling results for assemblies' Type B 105
Figure 4-12: Perforated block tie and fastened on blocks surface tie meshing, respectively. 106

Figure 4-13: Temperature distribution (Type A) 106
Figure 4-14: Temperature distribution and the heat flux distribution (Type B) 107
Figure 5-1: Components of masonry cavity walls with intermediate slab intersection 110
Figure 5-2 : Common shelf angles types..... 110
Figure 5-3: Convergence of the heat flux versus the number of nodes used in the mesh for intermediate floor intersection assemblies..... 114
Figure 5-4: A comparison between the results obtained from the validation modelling and literature 115
Figure 5-5: Type and dimensions of the 3D studied intermediate floor intersections finite element assemblies 116
Figure 5-6: Equivalent isothermal circuits for clear wall part (all shown images are side view)..... 119
Figure 5-7: Equivalent isothermal circuits for shelf angle parts, (a) directly attached, (b) Brackets, (c) Knife plate and (d)HSS respectively..... 121
Figure 5-8: Adjusted method with respect to the finite element modelling results 124
Figure 5-9: Adjusted method with respect to the Finite Element modelling results for all intermediate floor assemblies 125
Figure 5-10: Thermal distribution for intermediate floor intersections using insulation R-20 and concrete block density of 2100 kg/m^3 126
Figure 5-11: The heat flux (on the brick veneer surface) for intermediate floor intersections using insulation R-20 and concrete block density of 2100 kg/m^3 127

List of Symbols

- $\boldsymbol{R}$**:** The thermal Resistance (m^2K/W).
- $\boldsymbol{U}$**:** The thermal transmittance (W/m^2K).
- $\boldsymbol{k}$**:** Thermal conductivity (W/m.K).
- $\Delta\boldsymbol{t}$: The temperature difference between two interfaces (K).
- $\boldsymbol{q}$*:* The heat flux in watts per area of the addressed wall in square meters (W/m^2).
- $\boldsymbol{r_{jk}}$**:** The Pearson correlation between variables X_i and X_k.
- $\boldsymbol{\alpha}$**:** The adjustment factors for the R-value obtained using the isothermal method.
- $\boldsymbol{\beta}$*:* The adjustment factors obtained using the parallel path method.
- $\boldsymbol{Q_B}$*:* The heat flow of the clear field of an assembly (W/K).
- $\boldsymbol{Q_A}$*:* The heat flow of the assembly with a portion of the clear field replaced with intersections (W/K).
- $\boldsymbol{U_o}$*:* The clear field thermal transmittance ($W/m^2 \cdot K$).
- $\boldsymbol{A_{total}}$**:** The total opaque wall area (m^2).
- $\boldsymbol{\psi}$**:** The point transmittance heat flow from the linear thermal bridge (W/ (m K)).
- ***L:*** *The* length of the linear thermal bridge (m).
- $\boldsymbol{\chi}$**:** The heat flow from the point thermal bridge (W/K).
- $\boldsymbol{U_T}$**:** thermal transmittance of the overall assembly including thermal bridging (W/m^2K).

1. Introduction

1.1. Background

For centuries, concrete masonry has been considered an established and trusted building material. Modern concrete blocks and masonry veneers are significant constituents in the transition to sustainable buildings. Masonry can be aesthetically pleasing, energy-efficient, and durable (Earle, Ergun, & Gorgolewski, 2014). With the rapid change and higher standards of thermal requirements for building envelopes, masonry construction needs viable design improvements to meet stringent building energy codes as the minimum effective thermal resistance (R-value) has increased over time. In the 2017 National Energy Code of Canada for Buildings (NECB, 2017), R-values have been increased by an average of 25% for some elements compared to its previous edition. This increase is expected to improve the overall energy performance of buildings by 10% to 15% in comparison to previous versions of the code (NECB, 2011; NECB, 2015). One of the significant changes to energy regulations and guidelines is the calculation requirements for the effective R-value. The previous revisions of the NECB permitted the exclusion of major structural elements and other highly conductive elements that penetrate envelopes, providing that they comprised less than 2% of the total wall area (Straube, 2017). The new code requires that all elements be considered in the effective R-value calculation due to the significant R-value reduction effects that the thermal bridging element causes. For instance, the selection of brick tie material and design can have a significant impact on the effective R-value of brick veneer walls, although the brick ties compromise a small percentage of the total wall area. According to the literature, the R-value reduction effect of veneer ties can range from 5% to nearly 30%, depending on the thickness of exterior insulation and backup wall structure (Finch et al., 2013a; Wilson, 2013). These current code changes require more accurate methods and tools to provide precise overall R-value estimates. Therefore, there is a need to review and improve the thermal resistance of masonry walls. Thermal and energy modelling also requires an accurate method for the estimation of R-values of the buildings' components. For these purposes, this research presents two different R-value estimation approaches to help designers perform a quick and precise estimate of the R-values of different masonry veneer wall configurations for the early design phases.

To improve buildings' sustainability, many regulations have been established in recent decades to enhance the energy efficiency of building envelopes, such as increasing their effective thermal resistance (R-value). To achieve high R-values, efficient resources (in terms of thermal properties, time, and cost) and accurate estimations are needed. However, the estimation is not a simple process due to the complexity of building envelope configurations, such as the presence of highly conductive structural components penetrating the insulating materials (e.g., insulation fasteners). Thermal bridging elements allow heat to flow in multiple directions through several layers of envelope materials, thereby substantially complicating the R-value calculation (Barnes et al., 2013). Thermal bridges significantly reduce the R-value of a building envelope and therefore should be considered if an accurate R-value estimation is desired (Lawton et al., 2010; Urban et al., 2011b; Ismaiel et al., 2021). Steel veneer ties and shelf angles are among the largest sources of thermal bridging in concrete masonry walls (Roppel et al., 2012; Liu, 2019). The shape, size, and material of ties and shelf angles have been revolutionized to improve structural and thermal performance, which increases the complexity of wall configurations and, consequently, their R-value calculations. Other than thermal bridging elements, another factor that impacts the thermal performance and complicates R-value calculation is the thermal properties of wall components (D'Aloisio et al., 2012; Kontoleon et al., 2013). In the early design phase, designers address various wall configurations with different material properties, mainly due to the trade-off between the structural and thermal performance. For instance, high concrete block density increases the block's compressive strength while reducing the thermal resistance of the blocks (Harmathy and Allen, 1973). In another instance, the choice of the ties and shelf angles' material and shape has a significant impact on the effective thermal and structural behaviour of masonry walls. Changing the shape and material of blocks, ties, and shelf angles can affect the masonry walls' thermal resistance to a great extent (Adam Di Placido et al., 2019a; Bai et al., 2017). It is considered a challenge to determine the optimum wall components' material properties in the early design phase to meet structural and thermal requirements.

The combinations of various materials' thermal properties, geometries of wall components, and three-dimensional heat transfer create a challenge in determining the R-values of masonry walls (Kontoleon et al., 2013). There have been a few methods for estimating the R-value of a composite wall (e.g., Isothermal Planes and Parallel Path methods). Some of these methods have insufficient accuracy if applied to masonry walls due to employing assumptions for

simplification purposes, such as ignoring the lateral heat transfer and assuming an even temperature distribution on the same plane (Theodosiou et al., 2021; McGowan and Desjarlais, 1995; Kosny and Christian, 1995). The rest of the methods depend mainly on computer numerical models (e.g., linear and point transmittance), which consume time and are costly (ASHRAE, 2017d; Hydro, 2016b). The inability to perform a quick and precise estimate of the R-values of masonry walls demands an efficient approach for the early design phases.

1.2. Research Objectives

The walls of a building couple the exterior environment with the interior environment in complex ways. The perfect wall is expected to be an environmental separator. To do this role efficiently, the wall assembly has to control rain, air, vapor, and heat (Lstiburek, 2008). The insulating properties of the building envelope and construction quality together control the way heat and moisture flow into or out of the building. The exterior walls contribute significantly to the quantity of heat flowing through the building envelope. About 21% of the heating load in residential buildings and 30% of the heating load in commercial buildings results from flows through exterior walls (Baldwin et al., 2015). Therefore, this research focuses on the common masonry veneer exterior walls.

Due to the unavailability of an accurate estimate of the R-values of masonry walls, this research aims mainly to provide efficient approaches to estimate the overall effective R-values of common masonry veneer walls considering the effect of thermal bridging. These approaches aim to guide the designers to choose the optimum wall components' material properties in the early design phase to meet structural and thermal requirements without using computer simulations or experimental investigations. Moreover, it helps in having a reliable estimation of energy needs for the building envelope. This research studies the thermal resistance of different masonry wall configurations using 3D finite element thermal modelling. Besides, experimental validation was obtained from the literature.

The objectives of this research can be summarized as follows:

1. Compare and summarize the limitations of the current R-value design calculations and considerations such as code compliance, materials' properties, insulation type, and location as well as the sources of thermal bridging in masonry walls. In addition, we present the common experimental and simulation approaches used to measure the thermal

resistance of assemblies with large dimensions. Moreover, identify the main challenges facing the overall R-value calculations and the latest progress made on these challenges.

2. Evaluate the relative impact of different walls' components and the influence of different factors on the overall R-value.
3. Present an approach for estimating the R-values of common concrete masonry cavity wall configurations in the form of simple design charts and R-value multipliers. The approach provides simultaneously the mechanical (the masonry compressive strength, fm′) and thermal (R-value) properties of different cavity wall configurations, allowing designers to obtain appropriate structural and thermal properties during a preliminary design phase without using computer simulations. In addition, the design charts and R-value multiplier help designers evaluate and compare the impacts of changes in different parameters on R-values, thereby facilitating their design development.
4. Suggest an adjustment of current thermal resistance estimation methods (e.g., isothermal plane and parallel path methods) to include the effect of the thermal bridge resulting from veneer ties and intermediate floor intersections in the R-value estimations.

This research is divided into three main phases. **Figure 1-1** simplifies all research phases.

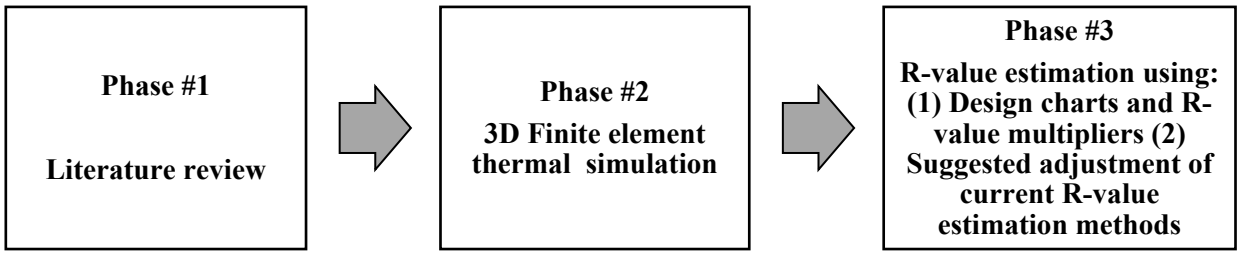

Figure 1-1: Research phases

This research is divided into three main phases; the first is a literature review on the influence factors, evaluation, and improvement of the thermal resistance of masonry veneer walls. The limitations of the current R-value design calculation methods are addressed. The main challenges facing the overall R-value estimations and the latest progress made on these challenges are presented. The second phase is determining a 3D finite element program for the thermal analysis simulation. ANSYS Workbench is used to perform steady-state finite element thermal analysis simulations. The FE simulations are performed to calculate the R-value for different masonry wall configurations. In this phase, the models are set up and validation is performed. The third

phase is the construction of design charts and R-value multipliers using the finite element results obtained from the second phase. The design charts help in structurally and thermally designing the common concrete masonry walls during the preliminary design phase. Besides, providing adjustments to the current thermal resistance estimation methods (e.g., isothermal plane and parallel path methods) using the results obtained from the second phase to include the effect of the thermal bridge resulting from veneer ties and intermediate floor intersections in the R-value estimations without the need for computer simulations or experimental investigations.

1.3. Thesis layout

The thesis consists of seven chapters as mentioned below. Chapters (2) and (3) were published as peer-reviewed journal papers, while Chapter (4) was published as a conference paper.

Chapter (1): Introduction

This chapter includes an introduction and a plan of the research work.

Chapter (2): Literature review

This chapter includes a brief review of the previous research work on the influence factors, evaluation, and improvement of the thermal resistance of masonry veneer walls. This chapter presents the research gap and the limitations of the current R-value estimation methods.

Chapter (3): R-value Estimation Using Design Charts

This chapter presents 3D Finite element thermal simulation, along with the limitations and boundary conditions considered in the modelling. Then a design chart that combines the R-value of the different masonry wall configurations, the blocks' density, and the masonry compressive strength (fm′) is presented.

Chapter (4): Adjustments of Existing Analytical Methods for Estimating the Effective Thermal Resistance of Masonry Veneer Clear Walls

This chapter suggests adjustments to current thermal resistance estimation methods (e.g., isothermal plane and parallel path methods) to include the effect of the thermal bridge resulting from veneer ties using the finite element models obtained from chapter (3).

Chapter (5): Adjustments of Existing Analytical Methods for Estimating the Effective Thermal Resistance of Masonry Walls with Intermediate floor intersection

This chapter suggests adjustments to current thermal resistance estimation methods (e.g., isothermal plane and parallel path methods) to include the effect of the thermal bridge resulting from intermediate floor intersections using the results obtained from chapter (4) and FEM modelling presented in chapter (3).

Chapter (6): Conclusions

This chapter is a synthesis of key points presented in this thesis. Moreover, it summarizes the conclusions and findings of each chapter.

Chapter (7): Research contribution and Future Recommendations

This chapter presents a summary of the outcomes of this research and its significance. Also, research future recommendations are presented.

2. Literature Review

2.1. Introduction

Increasing the thermal resistance of masonry wall systems is one way to reduce energy consumption in the operation of masonry buildings. This increase is also demanded by newer, more stringent energy codes. However, this approach has several challenges. One of them is thermal bridging, which occurs in places where highly conductive structural components penetrate insulating materials. Thermal bridging is common when connecting masonry veneers to structural backup walls that increase the complexity of wall configurations and, consequently, their R-value calculations.

The thermal properties of materials are key to the building's thermal performance. Due to their significant thermal energy storage capacity (i.e., thermal mass), masonry buildings can often provide superior thermal performance compared to light-frame buildings with similar thermal insulation values (ACI 122R-02, 2002; Huberman, N. & Pearlmutter, 2008; Huberman, Nora & Pearlmutter, 2004). Aside from thermal mass, thermal conductivity also has a significant influence on thermal performance. Changing the shape and material of blocks and bricks can increase their thermal resistance. However, thermal insulation is needed in masonry wall assemblies to significantly increase their overall or effective thermal resistance. Therefore, the configurations of masonry wall assemblies also play a key role in the thermal performance of a wall. One of the challenges in the assembly configuration is thermal bridging. Thermal bridging occurs when highly conductive structural components penetrate insulating materials, such as when structural members penetrate through an insulation plane (Association, 2013). The thermal bridging problem is common in many types of building envelope systems not only masonry walls (e.g., framing with steel, and wood). However, the elements' thermal material properties are significant to the thermal bridging effect. For instance, in a wood-framed system, an insulation layer is less effective because wood framing is less conductive than steel (Loghmanpour, 2014). Also, the distribution and the geometry of the highly conductive elements are significant to the thermal bridging effect on the systems' overall thermal resistance. Therefore, many suggestions were presented and investigated for reducing thermal bridging in steel and wood framing systems, such as increasing stud spacing, removing parts of the web, if

structurally feasible, and placing insulation between the framing members. Since the thermal bridging sources are simple in geometry and uniformly distributed in the wood and steel framing systems. The isothermal-planes method (presented in section 4.2.1) is appropriate for materials with conductivities moderately different from those of adjacent materials (e.g., wood frames with insulation). Moreover, the zone method (Adam Di Placido et al., 2019a; ASHRAE, 2021d) was presented to estimate the overall R-value of assemblies with metal elements of uniform cross-sectional areas (e.g., steel-framed constructions). However, the estimation of the overall R-value in wood and steel cavity walls is still a challenge due to the presence of ties (connectors) between the backup wall and the exterior cladding system. Additionally, in the case of masonry walls, the R-value estimation is not a simple process due to the complexity of building envelope configurations and the combinations of various materials' thermal properties, complex geometries of wall components, and three-dimensional heat transfer create a challenge in determining the R-values of masonry walls. Thermal bridging should be minimized in designs and carefully calculated as it is considered the main source of thermal performance deficiency in masonry walls.

Many regulations and guidelines have been established in recent decades to improve the thermal performance of building envelopes. The International Energy Conservation Code (IECC, 2012) provides and develops local codes for energy-efficient building design. Current Canadian building codes are influenced by energy considerations in the National Energy Code for Buildings (NECB, 2017). Three significant changes to energy regulations and guidelines have been added to the most recent revision. First, the overall thermal performance of the entire building envelope, rather than a single component, is considered in most regulations and guidelines. One type of thermal performance is the effective thermal resistance (R-value). The second change is the integration of many additional energy and thermal performance requirements, such as specific thermal properties of buildings, locations of different building elements, and the acceptable overall thermal resistance for different climates. The third significant change is the calculation requirement for the effective R-value. The previous revisions of the NECB permitted the exclusion of major structural elements and other highly conductive elements that penetrate envelopes, providing that they comprised less than 2% of the total wall area (Straube, 2017). The new code requires that all elements be considered in the effective R-value calculation. Therefore, due to the newly included thermal bridges, the

calculated effective R-value for many assemblies will now be smaller than previously determined. These significant changes require more accurate methods and tools to provide precise overall R-value estimates.

To comply with continuously evolving energy code requirements, the masonry and construction industries are developing new building techniques and are in search of an effective approach to calculate thermal resistance. Therefore, there is a need to review and improve the thermal resistance of masonry walls. Modelling also requires an accurate method for the estimation of R-values. To serve the aforementioned purposes, this chapter presents a comprehensive literature review on key factors that influence the overall thermal performance of masonry walls, methods to effectively estimate and measure thermal resistance (R-value); and improvements in thermal design. In addition to identifying the main technical and practical challenges and the corresponding progress made on each front, key design considerations, such as code compliance, material properties, insulation types, and location, as well as special ties and shelf angle types, are also discussed. This chapter also provides a review of available literature on the numerical calculations, computer simulations, and experimental investigations on the evaluation of thermal resistance are presented and discussed. This review indicates that a material's thermal properties are among the largest contributing factors to the thermal performance of masonry walls. This chapter summarizes critical information and recommendations that will help improve the thermal design of masonry walls, thereby reducing the energy consumption of buildings.

2.2. Influence and Improvement measures of different components

This research focuses on two common types of wall configurations: clear walls, and intermediate floor intersections as shown in **Figure** 2-1**.** A "clear wall" is defined as a planar area with regularly spaced structural components that is free of windows, doors, and other irregularities (Hershfield, 2022b). Clear wall configurations can contain thermal bridges from uniformly distributed secondary structural components, which are necessary to withstand loads. Examples of components included in clear field configurations are brick ties, girts, or studs that support cladding (Barnes et al., 2013). These thermal bridges do not include the ones related to intersections of the primary structure or between assemblies, such as intermediate floor intersections. The clear wall and the intermediate floor intersections make up the majority of the exterior wall surfaces and hence are chosen to be investigated in this research. The typical

components of concrete masonry walls are concrete blocks, mortar, insulation boards, shelf angles, veneer ties, and air gaps as shown in **Figure** 2-1.

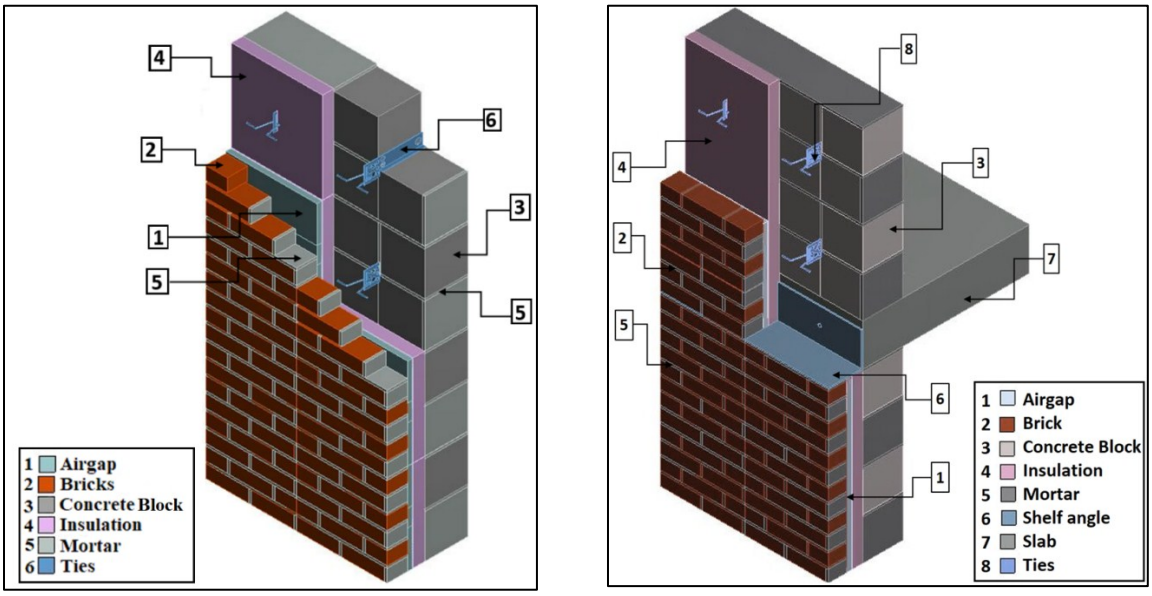

Figure 2-1: Two common concrete masonry cavity wall configurations and their typical components (clear wall and intermediate floor intersections, respectively)

2.2.1. Concrete Blocks and Clay Bricks

The shape, size, aggregate size, moisture content, and density of block and brick units have a significant effect on the thermal resistance. Research has been conducted to optimize the blocks' thermal design and obtain an accurate thermal resistance reading of different units. The thermal conductivity of concrete blocks or fired clay bricks mainly depends on the type of aggregate. For example, concrete thermal conductivity is generally correlated to concrete density (ESCSI, 2007). The type and shape of a hollow block can also have a large influence on the overall thermal performance. To enhance the thermal performance of masonry buildings, optimal thermal properties must be utilized correctly.

Voids in concrete blocks contribute significantly to the thermal resistance of masonry walls. The size, number, and distribution of a concrete block's voids contribute significantly to the overall thermal efficiency of a block. The staggered holes elongate the heat flow path through walls which improves the blocks' thermal resistance compared to aligned holes or solid blocks

(Pierzchlewicz, 1996). Bai et al. (2017) experimentally demonstrated that a hollow shale block with many rows of holes can achieve a thermal transmittance of 0.726 W/ (m^2·K) (thermal resistance of 1.37 m^2·K/W). After investigating the voids, studies were also conducted on web configurations. Bradfield et al. (2010) found that a smaller cross-sectional web area reduces the heat flow through wall assemblies. In addition, it was concluded that the smaller the intersection area between the web and the block's face shell, the better the thermal resistance of a block. A 30% reduction was noticed in the thermal resistance of concrete blocks with two webs over the typical three-web concrete block (NCMA, 2012). Based on similar studies, some manufacturers have developed concrete masonry units with two webs, instead of three to reduce the thermal bridging effect. Although insulation inserts can increase a concrete masonry unit's (CMU) thermal resistance, thermal bridging through solid webbing can reduce the effectiveness of the insulation (Kosny, 1995).

Lightweight aggregate with low thermal conductivity in lightweight concrete blocks can also reduce the thermal transmittance of blocks and bricks. With a large number of voids in the aggregate, lightweight aggregate concrete possesses a lower thermal conductivity and smaller density compared to normal concrete. Al-Jabri et al. (2005) experimentally compared the thermal conductivities of ordinary and lightweight hollow-core concrete blocks. Results showed that a 33% reduction in a block's density caused a 60% decrease in the resulting thermal conductivity. Lightweight aggregates from waste materials, such as demolition waste and agricultural residues, can be used to produce lightweight concrete blocks and achieve lower thermal conductivity (Callejas et al., 2017). Agricultural solid waste from maize and corn has been incorporated with cementitious powder to prepare lightweight concrete (Wang et al., 2020). The National Concrete Masonry Association suggested that the thermal resistance of lightweight concrete blocks is less sensitive to the thickness of blocks compared to normal-weight blocks (NCMA, 2013). A summary of the effects of concrete blocks on the overall R-value of masonry walls based on literature, along with recommendations to improve the thermal performance of masonry walls, is presented in **Table 2-7** section **2.6**.

2.2.2. Grout and Mortar

Cement-based grout and mortar have been widely used in most modern masonry construction; three types of mortar are being used for historic masonry projects; lime mortars, hydraulic lime

mortars, and Portland cement or masonry cement lime-based mortars. These types of mortar can differ significantly in their properties in both the plastic and hardened states, especially in compressive strength, flexibility, water and vapour transmission rate, and frost durability. The appropriate type of mortar is chosen based on the environmental conditions and structural requirements (Suter et al., 2001). Mortar is a thick paste that acts as a binder between CMUs and provides a levelling bed for units, resulting in reduced stress concentrations. Grout is used to fill hollowed cores in CMUs to provide a bond between the CMU and steel reinforcements through the cores. In general, grout reduces the overall R-value of a masonry wall. The grout effect depends mainly on the shape and thermal resistance of the concrete block. Kosny et al. (1995) observed that local thermal bridges caused by grout-filled cores have a large influence on the R-value. Also, results showed that the reduction in overall R-value caused by grout decreases as the CMU thermal resistance increases. **Figure 2-2** shows the shape of the units considered by Kosny et al. (1995), and **Table 2-1** shows the reduction percentage of the R-value in normal and lightweight grouted blocks compared to un-grouted (i.e., empty) blocks. The results showed that cut-web units are less sensitive to the grout reduction effect.

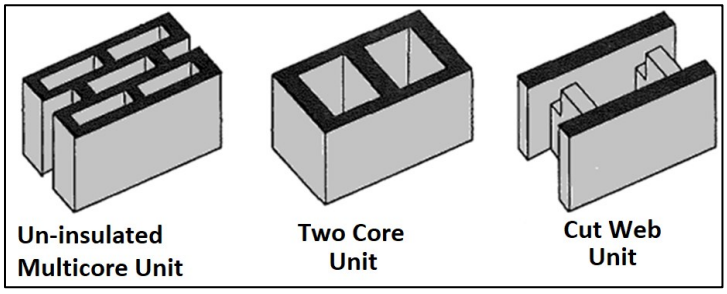

Figure 2-2: Shape of concrete masonry units.

Table 2-1: R-value reduction percentage caused by grout (Kosny, 1995)

	R-value reduction percentage caused by grout in comparison with the un-grouted cases		
	Uninsulated Multicore	**Two-Core**	**Cut-web Unit**
Normal-density blocks	12	10	7
Lightweight blocks	6	5	3

Mortar occupies only a small proportion (approximately 7%) of the total wall area in concrete masonry construction but causes a significant reduction in a wall's thermal resistance, depending on the thermal resistance of the concrete blocks. Kosny et al. (2011a) compared the effect of

mortar on the thermal performance of masonry concrete walls in two cases: walls with insulated and uninsulated blocks. It was concluded that the mortar reduction effect on R-value increases as the thermal resistance of concrete blocks increases. The R-value reduction due to mortar in the case of walls made of insulated two-core blocks was 12% more than the uninsulated two-cores. In addition, the mortar reduction effect on a wall's R-value is directly proportional to the thermal resistance value of a concrete block. Abdou et al. (1994) experimentally proved the reduction effect was about 8% in a conventional wall. To decrease the amount of heat loss due to mortar, it was recommended that less conductive mortars be used or the area of mortar joints should be decreased. Another suggestion was to replace the side mortar with mechanical interlocking.

Zedan et al. (2016) conducted whole building simulations to study the thermal bridges primarily caused by mortar joints between insulated building blocks. Results showed that the effects of thermal bridges resulting from mortar joints are significant and may cause an increase in the annual heating or cooling load by 11%.

2.2.3. Ties and Shelf Angles

Veneer ties and shelf angles are used to hold brick veneers in place. They are typical repeating sources of thermal bridging. In the past, repeated thermal bridging sources were considered insignificant. However, as expectations for envelope performance rise, repeated thermal bridging sources have attracted more attention. In recent studies, traditional steel masonry veneer ties and steel shelf angles are found among the largest sources of thermal bridging in masonry walls (Roppel et al., 2012; CCMP, 2013).

Research shows that tie material and shapes, and spacing can have a significant impact on the R-value of masonry veneer walls. Wilson (2019) showed that stainless steel ties with holes reduce the thermal resistance of exterior insulation over concrete/steel backup walls by 3% to 9%, compared to 8% to 25% for galvanized iron ties without holes. It was found that metal ties with a typical spacing between 400 mm and 600 mm, both horizontally and vertically, can contribute up to a 15% decrease in thermal resistance (Love, 2011).

Finch et al. (2013b), through numerical simulation, investigated the influence of different variables, such as tie material types and insulation levels, The variables addressed in this modelling were 2-inch x 16-gauge brick ties, with and without holes, made of galvanized steel

and stainless steel, and Basalt Fiber masonry cavity ties (proprietary UK product for a concrete backup wall). **Table** 2-2 shows the percentage of thermal degradation results compared to the no-tie case and using exterior insulation of R-20 and R-10 for all cases. The results concluded that as the exterior insulation R-value increases, the thermal degradation effect of a tie on the overall R-value increases.

Table 2-2: The percentage of thermal degradation results compared to the no-tie case

Brick ties type	Exterior insulation	Galvanized steel	Stainless steel	Basalt Fiber
With holes	R-20	21	7	0.5
Without holes	R-20	26	11	
With holes	R-10	14	6	0.2
Without holes	R-10	19	9	

The shape, size, material, and configuration of ties have been revolutionized to improve structural and thermal performance. Several tie shapes with different materials have been introduced to the market to minimize thermal bridging while meeting structural requirements (CCMP, 2013). Slotted ties (**Figure** 2-3**a**) can be fastened to the face shell of structural backing instead of being inserted in between blocks as traditional ties are typically used. Holes within the tie body are introduced to reduce the cross-sectional area, thus minimizing thermal conductance. Another type of tie is the block shear connector (**Figure** 2-3**b**), which has a horizontal embedment. This type of tie interlocks more effectively with blocks, helping to reduce the contact area (i.e., cross-sectional area), resulting in reduced thermal bridging.

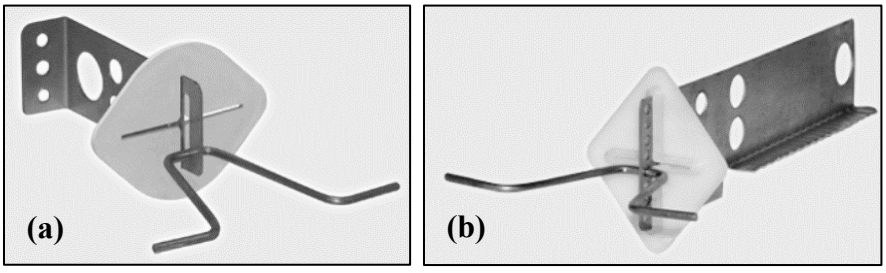

Figure 2-3: (a) Slotted ties and (b) block shear connector.

Shelf angles are anchored to structural backup using fasteners. Recently, intermittent structural support for shelf angles, which offset shelf angles from backing systems, such as knife plates (i.e., I-shape steel) and hollow structural section (HSS) tubes, are introduced to the market**.**

Figure 2-4 shows the common shelf angle types. In this way, only intermittent supports penetrate the exterior insulation instead of shelf angles. The amount of insulation displaced by market-available intermittent supports is practically the same.

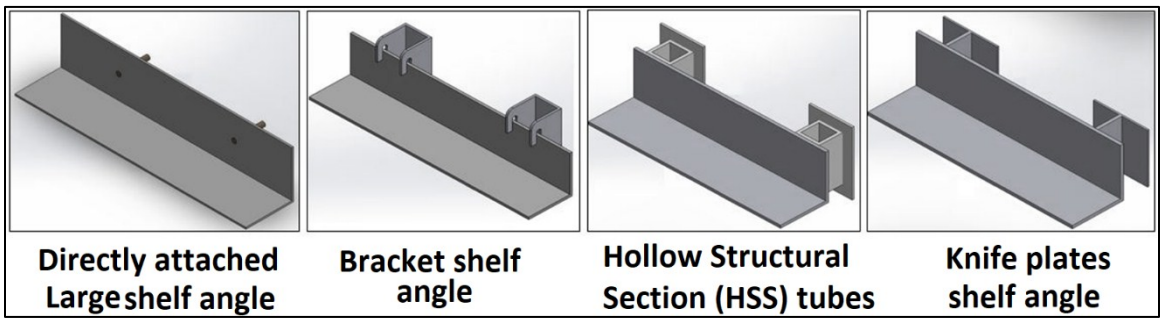

Figure 2-4 : Common shelf angle types

Finch et al. (2013b) studied directly attached masonry shelf angles and concluded that these shelf angles have poor thermal resistance and reduce the R-value reductions by 40% to 55% for typical exterior insulation thicknesses with stainless steel or galvanized ties. Shelf angles supported with intermittent knife plates or tubes resulted in much less reduction (12% to 22%). **Table 2-3** presents the influence of different shelf angle systems (namely knife plates, HSS tubes, and anchored large angles) on the R-value of a selected masonry wall (Wilson and Higgins, 2019). These studies confirmed that shelf angles supported on the outside of exterior insulation with intermittent supports result in less reduction in the R-value compared to the traditional approach (anchored large angles).

Table 2-3: R-values of different shelf angles (Wilson and Higgins, 2019)

	Knife Plate	**HSS Tubes**	**Anchored Large Angle**
R-value (RSI) RSI = 1 $m^2 \cdot K/W$	2.89	2.84	1.87

Another analysis of a wall assembly with shelf angles of different shapes and material properties was conducted using the data presented by Morison Hershfield (2016a). **Table** 2-4 presents the effect of different shelf angle systems on the R-value. The reduction in R-values ranges between 19% and 44% compared to the clear field's R-value of 3.13 $(m^2 \cdot K)/W$. "Clear field" is defined as planar areas with regularly spaced structural components that are free of windows, doors, and other irregularities (Barnes et al., 2013). This reduction range is based on the shelf angle shape

and material used in each assembly. It was recommended that fabricating the entire angle out of stainless steel would minimize the performance impact of a shelf angle.

Table 2-4: R-values for different shelf angles (Hershfield, 2016a)

Type	Clear field (without shelf angle)	Solid Angle Bolted	Spaced Shelf Angle	Thermally Broken Shelf Angle (steel)	Thermally Broken Shelf Angle (stainless steel)
R-value (m^2·K/W)	3.13	1.75	2.02	2.39	2.53
% Reduction	Reference	44.08	35.46	23.64	19.16

Another numerical and experimental study conducted by Placido et al. (2019a) showed that shelf angles supported with intermittent brackets with perforations can decrease the overall R-value reduction by approximately 15% compared to the traditional directly attached large shelf angles. It was concluded that, with the appropriate selection of shelf angle support designs, high R-value exterior-insulated masonry veneer walls were achievable.

Finch et al. (2013) studied directly attached masonry shelf angles and concluded that these shelf angles have poor thermal resistance and provide exterior insulation R-value reductions from 40% to 55% for typical exterior insulation thicknesses and stainless steel or galvanized ties. Shelf angles supported with intermittent knife plate or tube shelf angle supports with stainless steel or galvanized ties have a superior thermal insulation reduction (12% to 22%). Therefore, the author suggests the use of intermittently supported and thermally improved shelf angles.

2.2.4. Insulation for Concrete Masonry Walls

Commercial and residential buildings have various energy codes enforced across the world. In North America, the two most pertinent energy codes are the International Energy Conservation Code (IECC) in the United States (IECC 2012), and the National Energy Code for Buildings (NECB) in Canada (NECB 2017). The reference energy standard that the majority of Canadian provinces use is ASHRAE Standard 90.1(ASHRAE, 2019a). While specific versions of these regulations are applied to different jurisdictions, each one must consider the effectiveness of the installed insulation. For example, cladding attachments can reduce the exterior insulation

efficiency by 5% to 10% for high-performance systems and up to 80% for poor systems (Finch and Higgins, 2017).

The thermal performance of any building envelope is highly dependent on its insulation design (Schumacher et al., 2013). Insulation designs depend on an economic trade-off between the present initial cost of improving the envelope and the future cumulative cost of operational energy for space conditioning while considering durability and maintenance costs. Different insulation designs have been used in masonry wall construction, depending on the required thermal properties, climate conditions, and feasibility of construction, cost, and other design criteria. Insulation schemes are divided into three categories based on the insulation locations: interior, integral, and exterior. Common integral insulation schemes consist of insulation block inserts placed inside a block's cavities and granular fills in block core spaces. Exterior insulation systems completely cover all structural elements, such as columns and beams, to avoid thermal bridges and protect the structure from temperature variations (NCMA, 2013). **Table 2-5** summarizes the differences between various insulation strategies based on the insulation location and the advantages and disadvantages of each insulation strategy.

Table 2-5: Differences between various insulation strategies (NCMA, 2010)

Insulation Schemes	Interior Insulation	Integral Insulation	Exterior Insulation

Definition	• Insulation applied to the interior side of a backing wall
	• The interior wall surface is usually finished with a gypsum wallboard
		• Insulation placed between two layers of thermal mass, including:
		  ○ Insulation placed in concrete masonry cores
		  ○ Continuous insulation between two wythes of a masonry cavity wall
			• Walls that have insulation on the exterior side of a backing wall

Advantages	• Concrete masonry can fit both vertical and horizontal reinforcement with partial or full grouting without interrupting the insulation layer • Fast response to space heating and cooling • Less maintenance is required	• Masonry is in direct contact with indoor air, which allows excellent thermal mass benefits • Continuous cavity insulation minimizes thermal bridging • Cavity width can be varied to achieve different R-values • Thermal performance can be increased by insulating the cores of a backup	• Minimizes the effect of thermal bridging • Exterior insulation keeps masonry directly in contact with interior conditioned air • Provides the most thermal mass benefit • Reduces heat losses and moisture movement due to air leakage
Disadvantages	• Durability, weather resistance, and impact resistance of the exterior wall remain unchanged with the presence of interior insulation	• Insulation requires special installation procedures to provide tight joints between insulation boards, which guarantees thermal performance and helps reduce air leakage • Vertical and horizontal reinforcement with partial or full grouting might interrupt insulation inserts of cores	• Insulation requires a protective finish to ensure durability and effectiveness • Reinforcing mesh must be applied to reinforce the finish coating and improve crack and impact resistance • For historic masonry, water transport and drying can be blocked

Kosny et al. (1995) investigated the thermal efficiency of integral insulation for the arrangements shown in **Figure 2-5**. The research found out that the R-value difference between insulated and un-insulated blocks was only 20% to 40% of the thermal resistance of the added insulation.

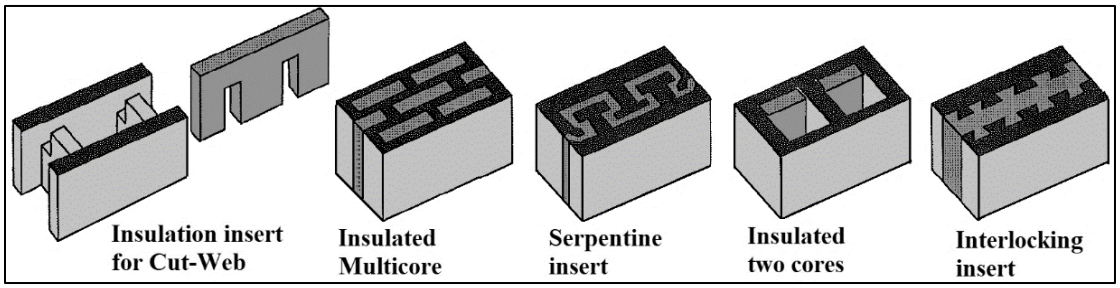

Figure 2-5: Arrangement of thermal insulation inside different block cavities.

McCall (1985) suggested that integral insulation with lightweight concrete blocks can increase the thermal efficiency value to 85%. Practical challenges in insulating masonry walls have been discussed by the European Insulation Manufacturers Association (Eurima, 2008). For exterior and interior wall insulation types, insulation boards should be in intimate contact with masonry to avoid air circulation from degrading the thermal resistance, and misalignments are mostly due to excess mortar between blocks and unclean wall surfaces. External insulation must be completely sealed at all perimeter edges to eliminate air infiltration between the panel and external wall. To address this issue, there should be a high level of construction quality control on-site.

2.2.5. Masonry Veneer and Air Cavity

In modern construction, traditional thick, solid masonry walls have been replaced with thinner and more energy-efficient ones, such as masonry cavity walls made of a masonry veneer (typically brick) wythe, which acts as a rain screen, and a backup (concrete block) wythe with a layer of continuous thermal insulation. Thermal insulation is typically installed on the exterior surface of the backup, leaving an air cavity between the insulation and veneer. The main purpose of the air cavity for drying any moisture or draining water presented in the cavity and preventing liquid transmission by providing a capillary break. Ventilation in the cavity occurs by weeps in the brick veneer, which are required to connect the cavity with outdoor air. There are three common types of cavity walls: unventilated, pressure-equalized, and ventilated, as shown in **Figure** 2-6. Unventilated cavity walls were commonly used until the late 1900s; newer designs, such as the pressure-equalized cavity wall, emerged to reduce moisture accumulation in the cavity. Pressure-equalized cavities function by allowing air to enter the cavity, thus reducing or eliminating the positive force of wind-driven rain against the veneer. However, this type of cavity is not effective in creating a true net-zero pressure differential across a veneer (Conway, 2016) and the accumulated moisture and water were not able to be dried or drained sufficiently. As a result, a more effective type of cavity wall was introduced for moisture management: the ventilated cavity wall, allowing airflow in and out of a wall cavity through weep vents located at the top and bottom of the veneer panels. The air circulation inside the cavity can potentially reduce the insulating effect of the cavity. Recent revisions in the 2017 National Energy Code of Canada for Buildings (NECB, 2017a) and 2015 National Building Code of Canada (NECB,

2015) state that: “materials installed towards the exterior of vented air space cannot be included in the calculation of effective thermal resistance of the assembly”. The contribution to the R-value of the wall from the air cavity and materials exterior to it is under on-going investigation. Stovall et al. (2004) found a temperature difference between cavity air and exterior for different air cavity configurations under different weather conditions. That means there is an insulating effect from the air cavity and brick veneer. Also, the ISO 6946 (ISO, 2017a) shows the thermal resistance values for vertically vented air cavities (e.g., in the case of masonry cavity walls) increased from 0.11 $m^2 \cdot K/W$ to 0.17 $m^2 \cdot K/W$ as the air cavity thickness increased from 5 mm to 15 mm. The value remains at approximately 0.18 $m^2 \cdot K/W$ when the air cavity is between 25 mm and 100 mm.

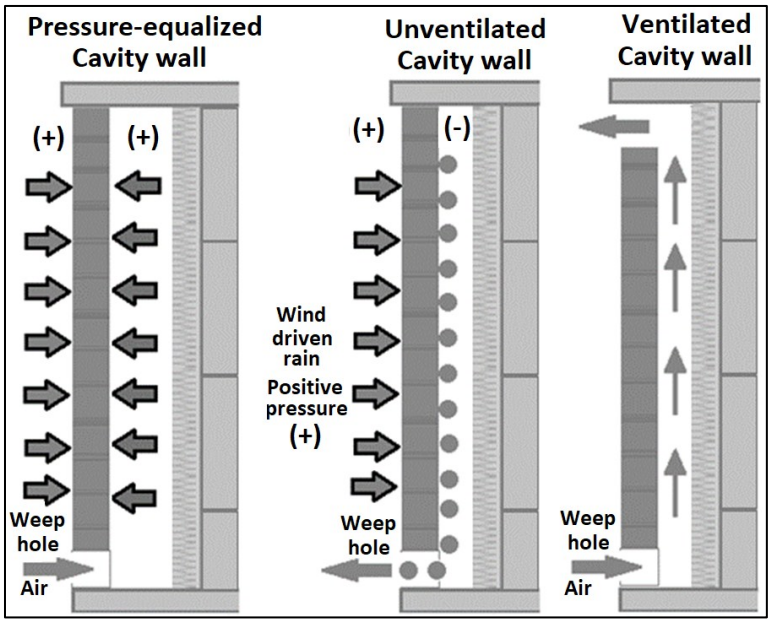

Figure 2-6: Types of cavity walls.

2.3. Overall Design Considerations

Due to masonry walls’ durability, high thermal mass, and versatility to adapt to a wide variety of insulation schemes, there is a high potential for masonry to have an excellent thermal performance. Thus, it is meaningful to provide designers and analysts with design information regarding building types and energy conservation alternatives. This section presents the effective wall conditions that are recommended to be considered in innovative insulation schemes and

block designs. The effects and consideration of significant design parameters will also be discussed.

2.3.1. Loading Effect of Cavity Walls

The relationship between structural loading and thermal performance of masonry walls is usually focused on subjecting masonry walls to extremely high temperatures (e.g., fire). Masonry tends to bend towards fire when subjected to high temperatures (Ono, 2007). Vertical loading tends to cause problems after a long period of fire exposure as the element tends to become laterally unstable due to high stresses produced by moments of lateral displacement (Rigão, 2012).

Numerical simulations were conducted by Nadjai et al. (2003) to address the influence of load application and wall slenderness on loading in fire conditions. The simulation results determined that the non-load bearing masonry wall showed displacements on both axes around the wall, and the maximum deformation occurred at the center of the sample, behaving as if it were fixed on four corners. For a load-bearing masonry wall, the displacements were smaller and restraint was only present at two sides of the wall: at the top and base of the masonry wall. It was concluded that loading has a direct effect on the displacement of masonry in fire conditions. Another study presented by Souza et al. (2019) identified the influence of loading on the fire behaviour of masonry walls. Six masonries made of clay bricks laid with mortar were tested experimentally. These specimens were tested with and without a loading of 10 t/m. The real-scale specimens were subjected to the standard ISO 834 (ISO, 1999) fire curve for four hours. During the test, the properties of stability, airtightness, and thermal insulation were assessed. Results showed that loaded specimens yielded smaller deformations compared to unloaded ones. The load application resulted in a thermal insulation reduction of 23.8%, while the unloaded specimen showed a decrease of 43.3%. Literature has shown few attempts to address the performance of load-bearing masonry walls with respect to high temperatures as well as the relationship between the structural and thermal performance of masonry walls. Further research is required as these attempts show that loading has a direct effect on the displacement of masonry in fire conditions.

2.3.2. Contact Resistance

The contact resistance effect can be significant on the overall R-value (ASHRAE, 2017c; McGowan and Desjarlais, 1995; Hershfield, 2016a). Guidance regarding the precise selection of

reasonable contact resistance values between non-metal materials is not popular, although the contact resistance between metal materials is provided by ASHRAE Handbook Fundamentals 2017 (ASHRAE, 2017c) and can range from 0.01 (m^2K)/W to 0.1 (m^2K)/W. Most of the currently available research data regarding contact resistances for buildings has been focused on light-gauge, steel-framed walls.

A study conducted by Morrison Hershfield (2016a) showed comparable results between modelled and experimental testing when using a contact resistance of 0.002 m^2K/W at steel-to-steel connections and 0.010 m^2K/W at steel-to-concrete interfaces. These values were further confirmed by Di Placido et al. (2019a). Their results also showed that contact resistances are significant, accounting for approximately 10% of the difference between modelled and experimental heat flow values.

2.3.3. Moisture Accumulation

Moisture accumulation in masonry wall systems causes adverse health effects on occupants. Besides, moisture could cause physical and chemical damage to the building's contents and reduce the efficiency of the buildings' mechanical systems. Controlling moisture is required to protect both the occupants and buildings from the accumulated moisture effect and to reduce the maintenance cost. Buildings must be designed, constructed, and operated so that the materials manage to dry quickly in case they get wet (Xhexhi et al., 2020). Moisture and water are often entrapped in the air cavities in cavity walls. Weep holes on the brick veneer are created for draining moisture from the air cavity to the exterior and for allowing airflow in the cavity to dry the moisture. Unfortunately, during construction, excess mortar falls into the air cavity behind the bricks, causing the blocking of the weep holes with mortar (Schulenburg, 2000). To overcome weep plugging during construction, several devices and inventions have been developed (Sourlis, 1993; Sourlis, 2000; Schulenburg, 2000; Koester, 2006).

2.3.4. Temperature Dependency of Material Properties

In building designs and performance simulations, the thermal properties of materials (e.g., thermal conductivity, specific heat) of construction are often assumed to be invariant to temperature, moisture, and time. For example, the thermal conductivity of an insulating material is often advertised using a single value that is implied to be constant. The value is usually

obtained through laboratory tests according to standards, such as ASTM C518 (ASTM, 2015a), which shows the standard testing method for steady-state thermal transmission properties using a heat flow meter. Laboratory testing requires examining insulation materials under specific conditions, such as a mean temperature of 24°C with a temperature difference of 20°C using a one-dimensional heat flow meter. Research has shown that these testing conditions are not representative of the realistic environmental conditions that insulation is typically subjected to (Berardi, 2017). Research has further shown that most insulating materials have an effective conductivity that may change over a range of environmental parameters (e.g., temperature, moisture levels, and material ageing).

Many studies showed that the thermal conductivity of concrete at room temperature is in the range of 1.4 and 3.6 W/ (m K) and varies with temperature and moisture (Bažant et al., 1996; Kodur and Sultan, 2003; Lie and Kodur, 1996; Shin et al., 2002; Harmathy and Allen, 1973; Phan and Phan, 1996). Measuring materials' thermal properties is a challenge as there are few standardized methods available for measuring materials' thermal properties. Overall, concrete thermal conductivity decreases gradually with temperature and this decrease is dependent on the concrete mix properties (e.g., moisture content and permeability) and is suggested to be as a result of the increment in pore volume in the cement-sand matrix and the change in grain size due to the development of fracture planes within the coarse aggregates (Malik et al., 2020). Also, the variation of moisture content with an increase in temperature was suggested to be the main reason for this decreasing trend in concrete thermal conductivity (Bažant et al., 1996). Specific heat increases with an increase in temperature up to about 400°C and remains constant thereafter. Concrete consisting of blended cement with slag or fly ash and lightweight aggregates exhibits good thermal performance at elevated temperatures (Malik et al., 2020). Insulation materials' thermal properties are also dependent on temperature variations. Experimentally, insulation materials made of inorganic fibres such as rock wool or fibreglass were tested. Linear temperature dependence of thermal conductivity has been noticed showing lower thermal conductivities at lower temperatures. However, foamed insulation materials like polyisocyanurate showed nonlinear temperature dependence with a significant deviation from linear behavior (Berardi et al., 2018).

2.3.5. Insulation and Materials Aging Effect

More accurate simulations must be considered to monitor the change in insulation's material properties through time and under cycles of different environmental conditions. Research emphasizes that the thermal behaviour assessments must be carried out with accurate data about the materials, considering the environmental and aging effects on the thermal properties of materials.

Berardi (2019) and Belanger et al. (2018) have shown that the aging of the foams and the operating temperatures have higher impacts on the polyisocyanurates than on polyurethane. Additionally, high moisture levels lead to lower performance in all foam materials, with open-cell foams experiencing the greatest thermal resistance reduction. Results showed that the effective resistance of closed-cell polyurethane and open-cell polyurethane was reduced by 15% and 18%, respectively, when subjected to different environmental conditions (Belanger and Berardi, 2018). Also, it was concluded that the thermal conductivity of aged materials can increase by 100% from their pristine conditions, especially when polyisocyanurate foams are used in cold and humid conditions.

Another study (Barnes et al., 2013) was performed on four different insulation materials (i.e., Dow Polystyrene, standard fibreglass, Aspen Aerogel, and Honeywell polyurethane), and these insulation materials were tested under controlled conditions to determine the effects of extended exposure to high temperatures and humidity on an insulation material's performance. Samples were exposed to steady-state temperature and humidity conditions in an environmental chamber for one week and one month. For the steady-state test conditions, the temperature and humidity were set to 150 °F (65.56°C) and 90%, respectively. Results showed that all four insulation materials experienced a reduction in R-value and thermal conductivity compared to the original samples. The R-value of the Dow Polystyrene and the standard fibreglass insulation materials was reduced by less than 3%, and there was no significant change between the one-week and one-month samples. The R-value of the Aspen Aerogel and the Honeywell polyurethane insulation materials were reduced by almost 10% and 25%, respectively. The Aspen Aerogel insulation degraded a further 3% between the one-week and one-month samples, while the Honeywell polyurethane insulation degradation remained constant. In addition to the reduction in thermal properties of the samples, minor physical changes to the specimens were also observed.

After conditioning, the Aspen Aerogel sample started to develop crystals on its surface, while the polyurethane samples began to bow and deform due to the exposure to high temperatures and humidity. The remaining two insulation materials showed no physical changes when exposed to high temperatures and humidity for an extended period (Barnes et al., 2013). Inaccurate assumptions about the thermal conductivity of materials cause inaccuracies in building performance. It affects design choices that will influence the thermal performance of the building. Designers should consider both the present and future climate conditions to avoid misleading assumptions.

2.3.6. Energy Efficient Wall Systems, Insulation Schemes, Materials and Block Design

The versatility of cavity walls to realize high-performance design requirements and insulation schemes has been discussed by Bradfield (2011). R-30 cavity wall can be designed by effectively arranging and selecting the correct insulation and by considering the wall tie analysis and its effect on thermal performance. Several studies have attempted to address energy efficiency, environmental effects in buildings, and building materials. Kumar et al. (2012) discussed the use of embodied energy and total energy in a sample room. This study focused on the comparison of two varieties of structures constructed using different types of bricks: clay brick and ash block structures. The ash blocks were manufactured using autoclaved aerated concrete material having 60% as the basic raw material, while other materials used were lime cement, gypsum, and aluminum powder. Due to millions of tiny pores, it has a low density and thermal conductivity. It was suggested that although ash blocks are more expensive than clay bricks, they can significantly decrease the size of air conditioning systems, energy usage, and total cost of building due to their lightweight and low thermal conductivity.

A comparative study between the thermal responses of conventional infilled frame construction and load-bearing masonry construction was performed by Abdou (1993). This study addressed the thermal performance of load-bearing concrete masonry wall assemblies under hot, dry climatic conditions. The assemblies were modelled under dynamic thermal analysis using computer simulation. Results showed that concrete masonry walls provide several advantages due to the relative mass of masonry walls, which results in a delayed migration as heat is absorbed. This event reduces peak heat flow and lowers the temperature differential, causing a

slower response to outdoor temperature fluctuations and more stable indoor air temperatures. It was concluded that load-bearing concrete masonry walls are generally superior to conventional infilled reinforced concrete frames with brick masonry. To improve the thermal performance of masonry walls, Su et al. (2019) developed a composite block that contains an inner hollow part, an outer solid part, and an extruded polystyrene layer sandwiched between the two components, as shown in **Figure** 2-7. This arrangement is consolidated by a set of tenons.

Different ratios of concrete mix were tested for the new composite. The mechanical strength and thermal properties of this innovative block (determined with experimental and numerical simulations) showed better performance compared to ordinary hollow-core concrete blocks. However, the thermal bridge at block joints must be considered, as well as the handling and transportation of the blocks, which require further consideration.

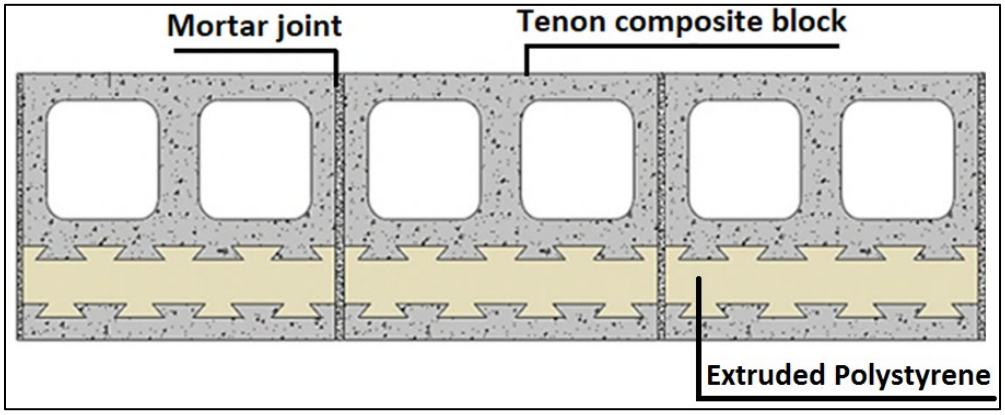

Figure 2-7: Horizontal schematic of a Composite block wall (Su et al., 2019).

2.3.7. Whole Building Thermal Analysis and Energy Consumption

Few studies consider the thermal analysis of a whole building. The majority of research is focused on local thermal bridging in a specific structural element. Whole building thermal bridges are significantly affected by the presence of concrete columns, slabs, and beams within the building envelope. These bridges create an easy path for heat transmission, which negatively affects air-conditioning loads.

A study performed by El Sayed (2002) addressed the effect of thermal bridging caused by columns and beams on energy consumption and peak load requirements of private residential

villas in Kuwait. The uninsulated skeleton structure of reinforced concrete (beams and columns), which forms 27% of the external total wall area, can have a significant effect on the thermal performance of a building envelope. Multi-dimensional heat transfer computer simulations were implemented to assess thermal performance, and these results were incorporated into a whole building energy simulation program to determine their impact on the overall thermal performance of the buildings considered. The steady-state three-dimensional heat transfer analysis showed that a 41% reduction in the thermal resistance of walls and a 48% reduction in the roof R-value was possible if columns and beams were not insulated, mainly due to the presence of a larger reinforced concrete slab area. It was concluded that the thermal resistance of construction could be reduced by 48% by using uninsulated roofs, columns, and beams. Moreover, the average impact of the reduction in the R-value of a whole building on the overall annual energy consumption and peak load demand was found to be 1.8% and 2.3%, respectively.

The yearly, monthly, and daily cooling and heating loads in a typical villa in Riyadh were investigated by Zedan et al. (2016). This study focused on the thermal bridges primarily caused by mortar joints between insulated building blocks. The effect of the mortar joint was addressed for the whole building rather than just one wall. The investigated villa had two levels with a total floor area of 400 m^2 and all walls were exposed to the environment. The thermal bridge effect was simulated in the whole-building energy analysis using 2D dynamic thermal analysis modelling. Results showed that the yearly cooling load increased from 3% to 11% based on a ratio of the thermal bridging mortar joint area and total wall area (0.02 and 0.08, respectively). On a monthly basis, the rate of increase was higher during the summer months. In August, the monthly cooling load increased between 5% and 15% for a mortar area to total wall area ratio of 0.02 and 0.08, respectively. It was concluded that the effects of thermal bridges resulting from mortar joints between building blocks are significant and may cause an increase in the annual heating or cooling load by 11%.

2.3.8. Construction and Design Recommendations

One of the main goals in the construction industry is to reduce energy usage in buildings while also ensuring comfort. Advanced construction techniques and materials with superior thermal properties can be used to reduce thermal bridging in masonry walls. One common method to

reduce the thermal bridging effect is the use of alternative steel or non-steel structural materials. Stainless steel is less conductive than normal steel and is highly encouraged to be used in the industry. Alternative materials, such as fibre-reinforced polymers (FRP) and thermal breaks, even though they are much less conductive, have issues common to new technologies. In many cases, a code-based acceptance procedure is not available for these new materials and alternative tests must be demonstrated and special approvals are required, which can cause reluctance when considering such details. Conventional construction and design approaches, as well as general recommendations for reducing thermal bridging, are as follows (Alshatshati et al., 2017; Barnes et al., 2013; Eurima, 2008; D'Aloisio et al., 2012).

- Reduce the frequency of penetrations and eliminate continuous thermal bridges whenever possible.
- Use structural elements with superior thermal resistance properties, such as FRP or stainless steel, which have an R-value three times greater than that of carbon steel.
- Accommodate manufactured structural thermal break assemblies for use at structural steel elements and encourage using an insulating shim (such as FRP) between the shelf angle and concrete surface.
- Insulation boards should be in intimate contact with masonry to avoid air circulation from degrading thermal resistance, and misalignments are mostly due to excess mortar between blocks and unclean wall surfaces.
- External insulation must be completely sealed at all perimeter edges to eliminate air infiltration between the panel and external wall.
- To avoid and control construction problems, there should be a high level of quality control and highly qualified technicians experienced in the construction industry working on site.
- During the design phase and before construction, heat transfer modelling should be considered to analyze unusual conditions where thermal bridging may occur.
- Develop strategies to minimize building energy loss due to thermal bridging before construction.

2.4. Estimation of Thermal Resistance

Kosny et al. (2001) showed that the thermal resistance of a wall can be overstated by up to 26.5% in construction details, such as corners and small thermal bridging items, are ignored. There is an increasing need for more accurate evaluations (prediction and testing) of the thermal

performance of masonry walls and their elements as energy codes become stricter and performance simulation is becoming more prevalent. Thermal resistance is commonly used in the industry to describe the ability to resist heat flow.

2.4.1. Simplified Analytical Approach

This section presents the difference between the current simplified analytical methods used to estimate the thermal resistance or transmittance of building elements. In addition to the assumptions and limitations for each method.

2.4.1.1. Thermal Resistance of Concrete Masonry Units

Two calculation techniques have been commonly used to determine thermal resistance: the parallel-path and series-parallel (e.g., isothermal-plane) methods. The parallel-path method is acceptable for calculating the thermal resistance of concrete masonry units (CMU), only if the units are not insulated (ACI, 2002). In this method, heat flow is assumed to be transferred through the CMUs in parallel flows. If the CMUs were hollow, the heat flow through the CMU (not including the mortar) would depend on the ratio between the web area and core area as shown in Equation (**1**):

$$R_T = \frac{R_w \times R_c}{a_c \times R_w + a_w \times R_c} \quad \textbf{(1)}$$

Where a_c is the fractional core area; a_w is the area percentage of the web; R_c is the thermal resistance of cores, empty or with fillings ($m^2 \cdot K/W$); and Rw is the thermal resistance of concrete webs ($m^2 \cdot K/W$). Note that the fractional area is the area of the studied element (core or webs) over the total area of the block.

The series-parallel method is applicable for both insulated and uninsulated masonry units and considers lateral heat flow in face shells (ACI, 2002; NCMA, 2013; ASHRAE, 2019a). This calculation divides the block into a series of thermal layers. The overall R-value is the sum of the resistance of each layer. The equation is described as follows:

$$R_T = R_i + \frac{R_f \times R_m}{a_f \times R_m + a_m \times R_f} + \frac{R_w \times R_c}{a_c \times R_w + a_w \times R_c} + R_a + R_V + R_O \quad \textbf{(2)}$$

Where a_c is the fractional core area; a_f is the fractional face shell area; a_m is the fractional mortar joint area; a_w is the fractional web area; R_a is the thermal resistance of cavities between the veneer and backup wall, including continuous insulation ($m^2 \cdot K/W$); R_c is the thermal resistance of cores, empty or with fillings ($m^2 \cdot K/W$); R_f is the thermal resistance of both face shells ($m^2 \cdot K/W$); R_i is the thermal resistance of inside air surface films ($m^2 \cdot K/W$); R_m is the thermal resistance of mortar joints ($m^2 \cdot K/W$); R_O is the thermal resistance of outside air surface films ($m^2 \cdot K/W$); R_T is the overall thermal resistance of a wall ($m^2 \cdot K/W$); R_V is the thermal resistance of veneers ($m^2 \cdot K/W$); R_w is the thermal resistance of concrete webs ($m^2 \cdot K/W$).

Applications of the series-parallel method for walls with configurations and materials were provided by the thermal catalog of concrete masonry assemblies (NCMA, 2012) and include fully grouted walls, walls with furring and gypsum, etc. For partially grouted walls, tables are available in National Concrete Masonry Association technical report number "TEK 06-02C" (NCMA, 2013) with R-values for walls of various grouting arrangements. The catalog has walls with different materials, such as perlite, vermiculite, polyurethane foamed-in-place, and others. It also presents values for blocks with different densities. The U-factor of a partially grouted single wythe wall without any thermal bridging elements (e.g., shelf angle, ties, fasteners or slabs) can be calculated from the weighted-area average of the U-factors of the grouted area and un-grouted areas as follows:

$$U = (a_{gr} \times U_{gr}) + (a_{ungr} \times U_{ungr}) \qquad (\text{Note } R = \frac{1}{U}) \qquad \textbf{(3)}$$

Where a_{gr} is the fractional grouted area of the wall, a_{ungr} is the fractional un-grouted area of the wall, U_{gr} is the thermal transmittance of the fully grouted wall ($W/m^2 \cdot K$), U_{ungr} is the thermal transmittance of the un-grouted wall ($W/m^2 \cdot K$), and R is the overall thermal resistance of a wall ($m^2 \cdot K/W$). These tables can be used to calculate the grouted area and un-grouted area based on the vertical and horizontal grout spacing in partially grouted masonry walls. The thermal transmittance of the grouted wall (U_{gr}) and the un-grouted wall (U_{ungr}) are provided in tables for various masonry units with different densities and core filling scenarios.

2.4.1.2. Series and Parallel Heat Flow Paths

Series and Parallel path methods are two of the most commonly used techniques for thermal resistance calculations. In the case of the series path method, the heat flows layer by layer

through a building assembly made of multiple materials stacked together. A single layer's thermal resistance to heat flow is given by the ratio of its thickness to its thermal conductivity. Accordingly, in series flow paths, the thermal resistance of a building assembly composed of uniform parallel layers (e.g., wall), consists of the sum of the resistances of all layers in series (ASHRAE, 2017a):

$$R_s = R_1 + R_2 + R_3 + R_4 + \dots + R_n \qquad \left(\text{where: } R_n = \frac{t_n}{K}\right) \quad \textbf{(4)}$$

where; $R_1, R_2, \dots, R_n$ are resistances of individual layers ($m^2 \cdot K$)/W, Rs= resistance of building assembly (overall resistance ($m^2 \cdot K$)/W), t_n= the thickness of individual addressed layers (m) and k= thermal conductivity of the individual addressed material (W/mK).

While in the case of the parallel path method, the heat flows through different pathways and is assumed to be transferred through the straight parallel lines through a building assembly. The Parallel Path Method is applied by assuming one-dimensional heat transfer perpendicular to the surfaces of the building element. This assumption is accurate when the materials on the same layer are having close thermal conductivity values (i.e., wood frame walls). In many building assemblies, components are arranged so that heat flows in parallel paths. If no heat flows through lateral paths, the average transmittance of the enclosure is calculated as follows (ASHRAE, 2017b):

$$U_{av} = AU_A + BU_B + \dots + NU_N \qquad \left(\text{where: } U_n = \frac{1}{R_n}\right) \quad \textbf{(5)}$$

where; $A, B, \dots, N$ are the surface-weighted path fractions for a typical basic area composed of several different paths with transmittances $U_A, U_B, \dots, U_N$.

Most building assemblies are a combination of layers in series and parallel pathways. Therefore, a combination between both methods is also used, called the series-parallel (e.g., isothermal planes) method. In the Isothermal Planes Method, it is assumed that heat can flow laterally in any component and the thermal resistances of adjacent components are combined in parallel, resulting in a path with series-parallel resistance combined. Isothermal planes are formed when heat can flow laterally with a small resistance value in any continuous layer, so that transverse

isothermal planes result (ASHRAE, 2017b). The assembly performs as a series of layers, of which one or more provide parallel paths. The total average resistance in that case is the sum of the resistance of the layers between the isothermal plans. Each layer is calculated and the results are weighted by the contributing surface area. This assumption is accurate when adjacent materials in the same layer have different conductivity values.

The parallel and isothermal-planes methods are often considered two separate calculation methods. Recently, the ASHRAE Fundamentals Handbook (ASHRAE, 2017b) suggests the actual U-factor lies between both methods. The ASHRAE fundamentals Handbook (ASHRAE, 1993a) suggested that these methods provide a range of upper and lower limits on the true thermal resistance. The obtained thermal resistance assuming parallel heat flow only is usually higher than that obtained assuming the isothermal planes method. Therefore, the isothermal plane and the Parallel Path method results are known as "the lower and the upper limit of the total thermal resistance", respectively. Generally, it was suggested that, if the construction contains a layer in which lateral heat conduction is high compared to heat flux through the wall, a value closer to the isothermal calculation should be used. If there is no layer of high lateral thermal conductance, a value closer to the parallel calculation is more accurate. However, the ASHRAE Fundamentals Handbook (ASHRAE, 1993a) generally recommended further experimental examinations of the required studied elements to reveal whether the actual thermal resistance value is closer to the higher or lower calculated range.

2.4.1.3. ISO 6946 Combined Method

The combined method is described in International Standard ISO 6946 (ISO, 2017d). This method is used to compute the thermal resistance of building elements consisting of homogeneous and inhomogeneous layers. It may also be applied to building elements, which may contain an air layer up to 0.3 m thick. The combined method suggests computing the total thermal resistance by combining the Parallel Path Method and the Isothermal Planes Method results. The total thermal resistance is computed as an arithmetic average of the upper and lower thermal resistance limits obtained using the Parallel Path and the Isothermal Planes methods, respectively. In other words, the two R-values (upper and lower limits) have the same weight (0.5) in the total resistance calculation. However, there are some limitations to this method: (1) this approach is only applicable in the case where the ratio of the upper limit to the lower limit of the thermal resistance does not exceed 1.5. (2) this method is not valid in cases of thermal

insulation is bridged by metal and in the cases where there is a significant difference between the thermal conductivity of the materials in the same layer. (3) There are some corrections required to the thermal transmittance values for air voids, mechanical fasteners, and inverted roofs; the total correction in some cases exceeds 3%.

2.4.1.4. ASHRAE Method

The assumptions described in the parallel path method (the heat flow is perpendicular to the wall) are not accurate in the wall structure containing steel members next to materials with low thermal conductivity such as thermal insulation, where the thermal bridge effects become more significant (Barbour et al., 1994). Therefore, the ASHRAE Method was developed to address assemblies with widely spaced metal elements of uniform cross-sectional areas and adjacent materials with different conductivities (e.g., lightweight steel-framed constructions) (Adam Di Placido et al., 2019a). The ASHRAE method is considered an adjustment to the parallel path method. This method is applied as follows; the wall is divided into two sections: (1) containing the steel thermal bridge influence and (2) containing the remaining portion of the wall cavity without the thermal bridge influence. Factors in the form of charts were presented to determine the width of the assumed two sections based on the dimensions of the addressed steel element. By using an area "weighting factor" to the wall sections affected by the steel element thermal bridge (Cao et al., 2016), the thermal resistance values are computed and then combined using the parallel path method. This method is suitable for lightweight steel-framed constructions due to having simple geometries and uniform thermal bridging (e.g. steel stud); also, the factors provided to determine the sections' width are limited to steel studs and lightweight steel-framed walls.

2.4.1.5. Point and Linear Transmittances

In this approach, the thermal transmittance introduced by thermal bridging components additional to that of the clear field is called the point or linear transmittance, depending on the geometry of the thermal bridges. The linear transmittance Ψ (W/ (m K) due to linear thermal bridges (e.g., slab edges, shelf angles) can be calculated as follows:

$$\Psi = \frac{Q_A - Q_B}{L} \quad \textbf{(6)}$$

Where Q_B is the heat flow of the clear field of an assembly (W/K); Q_A is the heat flow of the assembly with a portion of the clear field replaced with intersections (W/K); and L is the assembly width (m), which represents the linear length of the intersection.

The point transmittance is similar to the linear transmittance but for point anomalies such as beam end penetrations and intersections between linear details. The point transmittance χ (W/K) is a single additive of the amount of heat, as shown in Equation (4)

$$\chi = Q_1 - Q_2 \quad \textbf{(7)}$$

Where, Q_1 is the heat flow of the whole assembly unit with intersections (W/K), and Q_2 is the heat flow of the assembly with no intersections (W/K).

In calculating the overall thermal transmittance of an entire building or wall, all thermal transmittances are categorized into three groups: clear field transmittance **(U_o),** linear transmittance (Ψ)**,** and point transmittance *(χ)* (Hydro, 2016b). The overall U-value (W/m^2·K) is calculated as follows:

$$U_T = \frac{\sum(\Psi \times L) + \sum \chi}{A_{Total}} + U_O \quad \textbf{(8)}$$

Where U_o is the clear field thermal transmittance (W/m^2·K), A_{total} is the total opaque wall area (m^2), ψ is the point transmittance heat flow from the linear thermal bridge (W/(m K)), L is the length of the linear thermal bridge (m), and χ is the heat flow from the point thermal bridge (W/K).

The overall U-value for a wall can only be determined using the Point and Linear Transmittances approach when the thermal performance values for the clear field (U_o), linear **(Ψ),** and point **(χ)** transmittances are known, which requires computer simulations or experimental testing. Besides, the dimensions and quantities of each element must be determined before performing any thermal resistance estimations.

2.4.2. Experimental Testing for R-value

Effective thermal resistance is influenced by many factors, such as air leakage, thermal bridging, moisture content, physical conditions, and installation defects. Sometimes, the accurate value can

only be captured by testing. Therefore, tests are often used to evaluate and improve the approaches and accuracies of analytical calculations and numerical simulations.

2.4.2.1. Laboratory Testing Using Hot Box Apparatus

The hot box method is the most common experimental approach to determine the thermal performance of assemblies with large dimensions (Lindsey, 1993). ASTM C1363 2011 (ASTM, 2011) provides minimum requirements to test the thermal performance of building assemblies under steady-state conditions and for homogenous and non-homogeneous specimens (McCall, 1985). There are two types of hot box apparatuses: the guarded hot box and calibrated hot box, as shown in **Figure 2-8**.

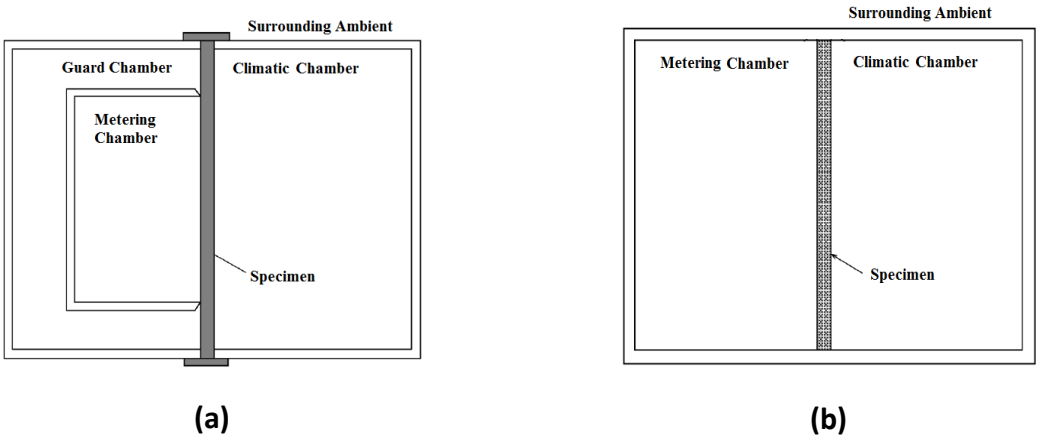

Figure 2-8: a-Typical guarded hot box; b- Typical calibrated hot box (ASTM, 2011)

A comparison between the advantages and disadvantages of the two hot boxes is shown in **Table 2-6**. The main components of both hot box apparatuses are the metering chamber, climatic chamber, loading frame, and ambient space surrounding the specimen. These four components should be designed to provide the required conditions for testing, such as air velocity, air temperature, and radiation conditions. The expected output information from these chambers provides an accurate measurement of the net heat transfer through the specimen.

Table 2-6: Comparison between guarded hot box and calibrated hot box

Points of Comparison	Guarded Hot Box (Self-Masking)	Calibrated Hot Box (Masked)
Advantages	Lateral heat flow at the edges of the metering chamber can be minimized.	Large specimen sizes can be tested

Disadvantages	Smaller specimen is required since the metering chamber opening has to be smaller than the building element dimensions.	The heat flow not going through the specimens has to be calibrated for different testing conditions and specimen sizes.

Hot boxes typically measure heat transfer through a specimen under steady-state conditions when the environmental conditions on both sides of the specimen are constant. Tests are typically performed with a significant temperature difference across the specimen. Air velocities on both sides of the specimen are measured and remain constant during the test. Once the steady-state condition is reached, the net heat flow (Q) through the specimen is carefully measured or calculated (ASTM, 2011). The following general equation is used to calculate the R-value of a specimen:

$$R = \frac{A \times \Delta T}{Q} \quad \textbf{(9)}$$

Where Q is the heat flow through the metered area (W), R is the thermal resistance of the specimen ($m^2 \cdot K/W$), A is the metered area (m^2), and ΔT is the difference in surface temperature across the specimen (K).

Aside from measuring R-values under steady-state conditions, R-values can also be measured under dynamic conditions with temperature changes. Dynamic tests can be performed, with the calibrated hot box by maintaining a constant indoor air temperature while the outdoor air temperature is varied using a predetermined time versus temperature relation. The energy required to maintain a constant indoor air temperature is recorded as a function of time (Van Geem et al., 1982). The dynamic response of a hot box to dynamic excitation needs to be determined and separated from the response of the specimens (Brown and Stephenson, 1993a; Brown and Stephenson, 1993b). Brown et al. (1993b) presented the test procedure to measure dynamic heat transfer characteristics of full-scale wall specimens using a guarded hot box apparatus. Fiorato et al. (1979) used a hot box apparatus to study different masonry wall configurations based on dynamic and steady-state conditions. The ASHRAE research project 1365-RP's (Roppel et al., 2012) used guarded hot box testing under steady-state conditions. Also, the experimental results using hotbox of many previous studies were used to validate recent numerical simulations' results or calculation methods (Brown and Stephenson, 1993a;

Brown and Stephenson, 1993b; Kosny, 1995; Kosny and Christian, 2001; Desjarlais and McGowan, 1997).

2.4.2.2. R-Value Measurements Using Thermal Imaging

Thermographic imaging consists mainly of taking photographs in the infrared spectrum. The camera estimates and creates an image of long-wave radiation that is converted to the visible color scale. From these long-wave measurements, the temperature can be deduced. Emissivity must be assumed in this technique as the camera is incapable of recognizing the boundary between different elements, such as bricks and steel door frames. The emissivity assumption is considered to be one of the main sources of error in this technique. In addition, ASTM C1060-11a provides practical techniques and recommendations for the thermographic inspection of insulation installations in envelope cavities of frame buildings (ASTM, 2015b). Thermographic imaging is considered a practical and rapid method for inspecting and analyzing improperly installed or damaged insulation. However, care must be taken during the interpretation of thermal bridging from thermographs because some temperature irregularities can be caused by air leakage (Barnes et al., 2013). A lower-cost automated approach for rapidly evaluating the energy effectiveness of buildings is needed. An automated measurement approach to estimate building envelope R-values was presented by Alshatshati et al. (2017). Estimated wall and window R-values used in this approach were obtained by thermal imaging. The measured exterior wall temperatures were calibrated to known and measured R-values for a small group of residences. In this approach, two steps were performed: (1) visual imagery was used to determine wall emissivity based on the colour of the walls and the temperature was estimated, and (2) a random forest model was developed using the training set obtained from the studied residences with a known R-value. This model can be used to estimate the R-values of other houses based on their measured exterior temperatures using thermal imaging. Results showed that the proposed approach was capable of accurately estimating envelope thermal characteristics and capacitances.

2.4.2.3. On-Site Overall R-Value Measurements for Masonry Walls

The thermal performance of a new building design can be evaluated through laboratory tests and numerical simulations, but evaluating the thermal performance of existing masonry walls is more complicated due to many factors, such as the degradation of material properties over time and

imperfect workmanship. Practical, non-destructive, and in-situ measurements are needed for the evaluation process.

ASTM C1155-95 (ASTM, 2013) provides guidelines to obtain in situ measurements of heat fluxes and temperatures and uses the data to compute the thermal resistance of building envelopes. This practice provides estimation methods for thermal resistance values in the range of temperatures obtained during the measurement of temperatures and heat fluxes. Two techniques are presented: the summation technique and the sum of least squares technique.

Deconinck et al. (2016) presented a comparison of in situ characterization methods for determining the thermal resistance of building components. The most accepted method is the average method described in ISO 9869 (Rasooli and Itard, 2018). Essentially, the average method relies on semi-stationary boundary conditions, using averaged measurement data as an approximation of stationary conditions. For the method to be valid, the averages should be taken over a sufficiently long period. More advanced data analysis methods, such as regression modelling, Auto-Regressive with eXogenous input (ARX)-modelling, or stochastic grey-box modelling, can be used to handle dynamic conditions. A comparison of these dynamic methods was completed for simulated measurements of an insulated cavity wall in a moderate European climate. Performances were tested for actual measurements of a similar test wall. These results showed that the semi-stationary methods were more practical and reliable when applied to winter measurements. The dynamic methods were more complex but offered more versatile applications.

An investigation presented by Soares et al. (2019) reviewed laboratory and in situ non-destructive methods to evaluate the thermal transmittance and behaviour of walls. The research described five methods: heat flow meters; guarded hot plates; guarded hot boxes; calibrated hot boxes; and infrared thermography. Regarding the in-situ methods, the majority of studies found in the literature refer to homogeneous or moderately homogeneous walls, and more research should be conducted to provide reliable methodologies that use quantitative infrared thermography to measure the thermal transmittance of non-homogeneous construction elements. It was concluded that further research is required to quantify the influence of several parameters, such as emissivity, surface heat transfer coefficients, air velocity, and thermal bridges. Calculating thermal resistance from in situ data represents in-service conditions. However, field

measurements of temperature and heat flux may not achieve the accuracy obtainable in laboratory apparatuses.

2.4.3. Numerical Simulation

Experimental measurements of an element's thermal behavior can be expensive, especially for large-scale specimens. Computational numerical simulation is considered a practical alternative, as this method is cost-effective and accurate. Many thermal analysis programs are designed to simulate thermal problems in two dimensions, such as THERM, HEAT2, Energy2D (Xie, 2012), and three dimensions, such as ANSYS, ABAQUS, HEAT3, and SIEMENS. A number of studies on masonry walls have been conducted to improve and validate the simulation approaches with experimental data (del Coz Diaz et al., 2006; Norris et al., 2012a; Desjarlais and McGowan, 1997). Those studies showed good agreement (typically about 3% discrepancy) between numerical simulation and experiment results. Validated simulation approaches were then used to simulate the thermal performance of other wall configurations. The collection of data (i.e., a catalog) allows designers to have quick and easy access to the accurate thermal performance of many design options (Norris et al., 2012a; Hershfield, 2016a).

2.5. Research Gap and Recommendations

Many studies have investigated the thermal performance of masonry concrete blocks, introduced insulation patterns, and estimated thermal efficiency using different approaches and techniques. There are a few methods to estimate the R-value of a complete wall, including all of its components (i.e., air gaps, ties, and shelf angles). Some of these methods are insufficient due to limitations on specific cases and conditions. These methods must be modified and further investigated to provide a reliable estimation method for the effective R-value of different masonry walls that can represent any detail required with no limitations on the conditions, configurations, or material properties. The remaining methods depend primarily on computer simulations (e.g., linear and point transmittance). There is a need for practical methods that are independent of computer simulations and experimental tests to simplify the application process for designers. These practical methods should be able to provide sufficient accuracy without compromising efficiency and increasing costs. The significance of such work would help provide design guidelines for the construction industry. It would also help designers predict the R-value

of masonry walls with different conditions and analyze the effect of interruptions, such as intersections of slabs or balconies, on the overall thermal performance. It is apparent from the literature reviewed that the estimation of a masonry wall's thermal performance is a sensitive process that can affect the total estimated energy use of a building.

A research gap was also found on significant topics that have a direct effect on the thermal performance of masonry walls and buildings (e.g., the relationship between the structural and thermal performance of masonry walls), the insulation aging effects, and the effect of building components on the whole building thermal analysis rather than one element (e.g., walls). Few types of research address the thermal inertia of masonry walls. Unlike thermal insulation, which can be characterized by thermal resistance, thermal inertia (the capacity of a material to store heat and to delay its transmission) is difficult to quantify a single parameter. Different indicators to characterize thermal inertia have been used over the years. Thus, coefficients like thermal diffusivity or the effective heat capacity per unit area are widely used. This property also has a significant effect on the effective thermal resistance between the interior and the exterior; besides, the thermal inertia causes a link between the maximum external temperature and the maximum instantaneous heat flux transmitted to the interior (Evola et al., 2017; CIANFRINI et al., 2015). Both effects can be used to reduce the energy consumption of the HVAC equipment. Further research is required to address these factors and topics.

The purpose of this review is to provide a critical discussion of the significant factors that influence the thermal performance of masonry veneer walls. Different methods of thermal design and evaluations of masonry walls were presented and discussed by reviewing the available research and practice literature. The effects of different wall components (e.g., concrete blocks, grout, mortar, ties, shelf angles, insulation, and veneer air gaps) and thermal bridging were also discussed, as well as subtle design considerations that influence the thermal performance of a wall, such as the choice of material for concrete block masonry ties and shelf angles. Analytical approaches were presented to demonstrate the resistance calculations for concrete masonry units, while the linear transmittance method and experimental investigations were discussed to illustrate efficient R-value measurements and calculations. The advantages and limitations of each method were also provided. Technical and practical challenges were highlighted, as well as the precautions required to achieve the best thermal performance.

From the review, it is clear that the thermal properties of materials are one of the dominant factors in thermal resistance and should be carefully considered. Tie material and design can have a significant impact on the effective R-value of masonry veneer walls. Traditional steel shelf angles appeared to be the highest contributors to thermal bridging in concrete masonry cavity walls. The R-value reduction of assemblies depends on the shape and materials of shelf angles and ties. Different shapes were introduced to the market to minimize the reduction in thermal resistance. There are many recommendations for the fabrication of stainless-steel shelf angles and ties, which could decrease their thermal bridging effects. This study summarizes critical information and recommendations that will help improve the thermal design of masonry walls, hence reducing the energy consumption of buildings.

2.6. Summary of Influence and Improvement measures of different components

A summary of the effects of different parameters on the overall R-value of masonry walls based on literature, along with recommendations to improve the thermal performance of masonry walls is presented in **Table 2-7**.

Table 2-7: Summary of the effect of different variables on thermal resistance

	Parameter	Effect on Thermal Resistance	Recommendation	Reference
Concrete Blocks and Clay Bricks	*Air cells in concrete masonry blocks*	• Air cells in concrete blocks increase the thermal resistance of the overall wall by 25% compared to solid blocks	• Air cells in concrete blocks contribute significantly to the thermal resistance of masonry walls • Cavity concrete blocks should be used	(Abdou and Murali, 1994)
	Distribution of air cells in concrete masonry blocks	• Blocks made of staggered holes (air cells) performed 2.6 times better compared to blocks made of aligned holes • Blocks made of aligned holes performed 3.4 times better than solid blocks	• Thermal performance of staggered holes has the best thermal resistance compared to aligned holes or solid	(Al-Jabri et al., 2005; Bai et al., 2017; Pierzchlewicz, 1996)
	Concrete block density	• A 33% reduction in block density caused a 60% increase in thermal resistance	• Lightweight aggregate with low thermal conductivity in lightweight concrete blocks	(Al-Jabri et al., 2005; NCMA,

			can provide an alternative cost-effective solution	2013)
	Block size effect	• R-value of walls made with normal weight concrete blocks is more sensitive to thickness variations than walls made with lightweight blocks • Block density effect on overall thermal resistance increases directly with block size	• Block size is a significant factor in the overall R-value calculation	(NCMA, 2013)
	Block's web effect	• A 30% reduction in the thermal resistance of two webs concrete block was noticed compared to three webs concrete block	• Concrete masonry units with two webs are recommended (instead of three) to reduce the webs' thermal bridging effect	(Bradfield and Szoke, 2010; IECC, 2012; Urban et al., 2011a)
Grout and Mortar	*Grout*	• Grout reduces the overall R-value of masonry walls between 3% and 12% compared to empty block cores, depending on the block's shape and density	• Must address many parameters (e.g., block's core number, density and shape) to optimize thermal design	(Abdou and Murali, 1994; Kosny, 1995)
	Number of grouted cores	• Reduction effect of grout on the overall R-value increases directly with the number of block cores	• Multicore units and blocks with many air gaps (even staggered air gaps) are not recommended for fully or partially grouted walls	(Kosny, 1995)
	Density of concrete block in grouted walls	• Reduction of the overall wall R-value caused by grout decreases as CMU thermal resistance increases	• Lightweight concrete blocks are recommended to grout the block's core (fully or partially)	(Kosny, 1995)
	Effect of mortar on insulated blocks	• Mortar reduction effect on R-value increases as thermal resistance of block concrete increases • R-value reduction can exceed 12% in insulated two-core blocks compared to uninsulated two-cores	• Should use less conductive mortars or decrease area of mortar joints • Should also replace side mortar by mechanical interlocking means	(Urban et al., 2011a)
Shelf	*Tie material*	• Stainless steel ties reduce thermal bridging effect and can reduce overall R-value by 3% (versus 8% for galvanized iron)	• Stainless steel has a better thermal performance and lower thermal bridging effect	(Finch et al., 2013b)

		• Fibre ties have the best performance in reducing the thermal bridging effect; can reach 0.2% based on exterior insulation	compared to ordinary steel • Fibre ties have the best performance, but require alternative properties' tests and special approvals	
	Slotted ties	• Holes over the tie body are introduced to reduce the cross-sectional area and minimize thermal conductance, • Holes are also used to elongate heat flow path through the tie	• Effect of ties can vary based on the studied case; however, slotted stainless steel ties are generally recommended for thermal performance improvement	(Finch et al., 2013b)
	R-value of exterior insulation	• Exterior insulation used in cavity walls is directly proportional to a tie's thermal degradation effect on the overall R-value • Effective reduction can range from 5% to almost 30%, depending on exterior insulation thickness and backup wall structure • Exterior insulation with higher R-values experience higher thermal degradation	• Masonry tie material and design can have a significant impact on the effective R-value of masonry veneer walls, which can be an important consideration for energy code compliance	(Finch et al., 2013b)
	Shelf angle effect and insulation thickness	• Reduction in the overall R-value depends on the insulation thickness that is penetrated by shelf angles	• Thicker insulation boards are recommended to reduce a shelf angle's effect on the overall R-value reduction	(Finch and Higgins, 2017)
	Shelf angle shape and material	• R-value reduction ranges between 19% and 44% based on shelf angle shape and material • Intermittent brackets with perforations can decrease the overall R-value by approximately 15% compared to traditional shelf angles solid directly attached large angles • Direct attachment of a shelf angle tight to the wall structure was found to reduce the thermal performance of a wall by 40% to 55%	• Thermally broken stainless steel shelf angles and brackets with perforations have the smallest reduction effect on overall R-value	(Adam Di Placido et al., 2019b; Finch et al., 2013b; Hershfield, 2016a)

		• Alternatively, standing the shelf angle off the floor line structure with intermittent supports (e.g., structural steel knife plates, hollow steel section attachments, or proprietary brackets) can reduce the effective R-value of the above-grade wall by 12% to 22%		
Insulation	*Thermal resistance of blocks*	• Lightweight concretes (blocks with high thermal resistance) may be more efficient at increasing the thermal efficiency of insulation inserts in block cores • Thermal efficiency can reach 85% for blocks made of lightweight concrete	• Lightweight concrete blocks should be used for insulation inserts in block cores	(McCall, 1985)
	Construction	• Location of insulation panels and construction process have a large effect on the condensation potential in concrete masonry walls	• Insulation boards should be in intimate contact with masonry to avoid air circulation from degrading thermal resistance • Misalignments must be avoided	(Eurima, 2008)
Masonry Veneer and Air Cavity	*Variations in air velocity outside the wall*	• Maximum difference of 5 Kelvin was found for a few cases with very low wind speeds	• Few attempts have been made regarding nature and quantity of cavity airflow behind screen-type claddings with different venting strategies and cavity depths • Further research is required	(Stovall and Karagiozis, 2004)
	Wall height	• Variation in wall height did not affect thermal performance	• Wall height is not effective • Further research is required	(Stovall and Karagiozis, 2004)
	Wind direction	• Perpendicular wind direction is more effective on airflow inside wall cavity	• Wind direction must be considered in thermal calculations and air cavity design	(Rowley and Algren, 1937)
	Cavity thickness	• No significant difference in mass flow rates between cavity thicknesses of 19 mm and	• Thickness of the air cavity is one of the most important	(ISO, 2017a; Stovall and Karagiozis,

		50 mm • Thermal resistance of air cavity is equal to approximately 0.18 $m^2 \cdot K/W$ when thickness is 19 mm or greater	parameters that affects thermal performance of cavity walls	2004)
	Ventilation weep size	• Doubling the ventilation weep height doubled the airflow rate	• Ventilation slot size is a controlling factor for airflow rate	(Stovall and Karagiozis, 2004)
Structural Elements	*Beams, columns and roof*	• A 41% reduction in thermal resistance is possible if columns and beams are not insulated (for beams and columns occupying 27% of the total external wall area) • Uninsulated roofs in hot climate regions can reduce thermal resistance by 48%	• Insulation of structural elements is significant	(Omar, 2002)
	Concrete slab intersections	• Thermal resistance may be reduced by 7% to 36% based on concrete slab density and thickness	• Insulation of structural elements is significant	(Desjarlais and McGowan, 1997)
Cavity Walls Loading Effect	*Vertical axial loading*	• Deformation due to high temperature was smaller for masonry walls loaded vertically compared to unloaded walls • Load application resulted in a 23.8% reduction in thermal insulation, while the unloaded specimen showed a decrease of 43.3%	• Few attempts have been made on the performance of load-bearing masonries with respect to high temperature and the relation between structural and thermal performance of masonry walls • Further research is required	(de Souza et al., 2019; Nadjai et al., 2003)

3. R-value Estimation Using Design Charts

3.1. Introduction

The effective thermal resistance of masonry cavity walls is affected by thermal bridging, which is common in connecting masonry veneers to structural backup walls. Therefore, a precise estimation of the R-value of masonry cavity walls is currently a time-consuming task, which lengthens the design process, especially in the early design development stage where many design options (e.g., structural and thermal) need to be explored holistically. At this design stage, the designers are investigating specific materials and evaluating them for beauty, durability, price, structural and building envelope performance. Guidance providing elements' thermal and structural properties are required for the materials selection process and help in deciding the preliminary cost estimates. Moreover, advice to refine the design is required before solidifying the plans into action at this design stage. This chapter presents an efficient approach for estimating the R-values of common masonry cavity wall configurations in the form of simple design charts and R-value multipliers. Parameters such as the block density, thermal insulation value, and the types of ties and shelf angles are addressed in this study. The approach simultaneously provides the mechanical (the masonry compressive strength, fm′) and thermal (R-value) properties of different cavity wall configurations, allowing designers to obtain appropriate structural and thermal properties during a preliminary design development phase without using computer simulations.

To improve the sustainability of buildings, many regulations have been established in recent decades to enhance the energy efficiency of building envelopes, such as increasing their effective thermal resistance (R-value). To obtain a design with high R-values, efficient and accurate approaches (in terms of time and cost) are needed for R-value estimations. However, the R-value estimation is not a simple process due to the complexity of building envelope configurations, such as the presence of highly conductive structural components penetrating the insulating materials. Thermal bridging elements allow heat flow in multiple directions through several layers of envelope materials, thereby substantially complicating the R-value calculation (Barnes et al., 2013). Thermal bridges significantly reduce the R-value of a building envelope and therefore should be considered carefully when accurate R-value estimation is desired (Lawton et

al., 2010; Urban et al., 2011b; Ismaiel et al., 2021). Previous energy codes permitted R-value calculations to ignore major structural elements and other highly conductive elements that penetrate envelopes, provided that they comprised less than 2% of the total wall area (Straube, 2017). However, current energy codes require all elements to be considered in the R-value calculation (ISO, 2017b; NECB, 2017b). Therefore, the R-value calculations of envelopes require new methods and tools.

Steel veneer ties and shelf angles are among the largest sources of thermal bridging in masonry cavity walls (Roppel et al., 2012; Liu, 2019). The shape, size, and material of ties and shelf angles have been revolutionized to improve structural and thermal performance, which increases the complexity of wall configurations and consequently, their R-value calculations. Ties can be fastened to the face shell of structural backing instead of being inserted between blocks as traditional ties are typically used. Holes within the tie body are introduced to reduce the cross-sectional area, thus minimizing thermal conductance (Wilson, 2013). Intermittent structural support, which offsets shelf angles from backing systems (e.g., knife plates, brackets, and hollow structural section tubes), is being used to reduce the thermal bridging effect.

Other than thermal bridging elements, another factor that impacts the thermal performance and complicates R-value calculation is the thermal properties of the wall components (D'Aloisio et al., 2012; Kontoleon et al., 2013). In the early design phase, designers address various wall configurations with different material properties, mainly due to the trade-off between structural and thermal performance. For instance, high concrete block density increases the block's compressive strength while reducing the thermal resistance of the blocks (Harmathy and Allen, 1973). In another instance, the choice of the ties and shelf angles' material and shape has a significant impact on the effective thermal and structural behaviour of masonry walls. Changing the shape and material of blocks, ties, and shelf angles can affect the masonry walls' thermal resistance to a great extent (Adam Di Placido et al., 2019a; Bai et al., 2017). Many studies were performed to find material properties with shapes and elements designed to satisfy both the structural and thermal requirements of masonry wall components (Straube, 2017; Bai et al., 2017; Su et al., 2019). In the early design phase, it is challenging to determine the optimum wall components' material properties that meet both structural and thermal requirements.

The combinations of various materials' thermal properties, geometries of wall components, and three-dimensional heat transfer pose a challenge for determining the R-values of masonry walls (Kontoleon et al., 2013). There have been a few methods for estimating the R-value of a composite wall. The Isothermal Plane and Parallel Path methods are two commonly used techniques for calculating the thermal resistance. In the case of the Isothermal Plane method, the heat flows layer by layer through a building assembly made of multiple materials stacked together. Accordingly, the thermal resistance of a building assembly composed of uniform parallel layers (e.g., a wall) consists of the sum of the resistances of all layers in series (ASHRAE, 2017a). In the case of the Parallel Path method, the heat flows through different pathways and is assumed to be transferred by the straight parallel lines through a building assembly. The Parallel Path method is applied by assuming one-dimensional heat transfer perpendicular to the surfaces of the building element. This assumption is accurate when the materials on the same layer have close thermal conductivity values (i.e., wood frame walls) (ASHRAE, 2017b). Isothermal Plane and Parallel Path methods have insufficient accuracy to be applied to masonry cavity walls due to employing assumptions for simplification, such as ignoring the lateral heat transfer and assuming an even temperature distribution on the same plane (Theodosiou et al., 2021; McGowan and Desjarlais, 1995; Kosny and Christian, 1995). Therefore, the ASHRAE Fundamentals Handbook (ASHRAE, 1993a) generally recommended further experimental examinations of the required studied elements to reveal the actual thermal resistance value. Another commonly used approach is linear and point transmittance (Norris et al., 2012b; ASHRAE, 2017e). This approach involves modelling the required building assembly with and without the thermal anomalies to obtain its heat flow in both cases. Then, the difference in the heat flows is attributed to individual contributions of point or linear loads. To estimate the overall heat flow in a wall assembly, all the linear and point loads can be added with the clear field heat flow (the heat flow through the assembly without the thermal anomalies). The idea of linear transmittance has been widely used in practice in various forms (ISO, 2017c; Hershfield, 2022b). However, the linear and point transmittance methods depend mainly on computer numerical models, which consume time and are costly (ASHRAE, 2021c; Hydro, 2016b).

Analytical and numerical approaches were presented for computing R-values using the solution of two-dimensional steady-state heat transfer. Tawade (Tawade) introduced an analytical and numerical approach to resolve a two-dimensional steady-state heat conduction problem of a

rectangular plate. The results showed that rigorous analytical solutions are available only for a few simple boundary conditions, and these conditions do not seem to be favourable for complex boundaries. Another study that focused on the determination of parameters such as the thermal conductivity, the heat transfer coefficient, and the heat flux in 3-D steady-state heat conduction problems was investigated by Mohebbi et al. (Mohebbi and Sellier, 2016). The methodology of the analysis used a 3-D elliptic grid generation scheme to generate a grid over the conducting body by mapping the irregular 3-D physical domain onto the regular cuboid computational domain. The steady-state heat conduction equation was then solved using the finite difference method to determine the temperature at every grid node generated by the grid generation technique. The obtained results confirm that the proposed algorithm is accurate. However, the method is complicated in the case of analyzing objects that have various materials.

The inability of the existing methods to perform a quick, simple, and precise estimate of the R-values of masonry walls demands a new R-value estimation method, especially for the early design phases. This chapter aims to develop an efficient method for estimating the R-values of common concrete-block masonry walls and to facilitate their structural and thermal design. Design charts and R-value multipliers are presented to relate the key parameters (e.g., concrete block density and the shape and thermal properties of thermal bridging components) to the R-values of different wall configurations. By determining the configuration of a new wall that needs to be designed (e.g., concrete block density, mounting types and conductivity of the ties, and shelf angle types), the R-value can be estimated using the presented charts and/or the R-value multipliers. The R-value multipliers reflect the relative effects of changing the properties of key parameters (i.e., thermal conductivity and shapes of ties and shelf angles) on the R-values of common masonry wall configurations. By showing the effects of different parameters on the R-values, these intuitive charts and design multipliers can provide a guideline for improving the thermal envelope as well as facilitate the masonry walls' design development. This chapter is structured as follows: An introduction section is presented, followed by a methodology section in which descriptions of addressed configurations and parameters are discussed. Then, the results and discussion sections present the design charts and R-value multipliers. Finally, a comparison and a summary of the results are presented. For further clarification and validation purposes, illustrative examples are provided in the appendix section at the end of this chapter.

3.2. Methodology

This chapter focuses on two common types of concrete-block masonry cavity wall configurations: clear walls and intermediate floor intersections, as shown in **Figure** 3-1**.** A "clear wall" is defined as a planar area with regularly spaced structural components that are free of windows, doors, and other irregularities (Hershfield, 2022b). Clear wall configurations contain thermal bridges from uniformly distributed secondary structural components, which are necessary to withstand loads. Examples of components included in clear field configurations are brick ties, girts, or studs that support cladding (Barnes et al., 2013). These thermal bridges do not include the ones related to intersections of primary structures, such as intermediate floors intersecting exterior walls. The clear wall and the intermediate floor intersections make up the majority of the exterior wall surfaces. The exterior walls contribute significantly to the quantity of heat flow through the building envelope, about 21% of the heating load in residential buildings and 30% in commercial buildings results from flows through exterior walls (Energy, 2015), and hence were chosen to be investigated in this study.

The typical components of concrete masonry walls are concrete blocks, mortar, insulation boards, shelf angles, veneer ties, and air gaps as shown in **Figure** 3-1.

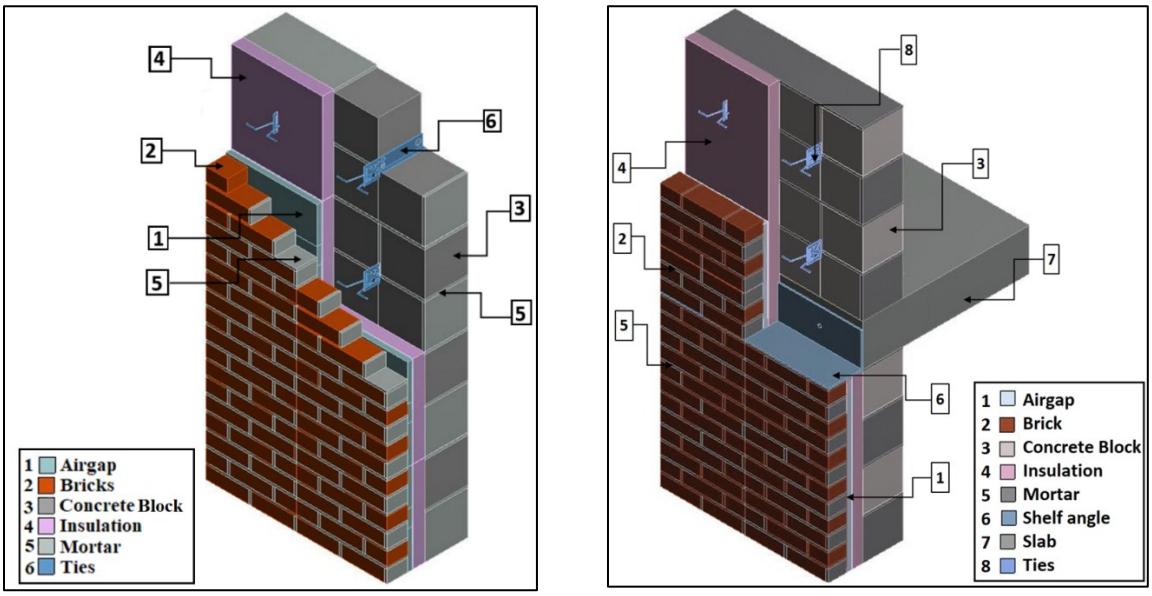

Figure 3-1: Two common concrete masonry cavity wall configurations and their typical components (clear wall and intermediate floor intersection respectively)

3.2.1. Configurations Types and Parameters

The clear wall configurations (labelled as "Type A" for brevity) addressed in this chapter consider four commonly used types of ties: solid and slotted block ties and solid and slotted on-surface ties (fastened on the block's surface) as shown in **Figure 3-2**. Intermediate floor intersection configurations (labelled as "Type B" for brevity) addressed in this chapter consider four commonly used shelf angles: directly attached shelf angle, shelf angles supported intermittently with bracket (Corporation, 2016), knife plate, and hollow structural section (HSS) as shown in **Figure 3-3**.

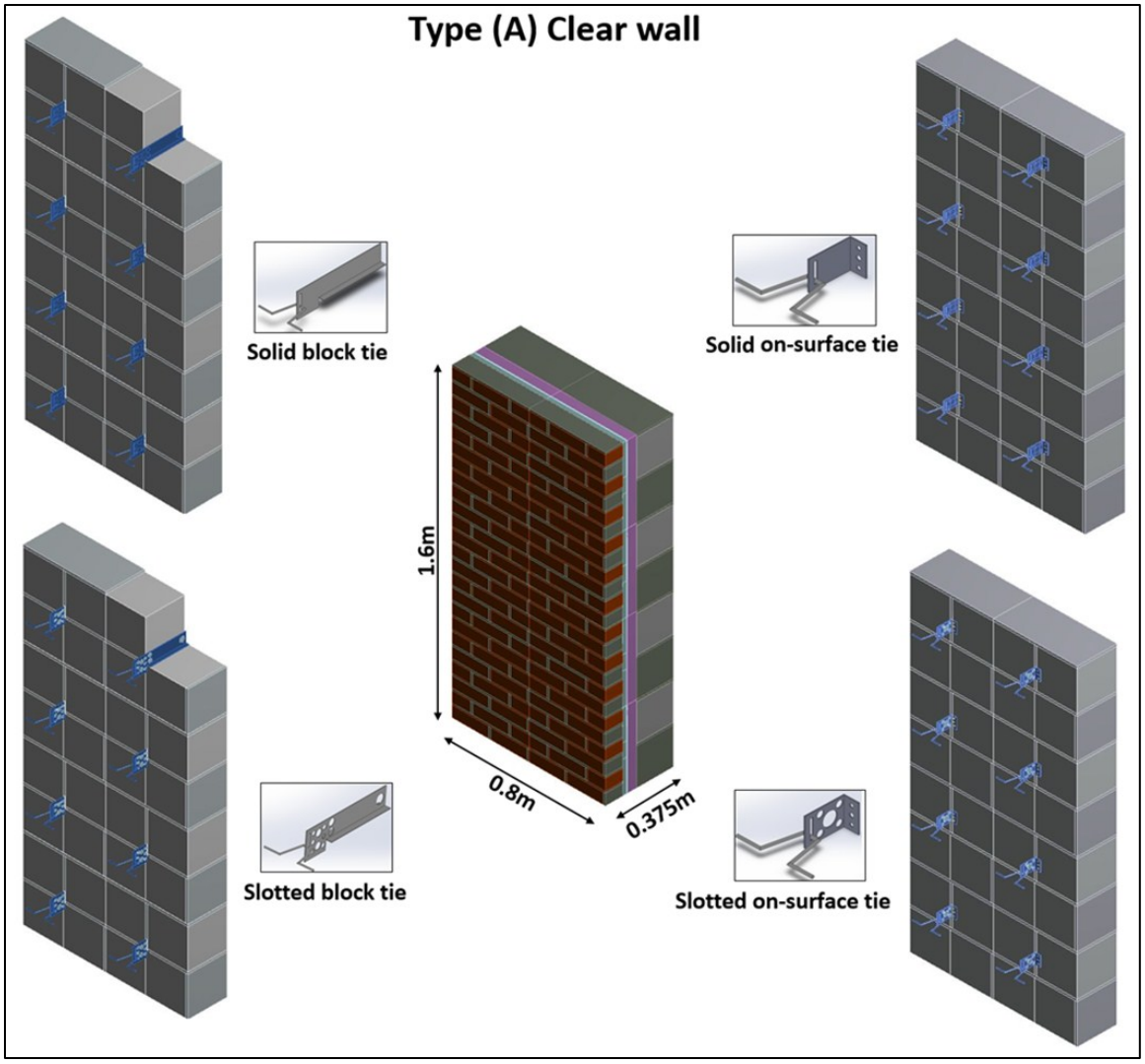

Figure 3-2: Type and dimensions of the 3D FE studied clear wall configurations (Type A)

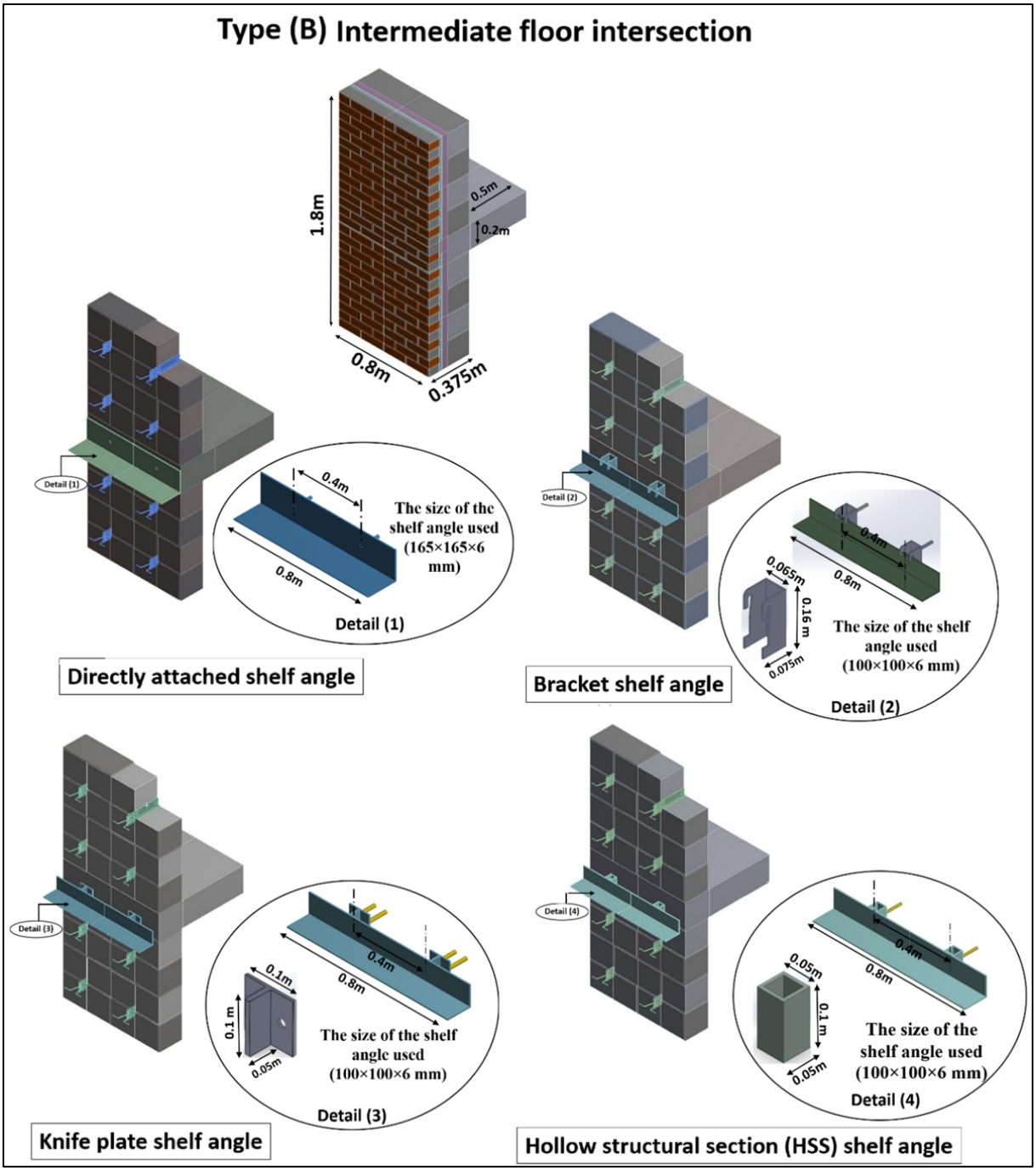

Figure 3-3: Type and dimensions of the 3D FE studied intermediate floor intersection configurations (Type B)

The appropriate dimensions and thermal and structural material properties for each component were selected from the ASHRAE Handbook and literature (Hershfield, 2022a; ASHRAE, 2021e; Hydro, 2016b). The component dimensions were obtained from the literature and the commonly used values in practice (Sturgeon et al., 2013a; Sturgeon et al., 2013b). The literature shows that the shape, size, and material of ties and shelf angles affect the R-value of masonry veneer walls and can reduce the thermal resistance of exterior insulation significantly (Finch et al., 2013a). Also, the block type and block unit density have a significant effect on the walls' thermal resistance (Concrete, 2007). Therefore, the investigated parameters of the wall configurations were selected based on the literature (del Coz Diaz et al., 2006; Norris et al., 2012a; Desjarlais and McGowan, 1997), and the parameter values used in this research were also obtained from the ASHRAE Handbook (ASHRAE, 2021e).

Table 3-1 presents the material properties common for all the studied configurations. An interior and exterior air film were considered in analysis for all the models with a nominal resistance of 0.11 and 0.03 m^2K/W, respectively. The thermal resistance of the air gap, 0.07 m^2K/W, between the wall thermal insulation and the brick veneer was obtained from the literature (Hershfield, 2022a; Roppel et al., 2011; Hydro, 2016b). To simplify the simulation process, the thermal insulation thickness was fixed in all of the addressed assemblies (50 mm). However, the insulation thermal conductivity varies to address different insulation R-values (R-15, R-20 and R-25). The insulation thickness is preferred to be reduced in practice to avoid designing thicker cross-sections and occupying larger spaces. However, increasing the insulation thickness may have an effect on the overall thermal resistance of the wall due to changing the ties' geometry and length. This effect was ignored in this research to facilitate the FE simulation process of different assemblies and parameters. Additionally, there are some modelling assumptions considered in this study; the model was analyzed at a steady state, and air leakage was not considered in addition, air spaces include convection and radiation. Only conduction was considered in air spaces (block cores, and air cavity between the insulation layer and the brick veneer layer). The intermediate floor thickness was considered 200 mm in all assemblies based on the common slab thickness used in practice. However, further work is required to address the impact of using different slab thicknesses on the overall walls' R-value.

Table 3-1: Common material thicknesses and properties used in the studied configurations

Component	Thickness (mm)	Conductivity (W/m K)
Standard concrete block Size Block 390X190X190 mm (Size block no.20) (Sturgeon et al., 2013a; Sturgeon et al., 2013b)	190	Varies
Concrete slab	200	1.8
Brick veneer	90	0.81
Cement mortar	10	1.2
Masonry ties (400mm on center)	14 gauge	Varies
Insulation	50	Varies

The studied parameters of the wall configurations include the shape and thermal conductivity of ties and shelf angles, the type and density of concrete blocks, and the thermal insulation value. In addition to the thermal properties, the present R-value design charts also consider the mechanical properties of different wall configurations. **Table 3-2** presents the parameters and thermal properties considered in this study. The charts combine the R-value of the assembly, the blocks' density, and the masonry compressive strength (f_m'). The masonry compressive strength was determined by using the unit strength approach, where f_m' is evaluated based on the masonry block's compressive strength and the mortar type. The f_m' values were obtained from the Canadian masonry standards (CSA S304 (2014)) which follow the unit strength approach for computing the masonry compressive strength. The density of the blocks was assumed to be 2100, 1800, 1550, 1380, and 1150 kg/m^3 respectively, and the compressive strength of units (f_b) was considered for each block type to be 35, 30, 20, 15, and 10 MPa respectively. The mortar used is S-type (clauses 5.1.3.3, 5.1.3.5.2, and D 6.1 Table 4 in the CSA S304 (Zorainy et al., 2018; 2014)).

Table 3-2: The parameters considered in each studied scheme

Schemes	Value range
Parameters considered for each configuration	Tie type, tie material, insulation R-value, concrete block density, concrete block type, shelf angle material, shelf angle type
Thermal insulation values in R, BTU/(ft^2·°F·hr) and in (m^{2}K/W)	R-15 (2.64), R-20 (3.52), R-25(4.40)

Block Density (kg/m^3) and corresponding conductivity (k=W/m K)	Hollowed: 2100 (k=1.17), 1800 (k=0.87), 1550 (k=0.66),1380 (k=0.6), 1150 (k=0.35) Fully grouted: 2100 (k=1.9), 1800 (k=1.13), 1550 (k=0.78), 1380 (k=0.6), 1150 (k=0.36)
Block Density (kg/m^3) and corresponding compressive strength (f_m') in MPa	For the grouted hollow units: 2100 and 1800 (f_m'=13.5),1550 (f_m'=10),1380 (f_m'=7.5) and 1150 (f_m'=5) For the hollow units: 2100 and 1800 (f_m'=17.5),1550 (f_m'=13),1380 (f_m'=10) and 1150 (f_m'=6.5)
Grout conditions	Hollow block wall, fully grouted wall
Tie type	Block solid tie, fastened on surface solid, block slotted tie, fastened on surface slotted (shown in **Figure 3-2**)
Tie thermal conductivity (k=W/m K)	Galvanized steel (k=50), stainless steel (k=17), glass fiber reinforced polymers GFRP (k=0.2)
Shelf angle type	Directly attached shelf angle, bracket shelf angle, knife plate, HSS shelf angle (shown in **Figure 3-3**)
Shelf angle materials (k=W/m K)	Galvanized steel(k=50), stainless steel (k=17)

360 configurations were studied for type A (4 types of ties x 3 tie materials x 3 insulation R-value x 2 grout conditions x 5 block densities = 360). In addition, 240 configurations were studied for type B (4 types of shelf angles x 2 shelf angle materials x 3 insulation R-value x 2 grout conditions x 5 block density = 240) to discuss different parameters and compare their effects on the thermal resistance of different wall configurations. By investigating many parameters and comparing assemblies, a relation between the effective thermal resistance of different masonry wall assemblies could be derived. Moreover, multipliers could be suggested to predict the effective thermal resistance of masonry wall assemblies in case of changing the tie, and shelf angle type and/or material without performing finite element thermal simulations.

3.2.2. Model Setup and Validation

To generate R-values of different wall configurations for producing the design charts and the R-value multipliers, the R-values of different wall configurations are estimated using a three-

dimensional finite-element modelling program, ANSYS (ANSYS, 2019). The Finite Element Method (FEM) has been validated and is widely considered to be a reliable numerical method for thermal analysis (Zieukiewicz and Taylor, 1991). ANSYS is regarded as a reliable FEM software for thermal analysis (Xie, 2012).

A steady-state heat transfer condition was considered. The governing equation, Fourier's law of heat conduction, is expressed in the differential form as follows (Ã–zisik et al., 1993);

$$\dot{Q}_n = -kA\frac{\partial T}{\partial n} \quad \textbf{(10)}$$

Where; n is the normal of the isothermal surface at the addressed point, $\dot{Q}_n$ is the rate of conduction heat flow at that point (W), k is the thermal conductivity of the material (W/m K), A is the heat conduction area normal to the addressed direction (m^2), $\frac{\partial T}{\partial n}$ is the temperature gradient.

The general heat conduction equation uses rectangular coordinates and considers a small rectangular element of length Δx, width Δy, and height Δz, as shown in **Figure 3-4**. Assume the density of the body is ρ and the specific heat is c. An energy balance on this element during a time interval Δt can be expressed as follows (Ã–zisik et al., 1993):

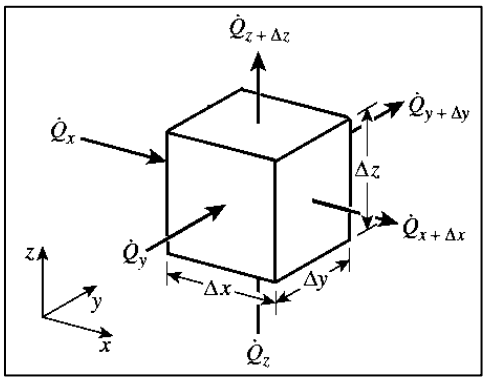

Figure 3-4:Three-dimensional heat conduction through a rectangular volume element

$$\dot{Q}_x + \dot{Q}_y + \dot{Q}_z - \dot{Q_{x+\Delta x}} - \dot{Q_{y+\Delta y}} - \dot{Q_{z+\Delta z}} + \dot{E_{generated}} = \frac{\Delta E_{element}}{\Delta t} \quad \textbf{(11)}$$

Where; $\dot{Q}_x, \dot{Q}_y and\ \dot{Q}_z$ are the rate of heat conduction at x, y, and z (rate of energy added), and $\dot{Q_{x+\Delta x}}, \dot{Q_{y+\Delta y}}\ and\ \dot{Q_{z+\Delta z}}$ are the rate of heat conduction at x+Δx, y+Δy and z+Δz (Rate of energy removed), $\dot{E_{generated}}$ is the rate of energy generation inside the element, and $\frac{\Delta E_{element}}{\Delta t}$ is the rate

of energy change within the element. Considering that the volume of the addressed element is expressed as follows;

$$V_{element} = \Delta x \Delta y \Delta z \quad \textbf{(12)}$$

The rate of the heat generation in the addressed element and the change in the energy content can be expressed as;

$$\Delta E_{element} = E_{t+\Delta t} - E_t = mc(T_{t+\Delta t} - T_t) = \rho c \Delta x \Delta y \Delta z \, (T_{t+\Delta t} - T_t) \quad \textbf{(13)}$$

$$\dot{E_{generated}} = \dot{e_{generated}} \quad V_{elemen} = \dot{e_{generated}} \Delta x \Delta y \Delta \boldsymbol{z} \quad \textbf{(14)}$$

By substituting equations 4 and 5 in equation 2 and dividing by the volume ($V_{element}$), the general energy balance equation is expressed as follows;

$$-\frac{1}{\Delta y \Delta z}\frac{\dot{Q_{x+\Delta x}} - \dot{Q_x}}{\Delta x} - \frac{1}{\Delta x \Delta z}\frac{\dot{Q_{y+\Delta y}} - \dot{Q_y}}{\Delta y} - \frac{1}{\Delta x \Delta y}\frac{\dot{Q_{z+\Delta z}} - \dot{Q_z}}{\Delta z} + \dot{e_{generated}} = \rho c \, \frac{T_{t+\Delta t} - T_t}{\Delta t} \quad \textbf{(15)}$$

By considering the heat transfer areas of the addressed element for heat conduction in the x, y, and z directions are $A_x = \Delta y \Delta z$, $A_y = \Delta x \Delta z$ and $A_z = \Delta y \Delta x$. And by taking the limit as Δx, Δy, Δz, and Δt tends to zero. The general heat conduction equation in rectangular coordinates. In the case of constant thermal conductivity is simplified to;

$$\frac{\partial^2 T}{\partial x^2} + \frac{\partial^2 T}{\partial y^2} + \frac{\partial^2 T}{\partial z^2} + \frac{\dot{e_{generated}}}{K} = \frac{1}{\alpha}\frac{\partial T}{\partial t} \quad \textbf{(16)}$$

where $\alpha = {}^{k}/_{\rho c}$ is the thermal diffusivity of the material. This equation could be reduced in our study to consider the steady-state condition with no heat generation (Laplace equation):

$$\frac{\partial^2 T}{\partial x^2} + \frac{\partial^2 T}{\partial y^2} + \frac{\partial^2 T}{\partial z^2} = 0 \quad \textbf{(17)}$$

Since the heat conduction equation does not involve any time derivatives in the steady conditions, the initial conditions are not required to be specified. However, three types of boundary conditions were considered in modelling; specified temperature, adiabatic boundary conditions, and interface boundary conditions. The specified temperatures were considered in the FE modelling to be constant at 21℃ and -18℃, for interior and exterior surfaces, respectively. While the remaining four sides of the wall were assumed to have adiabatic boundary conditions. Since the addressed walls are made up of layers of different materials, the solution of a heat transfer problem in such a medium requires the solution of the heat transfer problem in each layer. Therefore, the specification of the boundary conditions at each interface is required. The

boundary conditions at an interface were considered in the FE modelling based on the requirement that an interface cannot store any energy, and thus the heat flux on the two sides of an interface must be the same.

All FE models were analyzed at a steady-state thermal analysis, and air leakage was not considered. Contact resistance was not considered in the models because the most conductive contact surfaces between concrete and steel (between the shelf angle and the concrete slab), which are insignificantly present in the concrete-block masonry walls, and therefore the contact resistance has a minimum impact on the walls' thermal resistance (Roppel et al., 2011). The element used to simulate the wall components in the ANSYS modelling is SOLID70, given that its properties comply well with the configurations that need to be investigated. SOLID70 has a three-dimensional thermal conduction capability. The element has 8 nodes with a single degree of freedom – temperature – at each node. The element can be applied to a three-dimensional, steady state, or transient thermal analysis. Meshing was done by using ANSYS's advanced sizing feature. A mesh was generated that is sufficiently fine for each part of the model. This is a significant feature as some wall components (such as the ties) are relatively thin and need more elements and refined mesh, while the blocks, the brick veneer, and the insulation boards do not need the same size elements. A sequence of mesh convergence tests was conducted for a suitable balance between accuracy and computational time of clear wall and intermediate floor intersection assemblies. The convergence study on the mesh size was carried out by evaluating the variation of the heat flux versus the number of mesh nodes. It was found that the mesh size of 10 mm (which corresponds to 2,351,549 nodes for the clear wall models and 2,670,876 nodes for the intermediate floor models) is appropriate for the accuracy and model running time for all studied configurations. The RMS Error-values between the solution computed with a fine grid (i.e., 5 mm) and each solution computed with coarser grids have been reduced to an acceptable value of less than 10^{-4}, which is appropriate for the accuracy and model running time for all studied configurations. **Figure 3-5** shows the convergence of the average RMSE of the addressed configurations versus the number of nodes used in the mesh for the clear wall and the intermediate floor configuration, respectively.

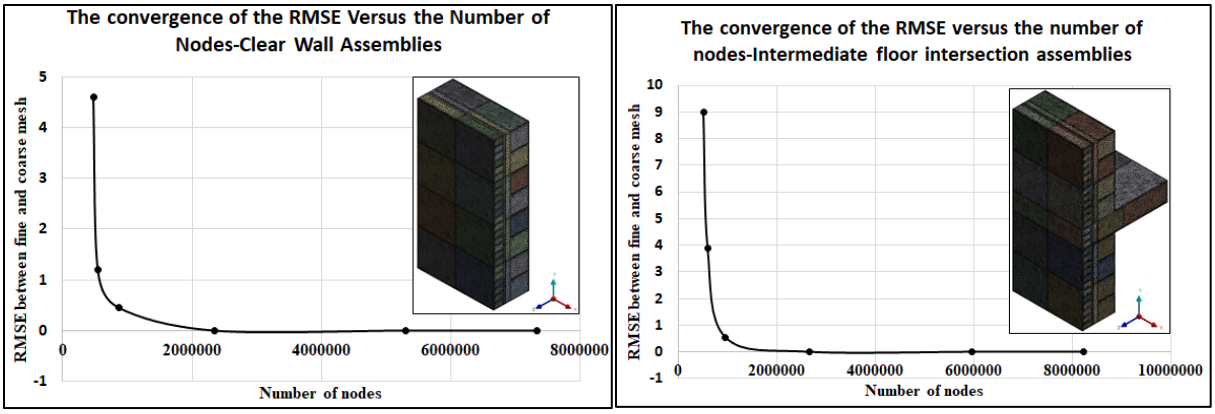

Figure 3-5: Convergence of the average RMSE of the addressed configurations versus the number of nodes used in the mesh for the clear wall and the intermediate floor configuration, respectively

For validating the modelling approach and the models, wall configurations presented in previous studies (Cui et al.; Norris et al., 2012b) were replicated using ANSYS and the simulation results were compared with the reported results. Results presented in the previous studies were obtained from three-dimensional finite element analysis and compared with experimental results obtained from guarded hotbox measurements and data provided in ISO Standard 10211 (ISO, 2017c). The validations addressed included five clear wall models with galvanized steel solid block ties in addition to five intermediate floor intersection wall models with directly attached galvanized steel shelf angles and solid galvanized block ties. All the models considered different insulation R-values (R-5, R-10, R-15, R-20, and R-25). When the results from the validation modeling and the literature were compared, the average differences were 6.8% for the clear wall and 7.13 % for the intermediate floor intersection assemblies.

From the results of the numerical modelling, an R-value was obtained for each addressed wall configuration using the overall heat transfer through the wall for defined internal and external environmental temperatures, as follows:

$$R=\Delta T/q \quad \textbf{(18)}$$

where R is the thermal resistance ($m^2 \cdot K/W$), q is the heat flux density in watts per area of the addressed wall in square meters (W/m^2) as predicted by the modelling, and ΔT is the difference in temperature between the inside and outside environment.

Design charts were constructed directly using the R-values of different studied wall configurations, and R-value multipliers were deduced from the R-values using an optimization technique (Deb, 2012). The following subsections explain the development of the design charts and R-value multipliers.

For validating the presented multipliers and suggested design approach, the measured data was randomly split into training (80% = 480 configuration) and validation (20% = 120 configuration) subsets, enabling validation (Berrar, 2019). While the training subset was used for design multiplier estimation, the validation subset was used to test the performance of the suggested multipliers on new data (validation data subset). The multipliers showed accuracy for both the validation and trained data sets, with an average coefficient of determination R^2 of 0.88, and RMSE of 0.9. A strong correlation between the measured and the predicted R-values was observed.

3.2.3. Design Charts and R-value Multipliers

To generate data for producing the R-value multipliers, the R-values of different wall configurations were estimated using a three-dimensional finite-element modelling program, ANSYS (Basiricò et al.), as stated earlier in subsection **(3.2.2)** and equation **(18)**. The R-value multipliers were deduced from the ANSYS results using an optimization technique (Deb, 2012). The optimization technique is a procedure that is executed iteratively by comparing various solutions until a satisfactory solution is achieved. The optimization objective is to minimize the Sum of Squared error (SSE) between the values obtained using the suggested R-value multipliers and the actual values obtained via ANSYS. **Figure** 3-6 shows a flow chart used for determining the R-value multipliers of the studied groups.

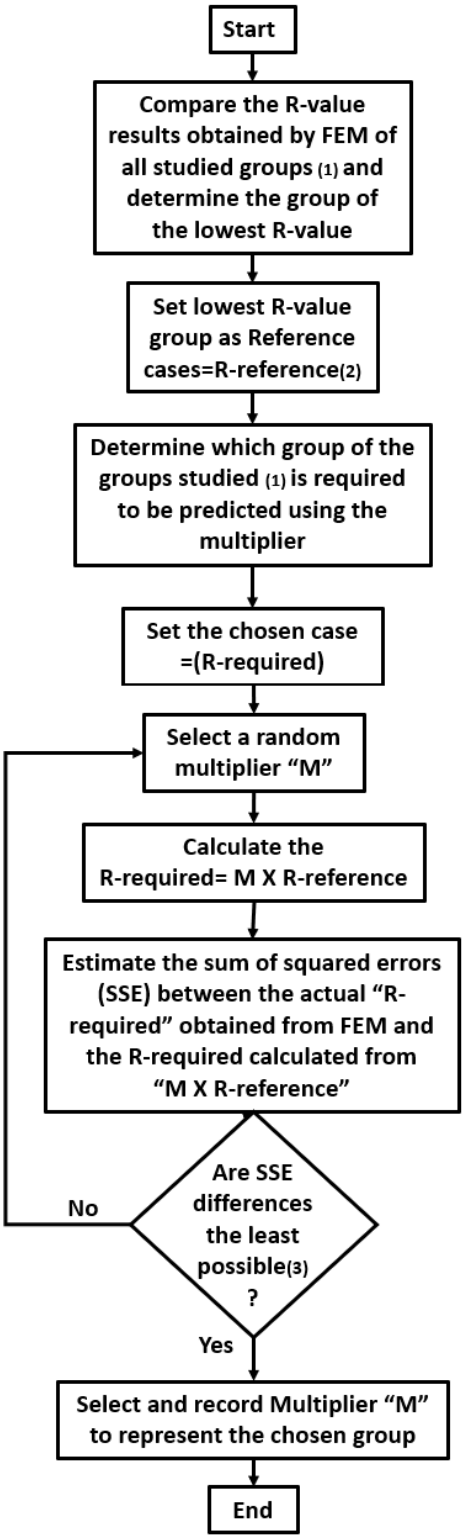

(1) The studied groups are as follows. For clear wall configurations; solid block tie, slotted block tie, solid on surface tie, and slotted on surface tie. All configurations were simulated using three tie materials (galvanized steel, stainless steel and glass fiber reinforced polymers GFRP). There was a total of 12 clear wall groups studied (3 tie types and 4 tie materials). Each group of the 12 studied clear wall groups consists of 30 different configurations addressing different parameters such as the insulation R-value, the block density and the block type (see Table **3-2**). For intermediate

intersection configurations; directly attached shelf angle, bracket shelf angle, knife plate, and hollow structural section (HSS). All intermediate floor intersection configurations were simulated using two shelf angle materials (galvanized steel and stainless steel). There was a total of 8 intermediate floor intersection groups studied (4 shelf angle types and 2 shelf angle materials). Each group of the 8 studied intermediate floor intersection consists of 30 different configurations addressing different parameters as the insulation R-value, the block density and the block type (see Table **3-2**).

(2) The reference case "R-reference" are: for the clear wall assemblies: galvanized steel solid block tie and for the intermediate floor intersection: galvanized steel directly attached shelf angle

(3) Optimization technique is executed iteratively by comparing various solutions of the multiplier value (M) until a satisfactory solution is achieved that will accurately represent all variables studied in each case; each studied case has variables such as block density, insulation board R-value and block type "fully grouted blocks or hollow blocks". Therefore, the multipliers are expected to satisfy all variables addressed for each studied group with the least possible error when compared to the actual values obtained by the finite element analysis.

Figure 3-6: A flowchart used for determining the R-value multipliers of the studied groups. Note: these steps are repeated for all the studied groups to obtain the required multiplier for each group

The minimization of an objective function involving unknown parameters in which the variables may be restricted by constraints is one of the core components of computational mathematics (Strobel, 1989). Optimization is concerned with the minimization of an objective function, i.e., F(x). Minimization will take place with respect to an n-vector, x, of real unknowns. The smallest value of (F) gives its minimum, while any corresponding values of x are a minimizer. The optimization objective in this study is to minimize the residual sum of squares (the sum of squared errors of prediction). The residual sum of squares essentially measures the variation of modelling errors. Generally, a lower residual sum of squares indicates that the regression model (suggested multiplier) can better explain the data, while a higher residual sum of squares indicates that the model poorly explains the data. Therefore, the residual sum of squares is the objective function that is required to be minimized:

$$F(x) = \sum_{i=1}^{n} \left(X_i - \hat{X_i}\right)^2 \quad \textbf{(19)}$$

where X_i is the measured R-value as estimated by the FEM (R-required) and $\hat{X_i}$ is the predicted R-value using the multipliers and could be represented as (M*R-reference). Unconstrained minimization is considered in our case, where we aim to minimize F(x). Minimize F(x) where x

ϵR^n and the objective function F: $R^n \rightarrow R$. The F(x) is at least twice continuously differentiable ($F \in C^2$). Optimality conditions for unconstrained minimization should be addressed. First, a local minimizer of F(x) is required to be obtained (multiplier M). The following two results provide first- and second-order necessary optimality conditions, respectively (Gould, 2006). In the first condition, suppose that $F \epsilon C^1$, and that M is the local minimizer of F(x), then g(M)=0. In the second condition, suppose that $F \epsilon C^2$, and that M is the local minimizer of F(x), then g(M)=0 and H(M) is positive semi-definite, that is $\langle s, H(M)s \rangle \geq 0$ for all $s \epsilon R^n$ Where g(M) is the gradient function, H(M) is the Hessian (matrix) and s is the step. Point M is considered the local minimizer in case the above-mentioned conditions were satisfied. Solver (Excel, 2021) was used to find an optimal (minimum) value for the objective function. Solver works with a group of variables, called decision variables or simply variable numbers that are used in computing the formulas for the objective function and constraint. The solver adjusts the values in the decision variable to produce the required result for the objective function. The GRG "Generalized Reduced Gradient" algorithm was chosen to be the solving method. This solver method focuses on the gradient or slope of the objective function as the decision variable changes and determines that it has reached an optimum solution when the partial derivatives equal zero.

The multipliers of the clear walls (Type A) can be used for the intermediate floor intersection (Type B) to account for the changes of tie type and material in the configurations studied for Type B (that will be explained later using **Table 3-9** in Section **3.4**). The R-value multipliers are applicable for predicting the effect of changing the key parameters (i.e., thermal conductivity and shapes of ties and shelf angles) on the R-values of many common masonry wall configurations. By knowing the concrete block density, the mounting types, and conductivity of the ties and shelf angle, the R-value can be estimated using the presented multipliers. Moreover, these R-

value multipliers are not limited to the groups studied in this chapter; the suggested R-value multipliers could be applied to predict the effect of changing the addressed parameters –such as the materials and shape of ties and shelf angles- on the effective walls' R-values for common masonry wall configurations regardless of the dimensions or the material properties of other wall components.

$$R_{new} = R_{Ref} \frac{M_{new}}{M_{Ref}} \quad \textbf{(20)}$$

R_{new} is the required unknown R-value, R_{Ref} is a known R-value (reference), either from the design charts presented in this chapter or calculated before (hand calculations, computer simulations or from literature in other studies), M_{new} is an R-value multiplier that corresponds to the required unknown case (R_{new}), M_{Ref} is an R-value multiplier that corresponds to the known case (reference). An illustrative example is presented in section 3.4 for intermediate floor intersection configurations, and further examples are provided in the appendix.

3.3. Results Discussion

The results obtained for the design charts and the R-value multipliers will be presented with the demonstration of their applications. The results and demonstration for the clear walls (Type A) will be presented first, followed by that of the intermediate floor intersection (Type B).

3.3.1. Clear Walls (Type A)

The R-value, density, and masonry compressive strength for both grouted and hollow clear wall configurations are shown in **Figure** 3-7. This chart presents only the studied group with galvanized steel solid block ties. The studied group shown in **Figure** 3-7 was found to have the lowest R-values compared to the others, such as stainless steel and glass fibre reinforced polymer (GFRP) ties. The solid block tie group was considered as the reference group for Type A models.

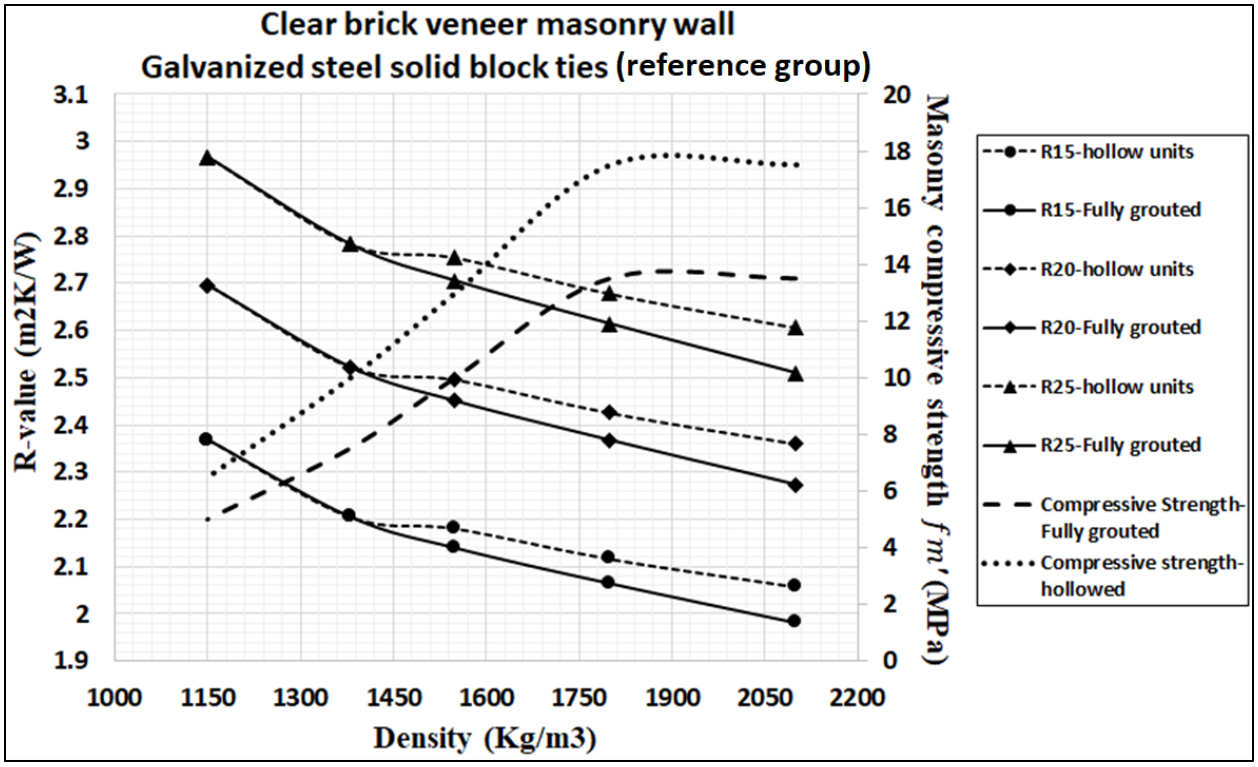

Figure 3-7: Masonry walls' R-value, density and f_m' for both grouted and hollow units clear wall configurations with different insulation and using galvanized steel solid block tie

The four types of ties used in clear wall configurations (Type A) were compared to the solid block galvanized steel tie (reference group) to find the improvement percentage of the walls' effective R-values. **Table 3-3** shows the percentage ranges for the R-value improvements for each group. The average, minimum and maximum percentages represent the percentage of R-value improvements for each group if compared to the chosen reference group based on the number of models studied for configurations type A (360 configurations studied).

Table 3-3: Percentages of R-value improvements for each group when compared to the solid block galvanized steel tie

		Solid block tie	Slotted block tie	Solid on surface tie	Slotted on surface tie
Galvanized steel	**Average**	Reference	7.75	16.37	25.13
	Maximum		9.85	21.00	30.51
	Minimum		5.86	12.79	20.46
Stainless steel	**Average**	20.59	28.79	33.70	42.68
	Maximum	27.07	38.32	43.64	57.19
	Minimum	15.83	21.05	23.54	31.28
GFRP	**Average**	60.07	59.71	64.74	64.49
	Maximum	84.96	84.48	90.57	90.18
	Minimum	40.40	40.22	44.35	44.17

By comparing all configurations' R-value results with the reference group, multipliers were obtained to represent the R-value of each studied group with respect to the reference group, as shown in **Table 3-4** and explained earlier in section (**3.2.3)**. The R-values for the other studied clear wall groups with different types and materials of ties can be estimated by constructing a graph (similar to **Figure 3-7)** for each studied group using the R-value multipliers presented in **Table 3-4**.

Table 3-4: R-values multipliers for clear wall configurations compared to the reference group

Schemes / **Tie material**	Effective R-values of the below groups could be estimated by multiply R-values obtained from **Figure 3-7** by the following multipliers			
	Block tie solid	**Block tie slotted**	**On surface tie Solid**	**On surface tie slotted**
Galvanized steel	1 (reference)	1.06	1.13	1.20
Stainless steel	1.16	1.21	1.23	1.31
GFRP	1.40	1.40	1.44	1.44

Example for illustration, considering a clear wall with a slotted fastened on surface stainless steel ties with insulation R-value of R-20, hollow block with density 1600 Kg/m^3; using **Figure 3-7,** the masonry compressive strength (f_m') is 14 MPa, while the effective R-value is 2.49 m^2K/W representing the reference case (from **Figure 3-7**) multiplied by 1.31 (from **Table 3-4)**. Therefore, the effective R-value for the stated case is 3.26 m^2K/W (Note that the FEM modelling result for this case is 3.4 m^2K/W). The difference between the simulation and the R-value multiplier results is 4.11%. Further examples are provided in appendix section.

The configurations with the highest insulation board R-values (R-25) showed the highest improvements in R-value percentages due to tie type when compared to the solid galvanized block tie configurations. The lowest improvement percentages were found in the configurations with the lowest insulation R-values (R-15). Therefore, it was concluded that the advancements in shape and material of the ties are more effective in configurations with higher insulation R-values. In addition, results show that, in the case of GFRP, the presence of slots and using different tie types did not show any significant effect on the overall R-values due to their low conductivity.

Regarding the block density, on average, the reduction of the concrete blocks' density by 10% showed an improvement in the effective R-value by 2.23% for clear wall assemblies. There is no significant change in the thermal resistance of the hollowed and fully grouted blocks for block densities lower than 1400 kg/m^3. **Table 3-5** shows the average R-value increase percentages that correspond to an average decrease in block density by 10% for each of the studied groups. **Table 3-5** shows that using galvanized steel ties is the most sensitive case to the block's density reduction. The galvanized steel ties showed the highest increase in the effective R-value by about 3.21% in the case of grouted configurations and 2.55% in the case of hollow block configurations, due to the reduction in the blocks' density by 10%. The lowest increase was noticed for the GFRP ties by 1.41% in the case of hollow block configurations and 1.7% in the case of grouted configurations. On average, using insulation boards with a low R-value (R-15) causes the most sensitivity to block density reduction. **Table 3-5** shows that the increased percentage in R-value that corresponds to an average of 10% decrease in the concrete block density by using R-15, R-20, and R-25, was 2.45%, 2.17%, and 2.07%, respectively. Therefore, it is concluded that the higher the conductivity of the ties, the more sensitive the R-value will be

to the reduction of concrete block density and thermal insulation. In addition, the lower the insulation R-value used, the more sensitive the total walls' R-value will be to concrete block density reduction. Also, using solid ties is more sensitive to block density reduction than using slotted ties. The fastened on-surface ties also showed greater sensitivity to the density reduction when compared to the block tie. Therefore, the highest thermal insulation benefit in the case of using lightweight concrete blocks could be achieved using solid ties with a high thermal conductivity value, fastened on the block's surface.

Table 3-5: Average range increase percentage in effective R-value that corresponds to an average of 10% decrease in the concrete block density

Insulation	Block type	Hollow blocks			Grouted blocks			Average
	Scheme\Tie material	Galvanized steel	Stainless steel	GFRP	Galvanized steel	Stainless steel	GFRP	
R-15	Block tie solid	2.58	2.32	1.74	3.28	2.87	2.09	**2.48**
	Block tie slotted	2.44	2.15	1.74	3.08	2.65	2.09	**2.36**
	On surface tie Solid	3.03	2.28	1.73	3.78	2.78	2.08	**2.61**
	On surface tie slotted	2.60	2.04	1.73	3.20	2.47	2.08	**2.35**
R-20	Block tie solid	2.44	2.10	1.37	3.13	2.62	1.64	**2.22**
	Block tie slotted	2.27	1.90	1.37	2.89	2.35	1.65	**2.07**
	On surface tie Solid	2.94	2.03	1.36	3.68	2.49	1.63	**2.36**
	On surface tie slotted	2.42	1.73	1.36	2.99	2.11	1.64	**2.04**
R-25	Block tie solid	2.37	3.42	1.13	3.07	2.50	1.36	**2.31**
	Block tie slotted	2.19	1.76	1.13	2.82	2.19	1.36	**1.91**
	On surface tie Solid	2.94	1.90	1.12	3.68	2.33	1.34	**2.22**
	On surface tie slotted	2.34	1.55	1.12	2.90	1.89	1.35	**1.86**
Average		**2.55**	**2.10**	**1.41**	**3.21**	**2.44**	**1.69**	**2.23**

Note: All the improvement R-value percentages represent an average range addressed for each configuration with a maximum block density of 2100 Kg/m^{3}and minimum block density of 1150 Kg/m^3

3.3.2. Intermediate Floor Intersection (Type B)

The thermal resistance of intermediate floor intersection configurations was obtained with the following parameters: insulation R-value, block type, shelf angle type, and material. All configurations were addressed using solid block ties only. **Figure** 3-8 shows the overall R-value, density, and masonry compressive strength for grouted and un-grouted directly attached galvanized steel shelf angles and solid block tie configurations. When compared to the bracket, knife plate, and HSS groups, which were also studied, the group shown in **Figure** 3-8 has the lowest thermal resistance values.

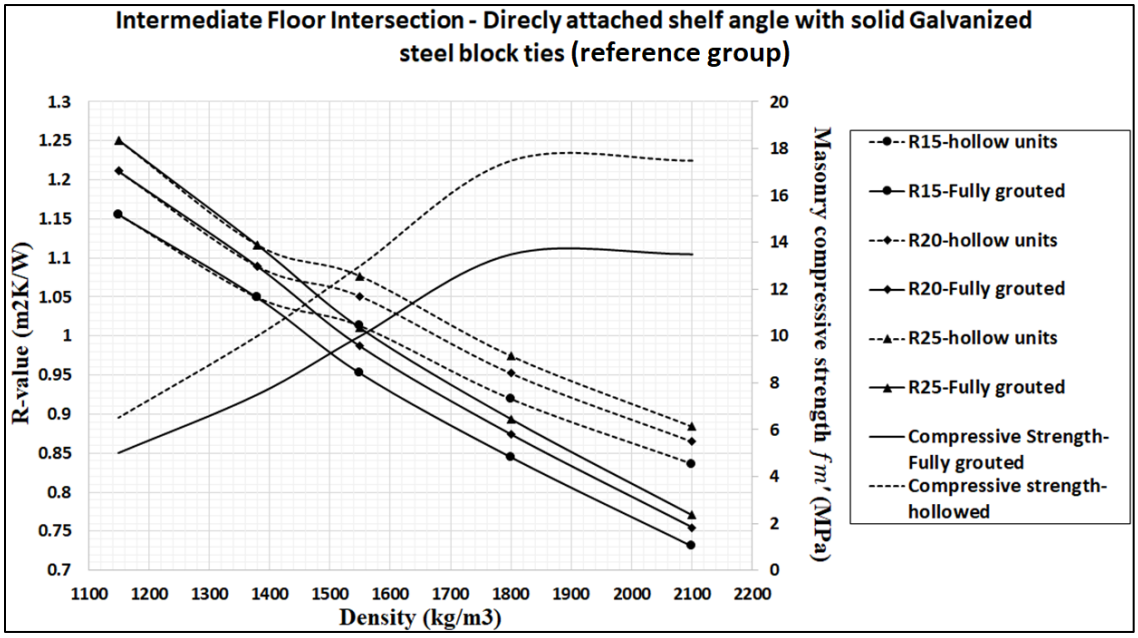

Figure 3-8: R-value, block density, and f_m' for both grouted and hollow units (un-grouted) intermediate floor intersections with different insulation and using galvanized steel solid block

A The four types of shelf angles studied (directly attached large shelf angle, bracket, knife plate, and HSS shelf angle) were compared to the directly attached large galvanized steel shelf angle to find the average improvement range in the effective R-values. **Table 3-6** shows the percentage ranges for the R-value improvements.

Table 3-6: Percentages of R-values improvements for each group when compared to the directly attached galvanized steel shelf angle

		Directly attached	Bracket	Knife plate	Hollow tube section
Galvanized steel	**Average**	Reference	18.11	28.11	32.34
	Maximum		44.53	61.21	66.56

	Minimum		5.86	10.01	13.54
Stainless steel	**Average**	29.72	47.09	63.12	58.32
	Maximum	41.45	85.58	100	100
	Minimum	23.13	30.44	37.09	33.69

By comparing all configurations' R-value results (Type B) with the reference group shown in **Figure** 3-8, R-value multipliers were obtained to represent the R-value of each group with respect to the reference group as shown in **Table 3-7.** It is possible to estimate the R-values for other studied intermediate floor intersection configurations with different shelf angle types and materials by constructing a graph similar to **Figure** 3-8 using the R-value multipliers presented in **Table 3-7.** In addition, the R-values of different intermediate floor intersection configurations and different tie types could be predicted by using both the R-value multipliers together as presented in **Table 3-4** and **Table 3-7** (Section 3.4**)** presents a table with both R-value multipliers for different groups). In addition, examples combining R-value multipliers obtained from **Table 3-4** and **Table 3-7** are presented in Section 3.4 and appendix section for illustration.

Table 3-7: R-value multipliers for intermediate floor intersection configurations with different shelf angle types and materials (all configurations have solid galvanized steel block ties)

Schemes / **Shelf angle** / **Material**	Effective R-values of the below groups could be estimated by multiply R-values obtained from **Figure** 3-8 by the following multipliers			
	Directly attached large shelf angle	**Bracket shelf angle**	**Knife plate shelf angle**	**HSS shelf angle**
Galvanized steel	1 (reference)	1.06	1.10	1.14
Stainless steel	1.246	1.30	1.41	1.37

For all cases, the configurations with the highest insulation board R-values (R-25) showed the highest improvement percentage range, similar to the clear wall configurations. The lowest improvement percentages were found in the configurations with the lowest insulation R-values (R-15). Therefore, it was concluded that the shape and material of the shelf angle are more effective in configurations with higher insulation R-values.

The effect of the block density was also studied in cases of intermediate floor intersection configurations. **Table 3-8** shows the average effective R-value increase percentages that correspond to an average decrease in block density by 10% for each of the studied groups. On

average, reducing the concrete block density by 10% showed an improvement in the effective R-value for the intermediate floor configurations by 3.5%. Configurations with an expected lower effective thermal resistance are more sensitive to the concrete block density. **Table 3-8** shows that cases using a directly attached galvanized steel shelf angle are the most sensitive to the block density reduction. In addition, cases using a galvanized steel shelf angle showed higher sensitivity to the concrete block density than those using stainless steel shelf angles. The grouted blocks also showed a higher improvement when compared to the hollowed blocks. The galvanized steel directly attached shelf angle showed the highest increase of the effective R-value by about 9.23% in the case of grouted configurations and 6.53% in the case of hollow block configurations, due to a 10% reduction in the block density by 10%. The lowest increase was noticed for the stainless-steel knife plate shelf angle, by 1.46% in the case of hollow block configurations and 1.97% in the case of grouted configurations. In addition, the increased percentage in effective R-value that corresponds to an average of 10% decrease in the concrete block density by using R-15, R-20, and R-25 was 3.5%, 3.49%, and 3.47%, respectively. Therefore, it is concluded that the higher the conductivity of the shelf angles, the more sensitive the R-value will be to concrete block density reduction. In addition, the grouted concrete blocks are more sensitive than the hollowed blocks to concrete block density reduction.

Table 3-8: Average increase percentage in effective R-value that corresponds to an average of 10% decrease in the concrete block's density for the intermediate floor intersection configurations

Insulation	Block type	Hollow blocks		Grouted blocks		
	Scheme\Shelf angle material	Galvanized steel	Stainless steel	Galvanized steel	Stainless steel	Average
R-15	**Directly attached**	6.08	4.75	8.72	6.62	**6.54**
	Bracket	3.95	3.00	4.56	3.53	**3.76**
	Knife plate	1.63	1.60	2.22	2.13	**1.90**
	HSS	1.68	1.63	2.28	2.18	**1.94**
R-20	**Directly attached**	6.34	4.98	9.02	6.88	**6.80**
	Bracket	3.72	2.68	4.32	3.20	**3.48**
	Knife plate	1.55	1.51	2.13	2.02	**1.80**
	HSS	1.60	1.54	2.20	2.07	**1.85**
R-25	**Directly attached**	6.53	5.17	9.23	7.07	**7.00**
	Bracket	3.59	2.49	4.19	3.00	**3.31**
	Knife plate	1.51	1.46	2.08	1.97	**1.75**
	HSS	1.56	1.49	2.15	2.02	**1.81**
Average		**3.31**	**2.69**	**4.43**	**3.56**	**3.50**

Note: All the R-value improvement percentages represent an average range addressed for each configuration with a maximum block density of 2100 Kg/m^3 and minimum block density of 1150 Kg/m^3

3.4. Summary of Results

The R-value multipliers and the relations obtained by comparing all the addressed groups to the reference groups considered (in our case, the solid steel galvanized block tie in the case of clear wall configurations and galvanized steel directly attached shelf angle in the case of the intermediate slab) are summarized in **Table 3-9.** The accuracy of using the presented approach was investigated by computing the coefficient of determination R^2 for the clear wall configurations and the floor intersection assemblies, which is equal to 0.94 and 0.71, respectively. These R-value multipliers are not limited to the cases studied in this chapter; they could be used for preliminary estimation of the R-value changes that may occur due to changing the type and material of ties and shelf angles of an addressed masonry wall. An illustrative example is presented in this section for intermediate floor intersection configurations, and further examples are provided in the appendix section.

Table 3-9: R-value multipliers summary and relations obtained by comparing all the addressed configurations

Shelf angle type / Ties' type		Clear wall	Shelf angle type for the intermediate slab configurations							
			Directly attached shelf angle		Bracket Shelf angle		Knife plate		HSS [1]	
			GS	SS	GS	SS	GS	SS	GS	SS
Block tie Solid	**GS [2]**	1*	1**	1.26	1.07	1.32	1.10	1.41	1.14	1.37
	SS [2]	1.16	1.16	1.46	1.24	1.53	1.27	1.63	1.32	1.59
	GFRP [2]	1.40	1.40	1.76	1.50	1.85	1.54	1.97	1.60	1.92
Block tie slotted	**GS**	1.06	1.06	1.33	1.13	1.40	1.16	1.49	1.21	1.45
	SS	1.21	1.21	1.52	1.29	1.40	1.33	1.71	1.38	1.66
	GFRP	1.40	1.40	1.76	1.50	1.85	1.54	1.97	1.60	1.92
On surface tie solid	**GS**	1.13	1.13	1.42	1.21	1.49	1.24	1.59	1.29	1.55
	SS	1.24	1.24	1.56	1.32	1.63	1.36	1.74	1.41	1.69
	GFRP	1.44	1.44	1.81	1.54	1.90	1.58	2.03	1.64	1.97
On surface Slotted	**GS**	1.20	1.20	1.52	1.29	1.59	1.32	1.70	1.37	1.65
	SS	1.31	1.31	1.65	1.40	1.73	1.44	1.85	1.50	1.80
	GFRP	1.44	1.44	1.81	1.54	1.90	1.58	2.03	1.64	1.97

*Reference group to all configurations of the lowest thermal resistance value - type A (**Figure 3-7**).

Reference group to all configurations of the lowest thermal resistance value - type B **(Figure 3-8).

[1]HSS: hollow structural section shelf angle.
[2]GS: Galvanized steel, SS: stainless steel and GFRP: Glass-fiber reinforced polymers.

FEM allows the modelling of complex geometrical and irregular shapes. The designer can use FEM to determine how critical factors might affect the overall thermal performance and the reasons for any deficiency in the thermal performance of the studied elements. Although the cost of simulating a standard FEA analysis is relatively high (ranging between 1,500-4,500 USD professional fees per configuration or 80-120 USD/hour based on the authors' knowledge and survey among professional organizations), FEM can be adapted to meet certain specifications for accuracy to decrease the need for experimental tests in the design process. Creating FE models is usually a costly and time-consuming process (McGowan and Desjarlais, 1995). Using the suggested multipliers and design charts, the designer can obtain approximate but sufficiently accurate R-values of different designs and materials without the need to simulate FEM or experimental testing. Moreover, the immense time required to simulate a detailed FEM model and the associated costs could be avoided with an expected accuracy of up to 6%. This study provides the designers with the expected thermal and structural behaviour of common masonry walls in the early design stage, where many design options need to be explored. The presence of design charts and multipliers simplifies the design of common masonry walls by considering numerous variables and material properties.

Illustrative Example:

Calculate the effective R-value and expected masonry compressive strength of an intermediate floor intersection assembly with the following details: (1) the ties are solid block ties; (2) the tie material is galvanized steel; (3) the insulation R-value is R-15; (4) hollowed blocks weigh1380 Kg/m^3; (5) the shelf angle type is knife plate stainless steel shelf angle (assuming the required assembly dimensions are the same as the addressed configurations Type B).

Solution

Step (1): The effective R-value and masonry compressive strength of the reference group (directly attached galvanized steel shelf angle configurations with galvanized steel solid block tie) are determined using **Figure** 3-8**.**

- The masonry compressive strength (fm′) is 9.7 MPa,
- The effective R-value is 1.05 m^2K/W, representing the reference case of solid galvanized steel block tie type and galvanized steel directly attached shelf angle.

Step (2): From **Table 3-7,** obtain the R-value multiplier that corresponds to the required case (block galvanized steel solid tie with knife plate stainless steel shelf angle). The R-value multiplier was found to be 1.41.

Step (3): Transfer the R-value obtained from **Figure** 3-8 to the required addressed case. This can be done by multiplying the reference R-value obtained from step (1) by the R-value multiplier obtained from step (2). Therefore, the effective R-value for the required case is estimated to be (1.05 X 1.41) = 1.4805 m^2K/W. Therefore, the expected masonry compressive strength is 9.7 MPa and the effective R-value is 1.48 m^2K/W.

The ANSYS simulation effective R-value result for the required case is 1.51 m^2K/W using finite element simulations. Therefore, the error percentage between the two results is 1.3%.

If the ties are changed from solid block galvanized steel to slotted stainless steel block ties for the same case;

Step (1): The effective R-value and masonry compressive strength of the reference group (directly attached galvanized steel shelf angle configurations with galvanized steel solid block tie) are determined using **Figure** 3-8**.**

- The masonry compressive strength (fm′) is 9.7 MPa,
- The effective R-value is 1.05 m^2K/W, representing the reference case of solid galvanized steel block tie type and galvanized steel directly attached shelf angle.

Step (2): From **Table 3-9,** obtain the R-value multiplier that corresponds to the required case (slotted stainless-steel block tie with knife plate stainless steel shelf angle). The R-value multiplier was found to be 1.71.

Step (3): Transfer the R-value obtained from **Figure** 3-8 to the required addressed case. This can be done by multiplying the reference R-value obtained from step (1) by the R-value multiplier obtained from step (2). Therefore, the effective R-value for the required case is estimated to be (1.05 X 1.71) = 1.8 m^2K/W. Therefore, the expected masonry compressive strength is 9.7 MPa and the effective R-value is 1.8 m^2K/W.

For validation, this example was simulated using ANSYS workbench. The corresponding effective R-value for the new required case is 1.9 m^2K/W using finite element simulations. Therefore, the error percentage between the two results is 5.26%.

The accuracy of using the presented approach is expected to be within the range of the presented coefficient of determination R^2 for the clear wall configurations and the floor intersection assemblies, which is equal to 0.94 and 0.71, respectively. These R-value multipliers are not limited to the cases studied in this chapter; they could be used for preliminary estimation of the R-value changes that may occur due to changing the type and material of ties and shelf angles of an addressed masonry wall.

3.5. Conclusion

This study presents design charts and R-value multipliers that aid designers in estimating and choosing the appropriate structural and thermal properties of common concrete masonry walls during the preliminary design phase without using computer simulations. In addition, a discussion and comparison of the impact of different parameters on the thermal resistance of masonry walls are addressed. The conclusion of this study is summarized as follows:

Regarding clear cavity wall configurations, the lowest thermal resistance values were for the galvanized steel solid block ties (reference group). The reference group was compared to other groups using galvanized steel but with different tie types (slotted block tie, solid fastened on surface tie, and slotted fastened on surface tie). The thermal resistance values of these groups were higher than the reference group by 7.75%, 16.37%, and 25.13%, respectively. Stainless steel was also compared to the galvanized steel solid block ties group. A significant improvement in the R-values was observed. On average, the R-value exceeds the reference group by 20.59%, 28.79%, 33.70%, and 42.68% for solid block ties, slotted block ties, fastened on surface solid ties, and fastened on surface slotted ties, respectively, in the case of using stainless steel ties. Glass fibre reinforced polymer (GFRP) tie material showed a remarkable increase in the R-value when compared to the reference group. The R-values increased by 60% in the case of block ties and 64% in the case of fastened on surface ties. The presence of slots did not show any significant effect on the R-values in the case of GFRP ties due to their low conductivity.

Regarding the intermediate floor configurations, four types of shelf angles were studied (directly attached large angle, bracket, knife plate, and hollow structural section HSS) and two shelf angle materials were considered; galvanized steel and stainless steel. Results showed that the galvanized steel for the directly attached shelf angle with solid galvanized steel block ties has the lowest R-value. The stainless steel directly attached large shelf angle has a higher average R-value by 30%, and the bracket galvanized and stainless-steel shelf angles have higher average R-values by 18% and 47%, respectively. The knife plate galvanized and stainless-steel shelf angles have higher overall average R-values by 28% and 63%, respectively. The hollow section tube HSS galvanized and stainless-steel shelf angles have higher overall average R-values by 32% and 58%, respectively, if compared to the directly attached large galvanized steel shelf angle.

For both intermediate floor intersection configurations (Type B) and the clear wall (Type A), the configurations with the highest insulation board R-values (R-25) showed the highest improvements in R-values percentages when each group was compared to the reference group. Therefore, it was concluded that the shape and material of the ties and shelf angles are more effective in configurations with higher insulation R-values. In addition, cases using solid ties are more sensitive to block density reduction than cases using slotted ties. The fastened on-surface ties also showed more sensitivity to the density reduction when compared to the block tie. Therefore, the maximum thermal insulation benefit in the case of using lightweight concrete blocks could be achieved by using solid ties with a high thermal conductivity value fastened on the block's surface. On average, the reduction of the concrete block density by 10% showed an improvement in the effective R-value of 2.23% in the case of clear wall configurations and 3.5% in the case of the intermediate floor configurations. In addition, configurations with an expected lower effective thermal resistance are more sensitive to the concrete block density. Using a directly attached galvanized steel shelf angle showed the highest R-value improvement of 7% when the concrete block density is reduced by 10%. The lowest R-value improvement, 1.75%, was noticed for the stainless-steel knife plate configurations. It is concluded that concrete block density is one of the dominant factors in the effective thermal resistance of masonry cavity walls and should be carefully considered.

Design charts that combine the masonry compressive strength, f_m', and the R-value properties according to the density of blocks for different cavity wall configurations were presented. The

introduced charts and R-value multipliers allow the designers to predict and choose the appropriate structural and thermal properties of common and typical concrete-block masonry cavity walls during a preliminary design phase without performing finite element simulations. These charts and design multipliers aim to provide a reliable preliminary estimation of energy needs for the buildings and present a guideline for improving the thermal envelope.

3.6. Appendix

This section presents examples to illustrate the steps used to calculate the effective R-values using the presented charts and R-value multipliers. Also, an example is included to discuss the prediction of the effect of changing the addressed parameters – such as the material and shape of ties and shelf angles - on the effective walls' R-values for common masonry wall configurations regardless of the dimensions or the material properties of other wall components. In this section, results are validated using ANSYS simulations and/or data obtained from the literature. In addition, this section presents figures showing the finite element simulation results of thermal distribution and heat flux for a few of the studied configurations.

3.6.1. Examples

Example (1): Clear wall assemblies:

It is required to calculate the effective R-value and expected masonry compressive strength of a clear wall assembly with the following conditions; (1) the ties are solid fastened on surface (2) tie material is stainless steel ties (3) insulation R-value of R-15, (4) hollow block with density 1800Kg/m^3. (Assume that the dimensions of the required configuration are the same as the addressed configurations Type A)

Solution:

Step (1): The effective R-value and masonry compressive strength of the reference case (lowest effective R-value) is determined from **Figure 3-7**

- The masonry compressive strength (fm′) is 17.5 MPa.
- The effective R-value is 2.1 m^2K/W representing the reference case of solid galvanized steel block tie type

Step (2): From **Table 3-4** obtain the R-value multiplier that corresponds to the required case (fastened on surface solid stainless-steel tie). The R-value multiplier was found at 1.23.

Step (3): Transfer the R-value obtained from **Figure 3-7** to the required addressed case. That could be done by multiplying the reference R-value obtained from step (1) by the R-value multiplier obtained from step (2). Therefore, the effective R-value for the required case is estimated to be (2.1 X 1.23) = 2.583 m^2K/W. Therefore, the expected masonry compressive strength is 17.5MPa and the effective R-value is 2.583 m^2K/W

For validation, this example was simulated using ANSYS workbench. The corresponding effective R-value for the required case was 2.69 m^2K/W. Therefore, the error percentage between both results is 3.97%.

Example (2): Using data from the literature for configurations Type A and Type B:

This example discusses the application procedure for the R-value multipliers presented in **Table 3-9**. These R-value multipliers can be applied to have a preliminary estimation of the changes that may occur in R-value due to changing the tie type, tie material, shelf angle type or material of an addressed masonry wall regardless of the dimensions or walls' components other than the ties and the shelf angles material properties. Data were obtained from the literature (Finch et al., 2013a) to validate that the usage of these R-value multipliers is not limited to the cases studied in this chapter and could be generalized.

Information about the literature data:

The literature data provided by Finch et al. (Finch et al., 2013a) presented a three-dimensional thermal analysis of various masonry ties and alternate cladding support techniques using HEAT3. This example focused only on the literature data investigated by Finch et al., discussing the discrete cladding attachment elements such as brick ties and brick veneer shelf angles. A series of thermal models were developed by Finch et al. to assess the thermal bridging impact of different masonry ties through exterior insulation and different backup wall types. Our study focuses on the 6" (150 mm) concrete back-up wall assemblies, which were modelled with varying levels of exterior insulation and the following different masonry tie options:

- Galvanized Steel 2-inch x 16 gauge fastened on surface brick ties (solid and slotted ties)
- Stainless Steel 2-inch x 16 gauge fastened on surface brick ties (solid and slotted ties)

- Basalt Fiber masonry cavity tie (proprietary UK product for concrete backup wall)

The case of the lowest effective R-value in the literature data was considered as the reference case for our calculations. **Table 3-10** shows calculations of the effective R-value of clear wall configurations and a comparison between the literature results and the estimated effective R-values obtained from R-value multipliers presented in this study. The average difference between both results was found to be 2.57%, as shown in **Table 3-10**.

Table 3-10: Calculations for clear wall configurations (Example 2)

Type of tie used	Effective R-value obtained from literature (Finch et al., 2013a)	R-value multipliers obtained from **Table 3-9**	Effective R-value estimated using the R-value multipliers (Explained by equation 21 below)	% difference from literature data and R-value multipliers
Solid Galvanized steel tie	2.46	Reference (1)	2.46	Reference
Slotted galvanized steel	2.64	1.2/1.13=1.06	2.46*(1.2/1.13) =2.62	0.88
Solid Stainless-steel tie	2.81	1.24/1.13=1.09	2.46*(1.24/1.13) =2.71	3.98
Slotted Stainless steel tie	2.99	1.31/1.13=1.16	2.46*(1.31/1.13) =2.86	4.53
Basalt Fiber tie	3.17	1.44/1.13=1.27	2.46*(1.44/1.13) =3.13	0.88
Note: The literature data was Clear wall fastened on surface ties with R-15 external insulation R-value				Average 2.57%

The reference case considered in **Table 3-9** should be transferred from solid galvanized block tie to solid galvanized steel fastened on surface tie to comply with the example requirements as follows;

The galvanized steel block tie solid*1.13=Galvanized steel fastened on surface tie solid

The galvanized steel block tie solid*1.24=Stainless steel fastened on surface tie solid

Stainless steel fastened on surface tie solid =1.24* $\frac{\text{Galvanized steel fastened on surface tie solid}}{1.13}$

To generalize

$$\text{Required case R-value} = \text{Any reference R-value considered} * \frac{\textbf{Factor for required case}}{\textbf{Factor for the refrence case considered}} \qquad \textbf{(21)}$$

The thermal impact of masonry shelf angles in addition to the impact of the masonry ties (solid 16 gauge stainless and galvanized fastened on surface slotted ties) was considered. The case of the lowest effective R-value in the literature data was considered the reference case for

calculations. **Table 3-11** shows calculations of effective R-value of intermediate floor intersection configurations and a comparison between the literature results and the estimated effective R-values obtained from R-value multipliers presented in **Table 3-9**. The average difference between both results was found to be 6.3% as shown from **Table 3-11**.

Table 3-11: Calculations for the Intermediate floor intersection configurations (Example 2)

Type of shelf angle and tie used	Effective R-value obtained from literature (Finch et al., 2013a)	R-value multipliers obtained from **Table 3-9**	Effective R-value estimated using the R-value multipliers (Using equation11)	% difference from literature data and R-value multipliers
Directly attached and galvanized steel ties	1.37	Reference (1)	1.37	Reference
Directly attached and stainless-steel ties	1.53	1.31/1.2 = 1.09	1.37*(1.31/1.2) =1.50	2.13
Knife plate and galvanized steel ties	1.62	1.32/1.2=1.1	1.37*(1.32/1.2) =1.51	6.74
Knife plate and stainless-steel ties	1.8	1.44/1.2=1.2	1.37*(1.44/1.2) =1.65	8.24
Note: The literature data was Intermediate floor intersection with fastened on surface ties and R-10 external insulation R-value. The shelf angle material for all studied configurations was galvanised steel.				Average 5.7%

3.6.2. Figures

Figure 3-9 and **Figure** 3-10 show a comparison between different walls showing the thermal distribution and the heat flux for cases with insulation value R-20 insulation - Fully grouted blocks and concrete blocks' density of 1550 Kg/m^3.

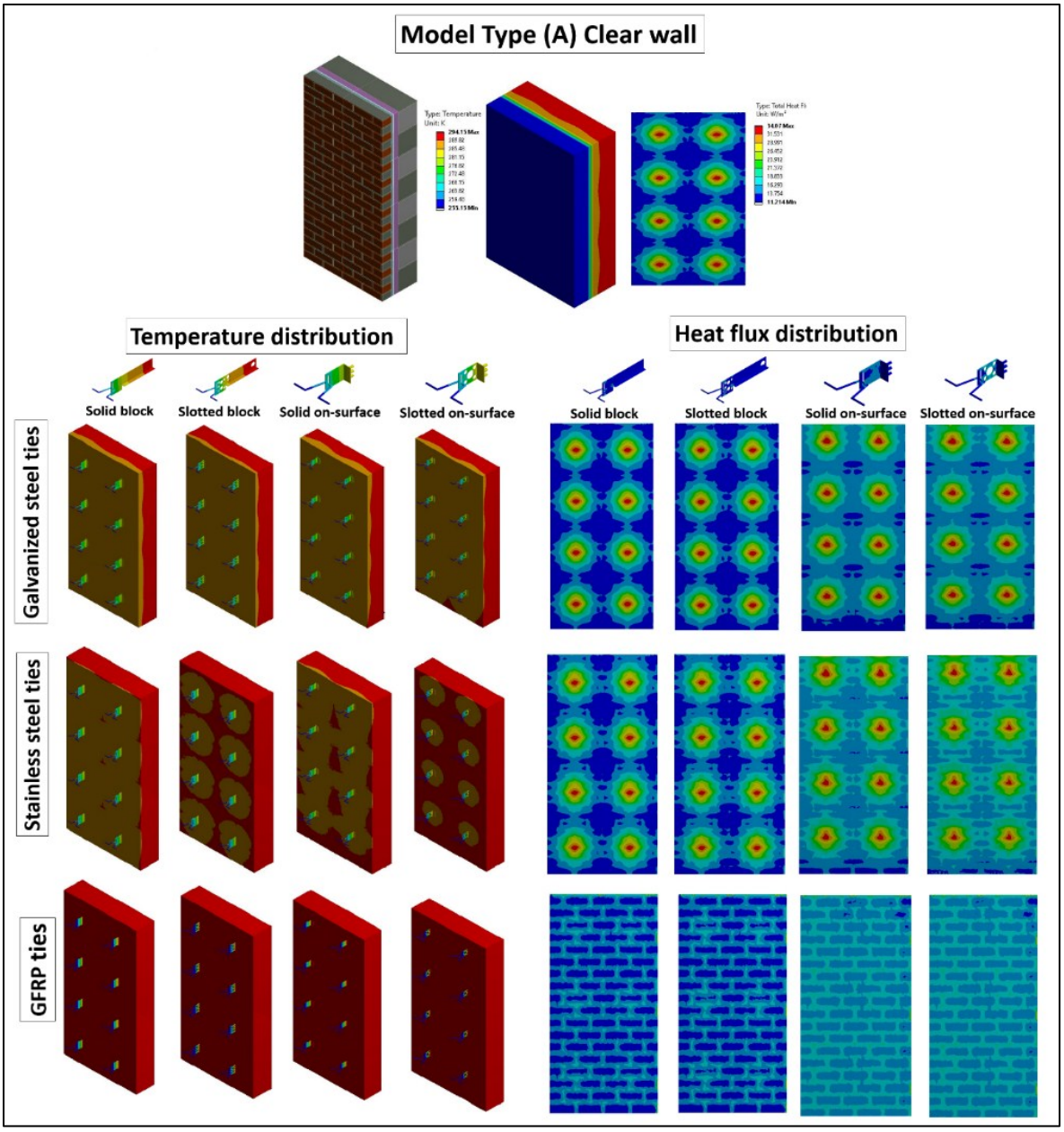

Figure 3-9: Thermal distribution and the heat flux for cases with insulation R-20 and concrete blocks' density of 1550Kg/m^3

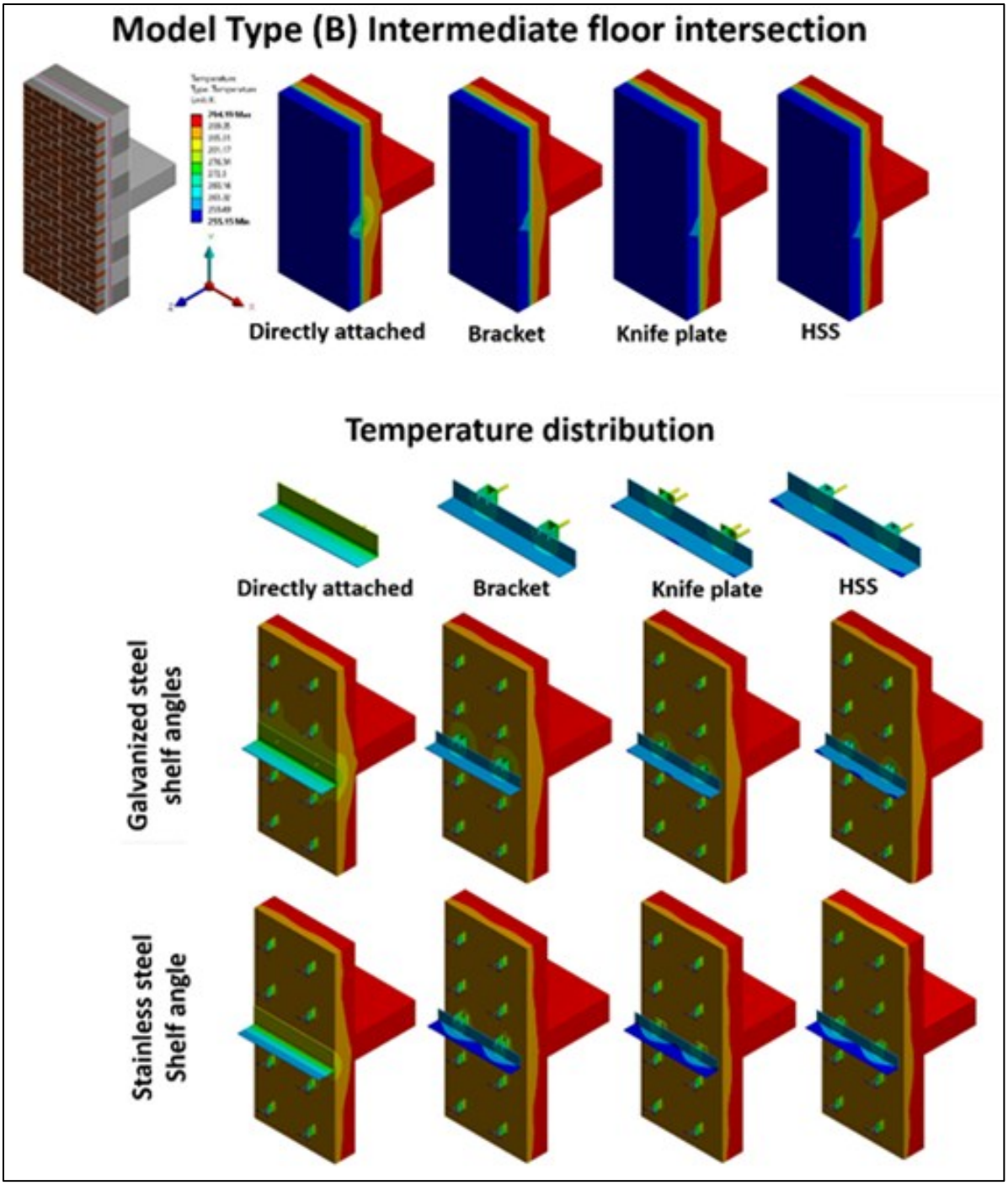

Figure 3-10: Thermal distribution for intermediate floor intersections using insulation R-20 and concrete block density of 2100 kg/m^3

4. Adjustments of Existing Methods for Estimating the Thermal Resistance of Masonry Veneer Clear Walls

4.1. Introduction

The demand for higher energy efficiency in buildings has driven higher levels of insulation to be used in masonry walls. However, the effective thermal resistance (R-value) is reduced significantly by highly conductive components—thermal bridges. Furthermore, the evaluation of R-values of the building envelope is essential for a reliable assessment of the thermal behaviour and energy efficiency of buildings. The lateral heat flows in multiple directions caused by thermal bridging elements are considered a challenge in the R-value estimations. This chapter suggests applying adjustment factors to current thermal resistance estimation methods (i.e., isothermal plane and parallel path methods) to accurately include the thermal bridging effects in the R-value estimations for the clear masonry cavity walls. The R- values obtained from analytical methods with or without using the adjustments were compared with numerical simulations using a 3D steady-state finite element method (FEM) in addition to experimental data available in the literature. The results showed an average accuracy of 2% in using the suggested adjustments, compared to 19% and 25% for the isothermal plane and parallel path methods, respectively.

In the transition to sustainable buildings, modern concrete blocks and masonry veneers can be significant constituents. Masonry is aesthetically pleasing and durable (Ismaiel et al., 2021). In Canada, a significant change in the calculation method for effective thermal resistance (R-value) was demanded in the National Energy Code of Buildings. The previous exclusion of major structural elements and other elements that penetrate the envelope as long as they make up less than 2% of the wall area is no longer accepted. The new calculation method requires considering all thermal bridging into the effective R-value calculations along with major structural elements such as balconies, beams, and columns to accurately recognize the impact of thermal bridging on the building elements. Moreover, the maximum R-values for opaque building assemblies and fenestration are increased to improve the thermal performance of the building envelope (Canadian Commission on and Fire, 2022). These changes require the use of new methods and tools to calculate envelope R-values accurately and account for all thermal bridges in the envelope. To comply with these continuously evolving energy code requirements, the masonry

construction industries are looking for an effective approach for thermal resistance calculation to help in the improvement of the thermal design of masonry walls.

The configurations of the masonry wall assemblies play a key role in the walls' thermal performance. One of the challenges in the assembly configuration is the thermal bridging, which takes place where highly conductive structural components penetrate insulating materials, such as at the structural members' penetrations through the insulation plane (e.g., veneer ties) (CCMPA, 2013). Traditional steel masonry veneer ties are among the sources of thermal bridging in concrete masonry walls (Adam Di Placido et al., 2019a). The shape, size, material, and configuration of ties have been revolutionized to improve thermal performance. Several tie shapes with different materials have been introduced to the market to minimize thermal bridging while meeting structural requirements. Slotted ties can be fastened to the face shell of structural backing instead of being inserted between blocks as traditional ties are typically used. Holes within the tie body are introduced to reduce the cross-sectional area, thus minimizing thermal conductance (Wilson, 2013).

The exterior masonry wall consists of a clear wall and interface details. A "clear wall" is defined as a planar area with regularly spaced structural components that are free of windows, doors, and other irregularities (Barnes et al., 2013). Clear wall assemblies can contain thermal bridges from uniformly distributed secondary structural components, which are necessary to withstand loads. Examples of components included in clear wall assemblies are brick ties, girts, or studs that support cladding. Intersections of the primary structure are not considered as parts of clear wall assemblies. The changes in construction or geometry that disrupt the uniformity of clear wall assemblies are known as interface details. These details include slab edges, wall transitions, parapets, corners, and wall penetrations. Determining the impact of heat flow through clear wall assemblies is necessary to accurately assess the thermal resistance of building envelope assemblies (ASHRAE, 2017c). This chapter focuses on the clear wall assemblies of concrete-block masonry cavity walls. The typical components of masonry concrete-block clear walls are concrete blocks, mortar, insulation boards, veneer ties, and air gaps in the case of brick veneer masonry walls. **Figure 4-1** shows the main clear wall components addressed in this study.

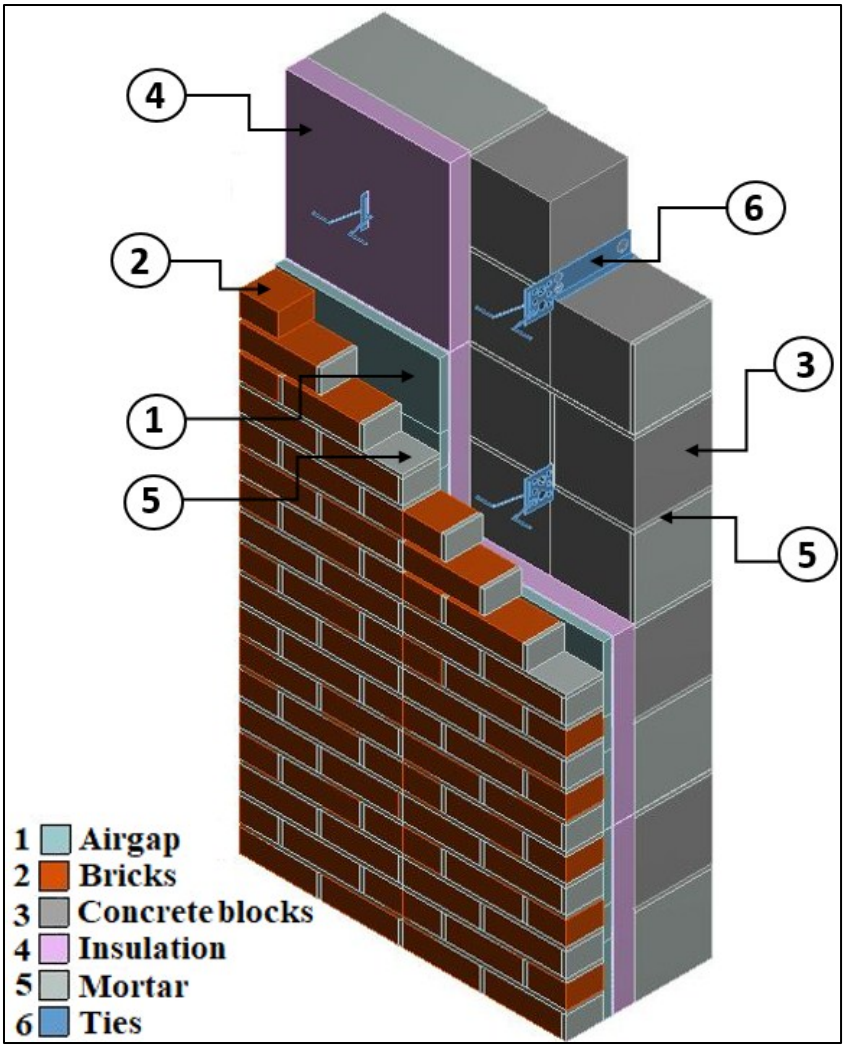

Figure 4-1: Components of a concrete-block clear masonry cavity wall

The combinations of various materials' thermal properties, geometries of wall components, and three-dimensional heat transfer pose a challenge for determining the R-values of masonry walls (Kontoleon et al., 2013). There have been a few methods for estimating the R-value of a composite wall. Series and parallel path methods are two of the most commonly used techniques for calculating thermal resistance (ASHRAE, 2017a). These methods are accurate when the materials on the same layer have close thermal conductivity values (i.e., wood frame walls) (ASHRAE, 2017b). Series and parallel path methods offer quick calculations but have insufficient accuracy to be applied to masonry cavity walls due to employing assumptions for simplification, such as ignoring the lateral heat transfer and assuming even temperature distribution on the same plane (Theodosiou et al., 2021; McGowan and Desjarlais, 1995; Kosny and Christian, 1995). Therefore, the ASHRAE Fundamentals Handbook (ASHRAE, 2021b)

recommended further experimental examinations of the required studied elements to reveal the actual thermal resistance value for assemblies including thermal bridging elements penetrating the insulating materials (e.g., veneer ties). Another commonly used approach is linear and point transmittance (Norris et al., 2012b; ASHRAE, 2017e). This approach is used for the interface details (assemblies contain thermal anomalies such as changes in construction or geometry that disrupt the uniformity of the clear field). The linear and point transmittance approaches involve modelling the required building assembly with and without the thermal anomalies to obtain heat flows in both cases. Then, the difference in the heat flows is attributed to individual contributions of point or linear loads. To estimate the overall heat flow in a wall assembly, all the linear and point loads from interface details can be added with the clear wall heat flow. The idea of linear transmittance has been widely used in practice in various forms (ISO, 2017c; Hershfield, 2022b). However, the linear and point transmittance method depends heavily on computer numerical models (ASHRAE, 2017d; Hydro, 2016b). This chapter aims to suggest adjustments to current thermal resistance estimation methods (i.e., isothermal plane and parallel path methods) to be applied to exterior masonry veneer walls considering the effect of the thermal bridge caused by the veneer ties. The significance of such work would help designers to estimate the thermal transmittance of clear field assemblies quickly and accurately, considering the thermal bridging effect caused by the veneer ties. In addition, accurate estimations of R-values will help with reliable estimation of energy needs for the buildings and improve the thermal envelope.

This chapter is structured as follows: after the introduction section, a literature review describing the commonly used analytically simplified methods and tools available in the previous studies for estimating the effective R-value is presented. This is followed by the methodology, including a description of the finite element models used in this study. Then, the explanation and application of the suggested adjustments along with a comparison with the finite element simulation results are presented. Finally, the results and main concluding remarks are discussed.

4.2. Current Analytical Methods

4.2.1. Isothermal plane and parallel path methods

Series and parallel heat flows are two idealized heat transfer scenarios in wall assemblies. The surface-to-surface thermal resistance of a flat building assembly composed of parallel layers (e.g., floor, or wall), consists of the sum of the resistances of all layers in series (ASHRAE, 2021b):

$$R_s = R_1 + R_2 + R_4 + \cdots + R_n \qquad \text{(where: } R_n = \frac{L_n}{K}\text{)} \qquad \textbf{(22)}$$

where; R_1, R_2..., R_n are resistances of individual layers (m^2K/W), Rs=resistance of building assembly (overall resistance (m^2K/W), L_n= the thickness of individual addressed layers (m) and k=thermal conductivity of the individual addressed material (W/m K).

In many building assemblies, heat flows in parallel paths through a layer consisting of different components. If no heat flows laterally within the layer, the average transmittance of the layer is calculated as follows (ASHRAE, 2021b):

$$U_{av} = AU_A + BU_B + \cdots + NU_m \qquad \textbf{(where: } U_m = \frac{1}{R_m}\textbf{)} \qquad \textbf{(23)}$$

where; A, B..., m are the surface-weighted path fractions for areas composed of several different paths with transmittances U_A, U_B,..., U_m (W/m^2K).

Most building assemblies are represented by a combination of materials connected in series and in parallel. Therefore, a combination of both series and parallel heat transfer scenarios can be applied, called the series-parallel (i.e., isothermal planes) method. In the isothermal planes method, it is assumed that the heat flows laterally in any component and the thermal resistances of adjacent components are combined in parallel, resulting in a path with series-parallel resistance combined. Isothermal planes are formed when heat can flow laterally with a small resistance value in any continuous layer, so that transverse isothermal planes result (ASHRAE, 2021b). The assembly functions as a series of combinations of layers, of which one or more provide parallel paths. The total average resistance in that case is the sum of the resistance of the layers between the isothermal plans. Each layer is calculated, and the results are weighted by the contributing surface area. This assumption is accurate when adjacent materials of the same layer have different conductivity values.

The parallel and isothermal-planes methods are often considered two separate calculation methods. The ASHRAE Fundamentals Handbook (ASHRAE, 2021a) suggests the actual U-factor lies between both methods. The ASHRAE Fundamentals Handbook suggests that these methods provide a range of upper and lower limits on the true thermal resistance (ASHRAE, 2021c). The obtained thermal resistance assuming parallel heat flow only is usually higher than that obtained assuming the isothermal planes method. Generally, it was suggested that if the construction contains a layer in which lateral heat conduction is high compared to heat flux through the wall, a value closer to the isothermal calculation should be used. If there is no layer of high lateral thermal conductance, a value closer to the parallel calculation is more accurate. However, the ASHRAE Fundamentals Handbook generally recommended further experimental examinations of the required studied elements to reveal the actual thermal resistance value.

4.2.2. ISO 6946 Combined Method

The combined method is described in International Standards ISO 6946 (ISO, 2017d). The combined method suggests computing the total thermal resistance by combining the results of the parallel path method and the isothermal planes results. The total thermal resistance is computed as an arithmetic average of the upper and lower thermal resistance limits obtained using the parallel path and the isothermal planes methods, respectively. In other words, the two R-values (upper and lower limits) have the same weight "0.5" in the total resistance calculation. This method is used to compute the thermal resistance of building elements consisting of homogeneous and inhomogeneous layers. It may also be applied to building elements, which may contain an air layer up to 0.3 m thick. However, this method has some limitations: (1) It is only applicable when the ratio of the upper limit to the lower limit of the thermal resistance does not exceed 1.5. (2) This method is inapplicable when thermal insulation is bridged by metal and there is a significant difference between the thermal conductivity of the materials in the same layer. (3) There are some corrections required to the thermal transmittance values for air voids, mechanical fasteners, and inverted roofs.

4.2.3. The Zone Method

The assumptions described in the parallel path method (the heat flow is perpendicular to the wall) are not accurate in wall assemblies containing steel members next to materials with low

thermal conductivity, such as thermal insulation, and the effects of the thermal bridges become more significant (Barbour et al., 1994). Therefore, the zone method was developed to address assemblies with metal elements of uniform cross-sectional areas (e.g., lightweight steel-framed constructions) (Adam Di Placido et al., 2019a; ASHRAE, 2021d). The zone method is considered an adjustment to the parallel path method. This method is applied as follows; the wall is divided into two sections: (1) containing the steel thermal bridge influence, and (2) containing the remaining portion of the wall cavity without the thermal bridge influence. Charts were presented to determine the width of the two assumed sections based on the dimensions of the steel element. By using an area "weighting factor" for the wall sections affected by the steel element (Cao et al., 2016), the thermal resistance value is computed and then combined with that of the no-steel section using the parallel path method. This method is suitable for lightweight steel-framed constructions due to its simple geometries and uniform thermal bridging (e.g., steel stud). Also, the charts provided to determine the sections' width are limited to steel studs and lightweight steel-framed walls.

Literature shows that the current analytical methods have insufficient accuracy to be applied to masonry cavity walls due to the geometry complexity and the presence of layers in which lateral heat conduction is high compared to heat flux through the wall. Therefore, there is a need to adjust the current methods or develop new R-value estimation methods to consider the effects of the thermal bridge element on the R-value.

4.3. Methodology

This chapter investigates the thermal resistance of the clear masonry wall assemblies analytically based on the results of intensive 3D finite element computer modelling. The objective of this study is to suggest an adjustment of current thermal resistance estimation methods (i.e., isothermal plane and parallel path methods) to include the effect of the thermal bridge resulting from different types of veneer ties in the total R-value estimations. First, 3D finite element models of simplified wall assemblies were used to investigate the effects of thermal bridging elements and thereby develop adjustments. In the simplified models (labelled as "Type A" for brevity), the clear wall geometries were simplified into regular shapes connected in series and parallel connections. The ties penetration in the air gap layer between the insulation and the outer brick veneer layer was ignored as shown in **Figure 4-3** and **Figure 4-4** due to its insignificant

reduction effect on the overall R-value (1.4%). The penetration of ties does not affect the overall R-value due to the low air velocity in the cavity and small area subjected to convection. Therefore, this penetration was ignored for simplification purposes. A wide range of values of the thermal properties and dimensions of wall components were investigated. Using the simplified models saves the immense execution and simulation time that the detailed assemblies require. The analysis of the simplified models facilitates comparing the results obtained from the adjusted isothermal and parallel path methods with those of the finite element models. For validating the suggested adjustments to actual masonry veneer walls, detailed clear masonry wall models were constructed (labelled as "Type B" for brevity). The suggested adjustments obtained from the simplified models' (Type A) analysis were applied to the detailed models (Type B) with a larger scale and different tie types. This section presents the Finite Element simulations used in this study. Then, a detailed description of the models and the suggested adjustments is presented.

4.3.1. Models Description

The simplified finite element models for the preliminary application of the suggested adjustments are presented in section **(3.1.1)**. The simplified finite element models (Type A) were addressed first. The Type A models represent the current common brick veneer tie types used in practice; Type $A_{(S)}$ represents the fastened on the block's surface ties; and Type $A_{(B)}$ represents the block ties. 60,000 simplified models were constructed for each tie type. 3D finite element modelling was used to perform steady-state thermal simulations to address many variables, such as the thermal conductivity and the dimensions of the wall components. After validating the suggested adjustments by comparing the simplified models' results obtained from the suggested adjustments with results obtained from ANSYS simulations, detailed clear masonry wall models are constructed (Type B) presented in section **4.3.1.2**). 360 detailed clear masonry wall finite element models were simulated using ANSYS. The detailed finite element models represent four types of the currently used brick veneer ties in practice: solid fastened on blocks' surface ties (Type $B_{(SS)}$), perforated fastened on blocks' surface ties (Type $B_{(PS)}$), solid block ties (Type $B_{(SB)}$) and perforated block ties (Type $B_{(PB)}$). **Figure 4-2** shows the shape of the tie types used in detailed models (Type B). The R-value of Type B models was estimated by applying the suggested adjustments to the isothermal plane and parallel path methods. Then, the results were compared to the values obtained from finite element simulations.

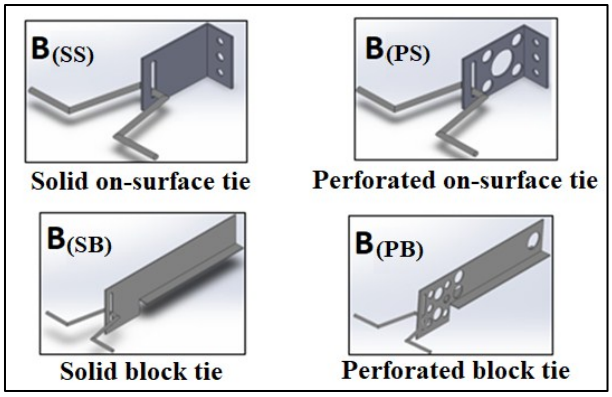

Figure 4-2: Shape of tie types used in detailed models (Type B)

4.3.1.1. Simplified Clear Wall Assemblies (Type A)

Due to the simplified clear wall geometry, addressing many variables such as the thermal properties and dimensions of wall components is possible without consuming immense execution and simulation time. Besides, it facilitates the comparison of the results obtained from the suggested adjustments of the isothermal and parallel path methods with the finite element results considering many variables. Therefore, simplified clear wall assemblies were used as a preliminary phase to develop the suggested R-value adjustments. Type A models were used to simplify the clear wall geometry into regular shapes connected in series and parallel connections. In addition, the effect of one tie only was considered in the center of each assembly. **Figure 4-3** and **Figure 4-4** show the simplified assemblies used (Type $A_{(s)}$ and Type $A_{(B)}$, respectively). Layers A, B, C, D and F represent concrete blocks, insulation boards, ties, air gaps and brick veneer, respectively. L_A, L_B, L_C, L_D and L_F represent the thickness (m) of concrete blocks, insulation boards, ties, air gaps and brick veneer, respectively. All dimensions shown in **Figure 4-3** and **Figure 4-4** are in meters. **Table 4-1** shows the range of dimensions used for each layer as well as the thermal conductivity range considered for each addressed layer.

Table 4-1: The range of dimensions and thermal conductivity used for each layer

Layer	Represents	Thermal Conductivity range (W/m K)	Thickness range (m)
A	Concrete blocks*	0.185 - 0.445	0.09 - 0.3
B	Insulation boards	0.02 - 0.07	0.025 - 0.15
C	Ties	50 - 0.2	0.002 - 0.01
D	Air gap	0.0415 - 0.7	0.025 - 0.15
F	Brick veneer	0.405 - 1.34	0.07 - 0.3

*The considered range of the concrete blocks' thermal conductivity reflects the cases of un-grouted (hollow) and fully grouted concrete blocks in the simplified models' simulation

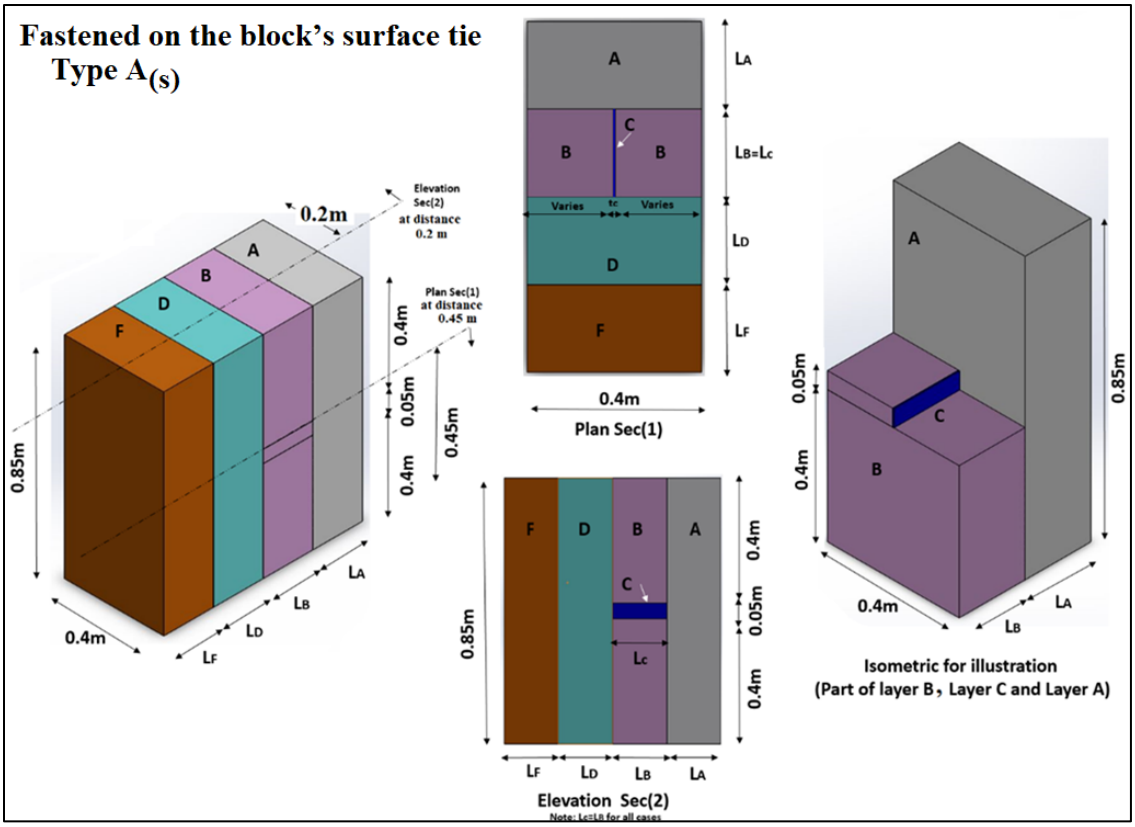

Figure 4-3: Simplified assemblies, Type $A_{(s)}$ representing fastened on-surface ties

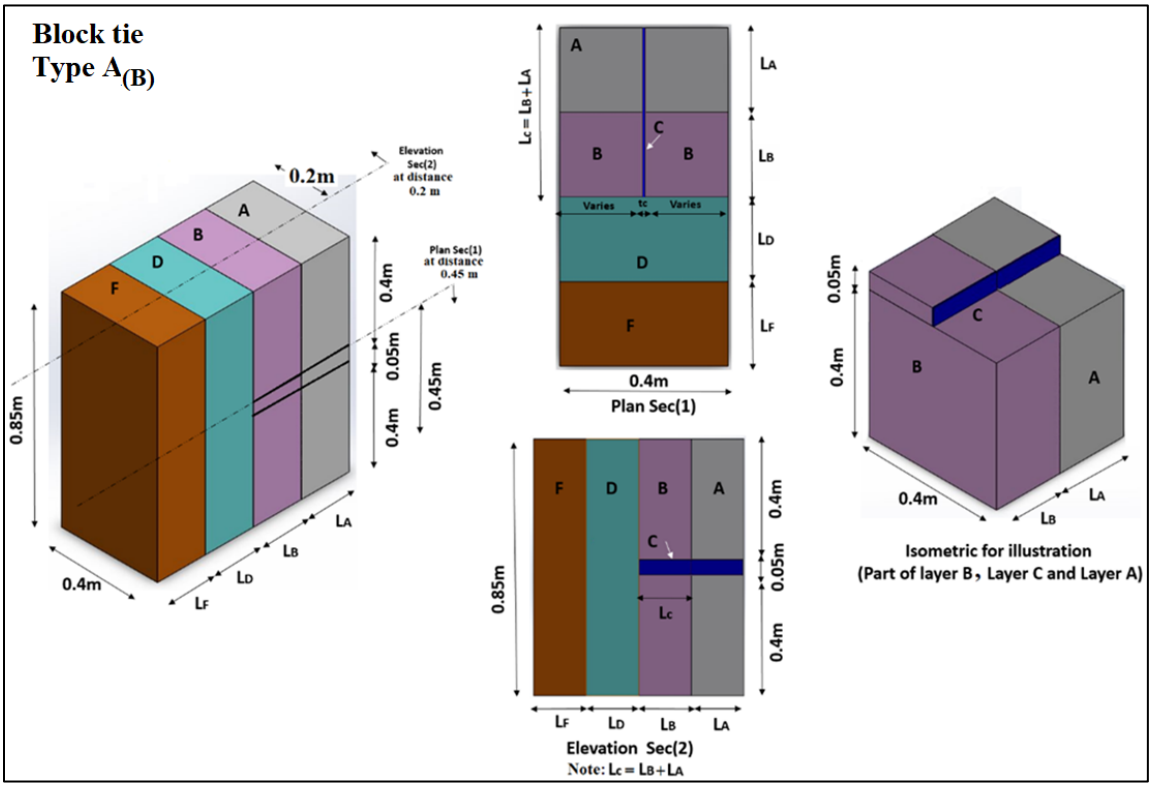

Figure 4-4: Simplified assemblies, Type $A_{(B)}$ representing block tie type.

4.3.1.2. Detailed Clear Wall Assemblies (Type B)

The detailed models of actual and complex geometries were used to validate the suggested adjustment calculation method obtained from the simplified models' analysis. **Figure 4-5** shows the detailed assemblies used: Type $B_{(SS)}$, $B_{(PS)}$, $B_{(SB)}$ and $B_{(PB)}$. **Table 4-2** presents the fixed material properties for all the studied assemblies. An interior and exterior air film were considered in the analysis for all models, with a nominal resistance of 0.11 and 0.03 m^2K/W respectively. The thermal resistance of the air gap, 0.07 m^2K/W, between the wall thermal insulation and the brick veneer, was obtained from the ASHRAE Handbook and literature (ASHRAE, 2019b; Hershfield, 2016b). 360 models (4 types of ties x 3 tie materials x 3 insulation R-value x 2 grout conditions x 5 block densities = 360) were studied for Type B to discuss different variables. **Table 4-3** presents the variables considered for each studied scheme.

Table 4-2: Material thickness and properties used in the studied schemes for Type B models

Component	Thickness (m)	Conductivity (W/m K)
Standard concrete Block* Size Block 390X190X190 mm (Size block no.20) (Sturgeon et al., 2013a; Sturgeon et al., 2013b)	0.190	Varies
Cement Mortar	0.01	1.2
Masonry ties (0.40 m on center) **	14 gauge	Varies
Insulation	0.05	Varies
Brick veneer	0.09	0.81

*In the case of estimating the thermal resistance (m^2K/W) of the hollow concrete block (R_{block}), the hollow block thermal conductivity value was considered from the ASHRAE Handbook (ASHRAE, 2019).
**There are several spacings of the masonry ties used in practice based on the structural requirements of the addressed wall. This study focuses on the minimum masonry tie spacing to address the highest masonry tie thermal bridging effect.

Table 4-3: The variables considered in each studied scheme

Scheme	Variables considered
General variables considered for each assembly	tie type, ties' material, insulation R-value, concrete block density, concrete blocks' type
R-values in BTU/(ft^2·°F·hr) and in (m^2K/W) for insulation	R-15 (2.64), R-20 (3.52), R-25(4.40)
Block Density (kg/m^3) (conductivity (k=W/m K)	Hollowed: 2100(k=1.17), 1800(k=0.87), 1550(k=0.66),1380 (k=0.6), 1150(k=0.35) Fully grouted: 2100(k=1.9), 1800(k=1.13), 1550(k=0.78), 1380(k=0.6), 1150(k=0.36)
Type of wall	Hollow block wall, Fully grouted wall
Tie type	Block solid tie, fastened on block's surface solid, block perforated tie, fastened on block's surface perforated
Ties materials (conductivity =W/m K)	Galvanized steel (k=50), Stainless steel (k=17), GFRP (k=0.2)

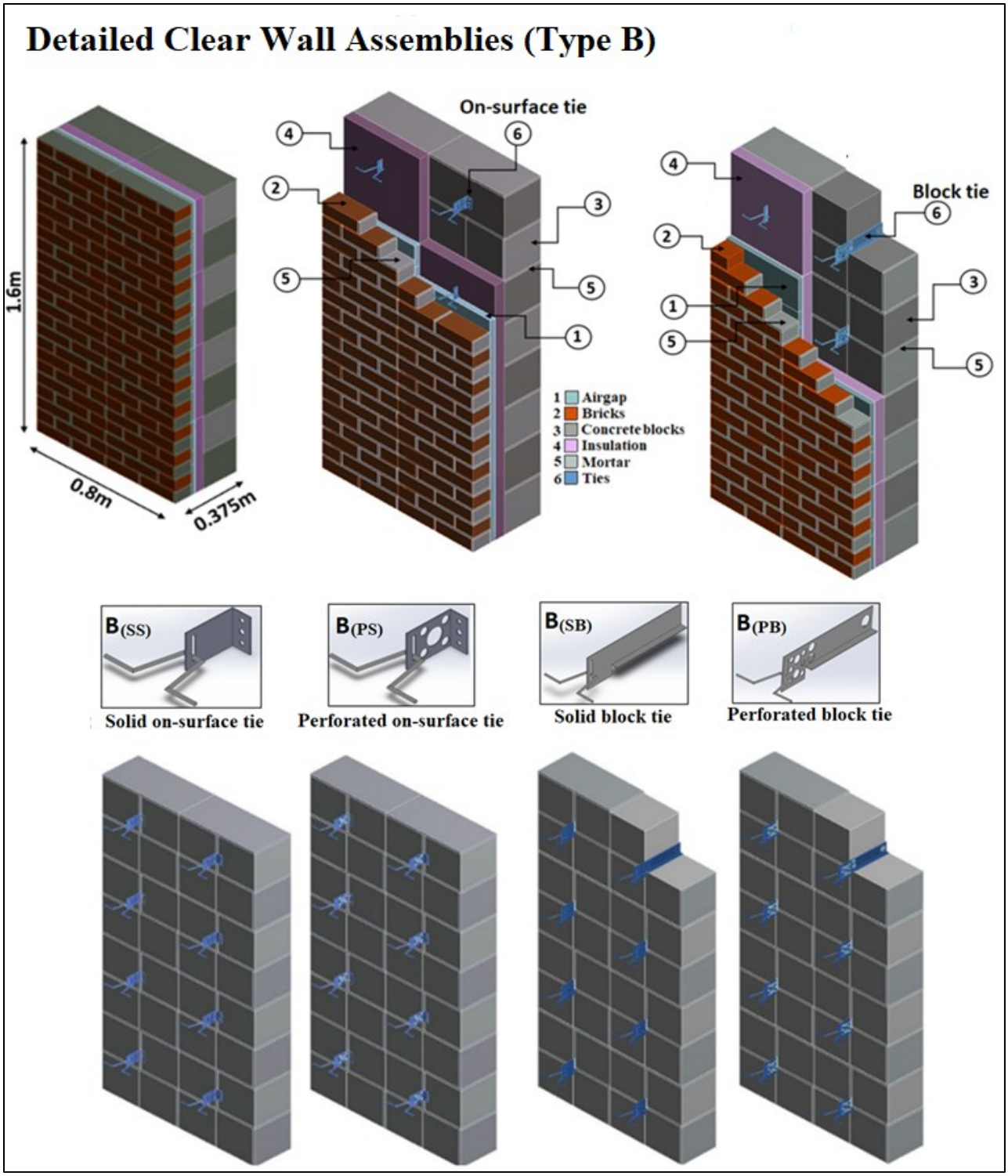

Figure 4-5: Detailed clear wall assemblies (Type B)

4.3.2. Finite Element Analysis Simulations

Experimental measurements of an element's thermal behaviour can be expensive, especially for large-sized specimens. If a physical test is not possible, computer simulation provides the next most accurate results. Computational numerical simulation is considered a practical alternative, as this method is cost-effective and accurate. Several thermal analysis programs are designed to simulate thermal problems in two dimensions, such as THERM, HEAT2, Energy2D (Xie, 2012), and three dimensions, such as ANSYS, ABAQUS, HEAT3, and SIEMENS. Several studies on masonry walls have been conducted to improve and validate the simulation approaches with experimental data (del Coz Diaz et al., 2006; Norris et al., 2012a; Desjarlais and McGowan, 1997). Those studies showed good agreement between the numerical simulation and experiment results. Validated simulation approaches were then used to simulate the thermal performance of other wall configurations. The results are expected to be within ± 5% of the test result (McGowan and Desjarlais, 1995).

The ANSYS Workbench (ANSYS, 2019) was used to perform steady-state finite element thermal analysis simulations of typical brick veneer cavity wall assemblies. Simulations were conducted to calculate the overall R-value for different wall configurations (discussed in sections **4.3.1.1** and **4.3.1.2**). There are some modelling assumptions considered in this study: all models were analyzed at a steady-state thermal analysis and air leakage was not considered. All the material properties were taken from the ASHRAE Handbook (ASHRAE, 2019b). Three types of boundary conditions were considered: specified temperature, adiabatic boundary conditions, and interface boundary conditions. In the FE modeling, the specified temperatures were assumed to be constant at 21°C and -18°C for the interior and exterior surfaces, respectively. Which is the case for steady heat conduction. While the remaining four sides of the wall were assumed to have adiabatic boundary conditions. Since the addressed walls are made up of layers of different materials, the solution of a heat transfer problem in such a medium requires the solution of the heat transfer problem in each layer. Therefore, the specification of the boundary conditions at each interface is required. The boundary conditions at an interface were considered in the FE modelling based on the requirement that an interface cannot store any energy, and thus the heat flux on the two sides of an interface must be the same. The element used to simulate the wall components in the ANSYS modelling is SOLID70 based on its properties, which complies well with the assemblies required to be investigated. SOLID70 has a

three-dimensional thermal conduction capability. The element has eight nodes with a single degree of freedom, temperature, at each node. The element can be applied to a three-dimensional, steady state or transient thermal analysis. Meshing was done by using ANSYS's advanced sizing feature. A mesh was generated that is relatively fine for specific parts of the model (such as the ties). A sequence of mesh convergence tests has been conducted for a suitable balance between the accuracy and computational time of the addressed models. The convergence study on the mesh size was carried out by evaluating the variation of the heat flux versus the number of mesh nodes. It was found that the mesh size of 10 mm (which corresponds to an average of about $2x10^6$ nodes for the detailed clear wall assemblies Type B and about $4x10^5$ nodes for the simplified clear wall assemblies Type A) is appropriate for the accuracy and model running time for all studied cases. **Figure 4-6** shows the convergence of the heat flux versus the number of nodes used in the mesh.

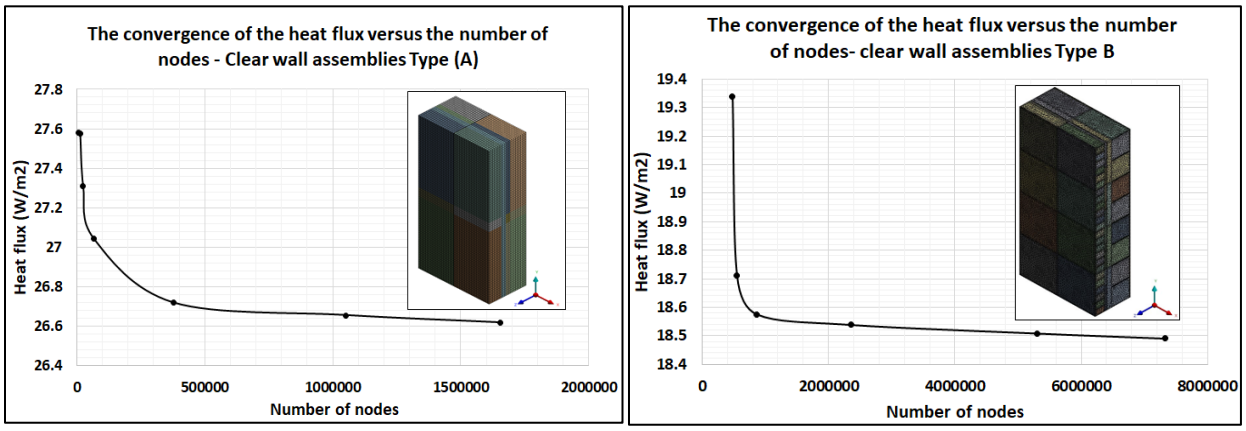

Figure 4-6: Convergence of the heat flux versus the number of nodes used in the mesh for the clear wall Type A and B, respectively.

The general heat conduction equation in rectangular coordinates in the case of constant thermal conductivity is simplified to consider the steady-state condition with no heat generation (Laplace equation) (ASHRAE, 2021a):

$$\frac{\partial}{\partial x}\left(k_x \frac{\partial t}{\partial x}\right) + \frac{\partial}{\partial y}\left(k_y \frac{\partial t}{\partial y}\right) + \frac{\partial}{\partial z}\left(k_z \frac{\partial t}{\partial z}\right) = 0 \qquad \textbf{(24)}$$

where: k_x, k_y, k_z = thermal conductivity in direction of x, y and z axes, (W/m.K), and $\frac{\partial t}{\partial x}, \frac{\partial t}{\partial y}$ *and* $\frac{\partial t}{\partial z}$ are the gradient of temperature (change in temperature per unit length perpendicular to isothermal surfaces) along x, y and z axis, respectively (K/m).

If the steady-state heat flux is only in one direction (e.g., perpendicular to the building envelope) and materials are assumed to be isotropic, heat transfer by conduction in a solid is governed by Fourier's law and can be simplified for each material layer within the building envelope as follows (ASHRAE, 2021a):

$$q = -k_m \frac{\Delta t}{\Delta x} = -U\,\Delta t = -\frac{1}{R}\,\Delta t \qquad \textbf{(25)}$$

where: Δt is the temperature difference between two interfaces of one material layer (K), Δx is the layer thickness (m), k_m is the mean thermal conductivity of material layer with a thickness Δx (W/m K), U is the thermal conductance of layer with a thickness Δx (W/ m^2 K), and R is the thermal resistance of layer with a thickness Δx (m^2 K /W).

From the results of the numerical modelling, an R-value was obtained for the overall wall. This R-value was determined from the overall heat transfer through the wall for defined internal and external environmental temperatures as mentioned earlier, as follows:

$$R = \frac{\Delta t}{q} \qquad \textbf{(26)}$$

where: q is the heat flux in watts per area of the addressed wall in square meters (W/m^2) as predicted by the FE modelling, and $\boldsymbol{\Delta t}$ is the difference in temperature between the inside and outside environment.

For validating the modelling approach, wall configurations presented in previous studies (Cui et al.; Norris et al., 2012b) were replicated using ANSYS and the simulation results were compared with the reported results. Results presented in the previous studies were obtained from three-dimensional finite element analysis and compared with experimental results obtained from guarded hotbox measurements and data provided in ISO Standard 10211 (ISO, 2017c). The validation addressed were five clear wall models with galvanized steel solid block ties. The

addressed models considered different insulation R-values (R-5, R-10, R-15, R-20 and R-25). The comparison between the results obtained from the validation modelling and literature showed an average difference of 6.8% for the clear wall assemblies.

4.4. Discussion and Results

4.4.1. Results for Type A

Isothermal and parallel thermal circuits were developed for $A_{(S)}$ and $A_{(B)}$ assemblies as shown in **Figure 4-7**.

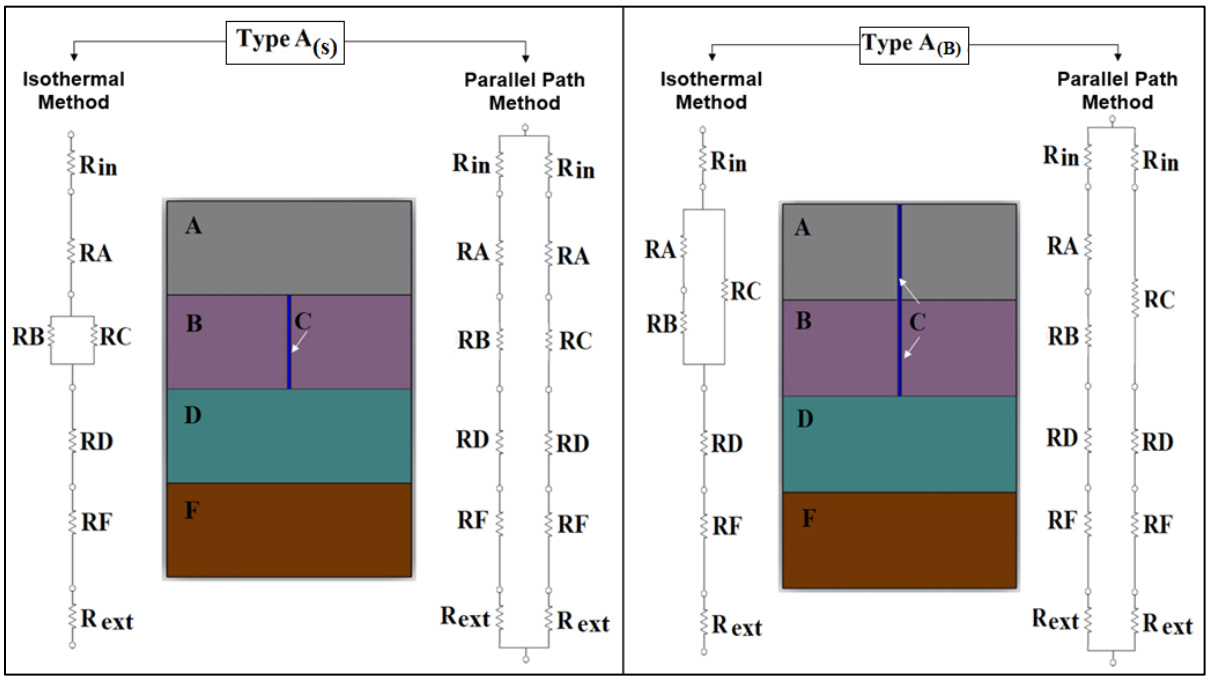

Figure 4-7: Model $A_{(S)}$, $A_{(B)}$ equivalent isothermal and parallel thermal circuit

(Note:R_{in} and R_{ext} are the interior and exterior air film resistance)

The simplified (Type A) assemblies' R-value was estimated by using the parallel path, isothermal, and FEM simulations. Results show that the finite element results are between the results obtained from the isothermal analysis and the parallel path method. This observation complies well with The ASHRAE Handbook (ASHRAE, 2021a) suggestion. In addition, a comparison between the R-values obtained from the parallel-path and isothermal-planes methods with respect to the R-values obtained by using finite element analysis was performed. **Table 4-4** shows a correlation matrix to identify the strength of the relationship between significant variables (i.e., thermal conductivity and area of ties and insulation) and the R-values obtained

from the FE simulation. A correlation matrix is a table showing correlation coefficients between variables. Each random variable (X_i) in the table is correlated with the other values in the table (X_j). The correlation matrix is a symmetric matrix, which refers to the symmetric array of numbers as shown below (Helwig, 2017);

$$R = \begin{bmatrix} 1 & r_{12} & r_{13} & \dots & r_{1N} \\ r_{21} & 1 & r_{23} & \dots & r_{2N} \\ r_{31} & r_{32} & 1 & \cdots & r_{3N} \\ \vdots & \vdots & \vdots & \ddots & \vdots \\ r_{N1} & r_{N2} & r_{N3} & \cdots & 1 \end{bmatrix}$$

$$r_{jk} = \frac{S_{jk}}{S_j S_K} = \frac{\sum_{i=1}^{n}(X_{ij} - \overline{X_j})((X_{ik} - \overline{X_k})}{\sqrt{\sum_{i=1}^{n}(X_{ij} - \overline{X_j})^2}\sqrt{\sum_{i=1}^{n}(X_{ik} - \overline{X_k})^2}} \quad \textbf{(27)}$$

where: r_{jk} is the Pearson correlation between variables X_i and X_k

Table 4-4: Correlation matrix between significant variables and the R-values obtained from the FE simulation

	k_{Block} (W/mk)	k_{ns} (W/mk)	k_t (W/mk)	Tie Area	Insulation Area	FEM R-total (3D)
k_{Block} (W/mk)	1					
k_{ins} (W/mk)	0.0001155	1				
k_t (W/mk)	0.0007660	0.0003700	1			
Tie Area	0.0002793	0.0001350	0.0008955	1		
Insulation Area	-0.0011149	-0.0005388	-0.0035736	-0.7398970	1	
FEM R-Value	**-0.1051358**	**-0.4615313**	**-0.4578149**	-0.0079835	0.0019328	1

Table 4-4 shows that the concrete block, tie, and insulation thermal conductivities have the strongest correlation with the FE simulation R-value results. The ratio between the summation of thermal conductivities of layers penetrated by the thermal bridging source and the thermal conductivity of the thermal bridging source (equation (28)) can be used to predict whether the actual R-values are closer to the isothermal plane method or the parallel path method. As shown in **Figure 4-8**, In the case of (Ratio $\leq$ 0.1), the actual R-values results were closer to the parallel

path method. While in the case of (Ratio > 0.1), there was no difference between the isothermal method and the parallel path method, both methods obtained similar R-value results.

$$\text{Ratio}=\frac{\sum k_i}{k_{TBS}} \quad \textbf{(28)}$$

where: k_i is the summation of thermal conductivities of layers penetrated by the thermal bridging source (W/m k) and k_{TBS} is the thermal conductivity of the thermal bridging source (W/m K).

Figure 4-8 shows the relationship between the average R-value results obtained from the isothermal, parallel path, and FE method (ANSYS) to the "Ratio" calculated using equation **(28).**

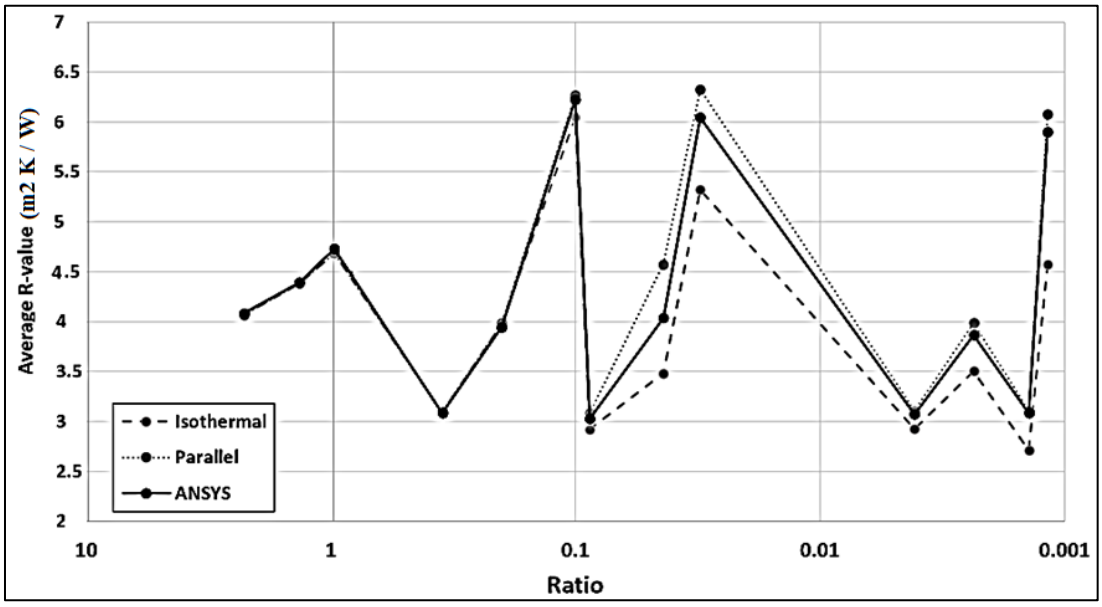

Figure 4-8: R-value results using isothermal, parallel path and ANSYS with respect to the Ratio

It is concluded that the results suggested by the Combined Method described in the International Standards ISO 6946 (ISO, 2017d), which suggested that "the total thermal resistance is computed as an arithmetic average of the thermal resistances obtained using the Parallel path and the Isothermal planes methods" is more accurate for masonry veneer walls with Ratio > 0.1. This ratio could be found in assemblies constructed using veneer ties with low thermal conductivity. Adjustment factors for Ratio ≤ 0.1 are required to satisfy the common design requirements and the possible wall cases and material properties used in practice. Adjustment

factors α and β in the form of equation **(29)** are suggested by this study to adjust and combine the values from the current analytical methods.

$$R_{\text{adjusted}} = \alpha * R_{\text{isothermal plane}} + \beta * R_{\text{parallel path}} \quad \textbf{(29)}$$

where: α and β are the adjustment factors for the R-value obtained using the isothermal method (lower limit) and the parallel path method (upper limit) respectively.

Using FEM results, adjustment factors were deduced by a procedure that is executed iteratively by comparing various solutions until a satisfactory solution is achieved. The unconstrained optimization technique was used in this study based on setting the design objective to minimize the resulting difference between the values obtained by using a suggested adjustment and the actual values obtained by the FEM simulations. The optimization objective was the minimization of the residual sum of squares (the sum of squared errors of prediction). The residual sum of squares essentially measures the variation of modelling errors. Generally, a lower residual sum of squares indicates that the regression model (suggested factors) can better explain the data, while a higher residual sum of squares indicates that the model poorly explains the data. Therefore, the residual sum of squares is the objective function that is required to be minimized. A solver was used to find an optimal (minimum) value for the objective function. The solver works with a group of variables, called decision variables or simply variable numbers, that are used in computing the formulas for the objective function and constraint. The solver adjusts the values in the decision variable (adjustment factors) to produce the required result for the objective function (the minimization of the residual sum of squares). The GRG (Generalized Reduced Gradient) algorithm was chosen to be the solving method. This solver method focuses on the gradient or slope of the objective function as the decision variable changes and determines that it has reached an optimum solution when the partial derivatives equal zero. Type A data were randomly split into training (80% = 96,000 configuration) and validation (20% = 24,000 configuration) subsets, enabling validation (Berrar, 2019).While the training subset was used for adjustment factors estimation, the validation subset was used to test the performance of the suggested factors on new data (validation data subset). Factors of α and β shown in **Table 4-5** were suggested based on the ratio shown in equation **(28).** The suggested R-value equation is as follows:

Table 4-5: Adjustment factors

	Ratio≤ 0.01	**0.01 < Ratio≤0.1**	**Ratio > 0.1**
α	0.56	0.605	0.5
β	0.455	0.385	0.5

The accuracy of the presented R-value adjustment factors was investigated for Type A models. The average error percentage between the ANSYS results and the suggested adjustments results was 4% (R^2=0.96). The average difference percentage between the results obtained by the parallel path and isothermal methods compared to the FEM results was 7% (R^2=0.943) and 12% (R^2=0.87), respectively.

4.4.2. Results for Type B

Equivalent isothermal and parallel thermal circuits were developed for $B_{(SS)}$ and $B_{(SB)}$ assemblies, as shown in **Figure 4-9** and **Figure 4-10** respectively. The case of on-surface tie assemblies was more challenging. As a result, as shown in **Figure 4-10**, three paths were considered: (1) through the wall component without ties (cavity path), (2) through the attached tie part on the concrete block (represented by R_{tie2} and R_{ins2}), and (3) through the tie body represented by R_{tie3}. In the case of addressing perforated tie types (assemblies' types B_{SB} and B_{SS}), the tie area perpendicular to the thermal flow was multiplied by factor $F_{slotted}$ presented in equation **(30)** to consider the thermal transfer reduction effect caused by the holes for the R_{tie} calculation in the thermal network.

$$F_{Slotted} = \frac{\text{Volume of the perforated tie}}{\text{Volume of the sloid tie}} \quad \textbf{(30)}$$

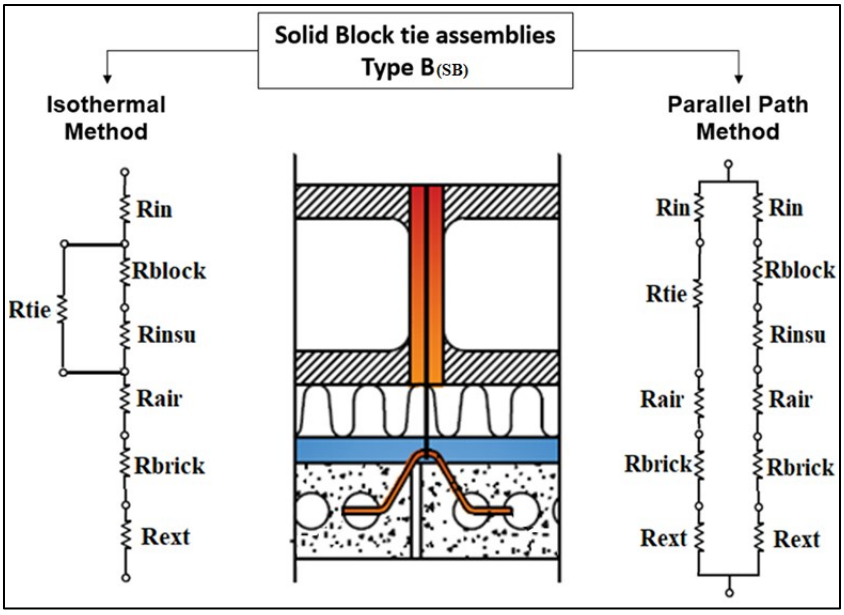

Figure 4-9: Equivalent isothermal and parallel thermal circuits for B_{SB} assemblies

(Note: R_{in} *and* R_{ext} are the interior and exterior air film resistances, R_{brick} is the thermal resistance of the bricks, R_{block} is the thermal resistance of the concrete block, R_{tie} is the thermal resistance of tie, R_{air} is the thermal resistance of the air gap, R_{insu} is the thermal resistance of insulation. All thermal resistances are in (m^2K/W))

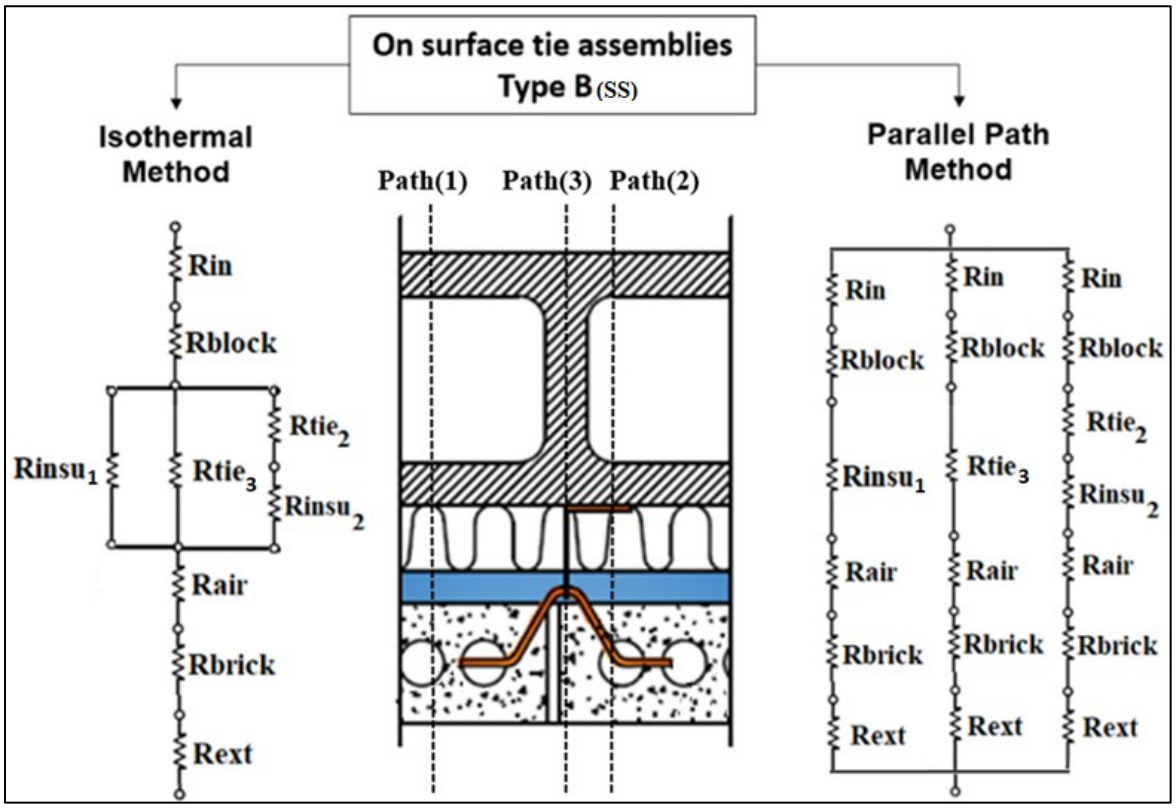

Figure 4-10: Equivalent isothermal and parallel thermal circuits for B_{SS} assemblies.

(Note: R_{in} *and* R_{ext} are the interior and exterior air film resistance, R_{brick} is the thermal resistance of the bricks, R_{block} is the thermal resistance of the concrete block, R_{air} is the thermal resistance of air gap, R_{insu} is the thermal resistance of insulation, R_{insu2} is the thermal resistance of insulation for path (2) as mentioned earlier, R_{tie3} is the thermal resistance of tie for path (3), and R_{tie2} is the thermal resistance of tie for path (2). All thermal resistances are in (m^2K/W))

The R-value of the detailed assemblies Type B was estimated using FEM simulations and the suggested adjustment factors (**Table 4-5)**. The average difference between the results obtained by the adjustments and the FEM results is 2 %. In addition, the coefficient of determination (R^2=0.98). While the average difference percentage between the results obtained by the parallel path and isothermal methods compared to the FEM results was 25.5% (R^2= 0.7) and 19% ((R^2= 0.8), respectively. **Figure 4-11** shows a comparison of the suggested adjustments with respect to the FEM simulation results.

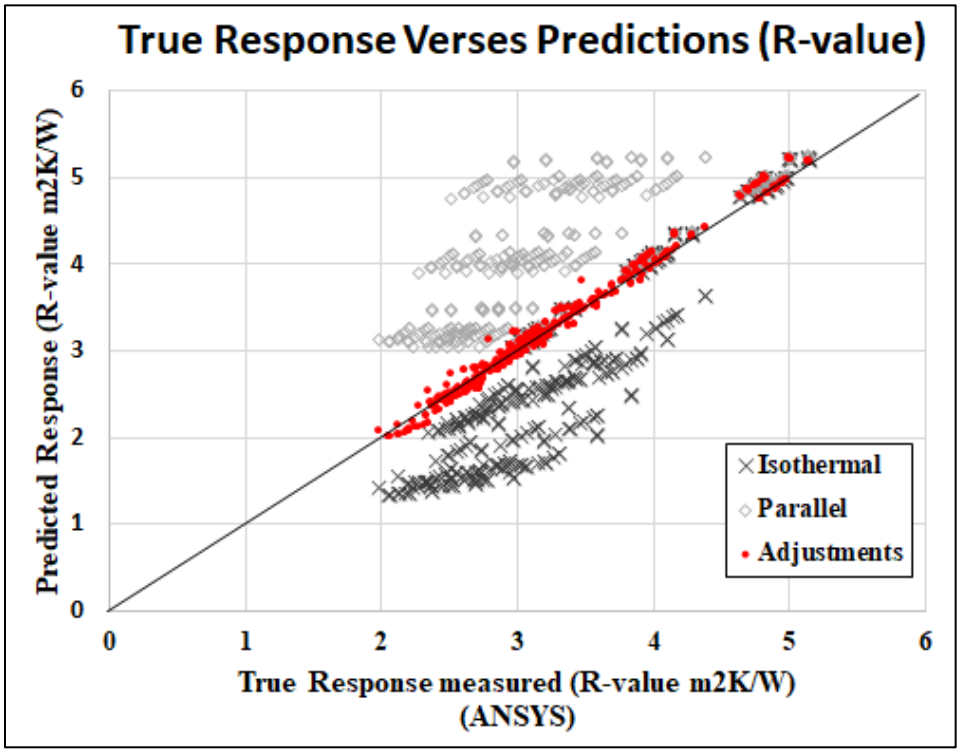

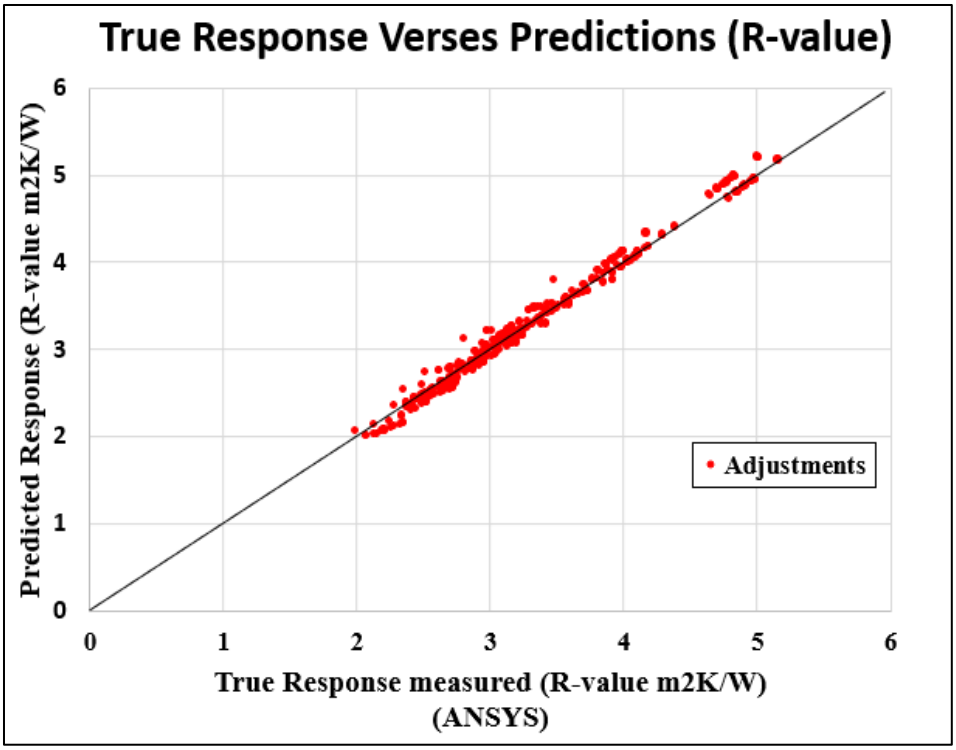

Figure 4-11: Adjusted method with respect to the Finite Element modelling results for assemblies' Type B

4.5. Conclusion

The results show that the ratio between the summation of thermal conductivities of layers penetrated by the thermal bridging source and the thermal conductivity of the thermal bridging source is a useful basis for estimating R-values for masonry walls with steel veneer ties. Results show that in the case of having a low conductive element penetrating the insulation layer, the results will be the same regardless of using the parallel path method or the isothermal plan method. In addition, the finite element simulation results were closer to the average of the isothermal and the parallel path methods in the case of the ratio between the summation of thermal conductivities of layers penetrated by the thermal bridging source and the thermal conductivity of the thermal bridging source being greater than 0.1. The suggested adjustment factors outlined above show good agreement with the modelled results, with an expected accuracy of 2%. The suggested adjustments are similar to the method outlined in ISO 6946 but with a more complex algorithm to find a suitable weighting between R-values obtained from isothermal plans and the parallel path method to represent complex geometries with thermal

bridging sources. Accurate estimations of R-values will help with reliable estimation of energy needs for the buildings, as well as improvement of the thermal envelope.

4.6. Appendix

The mesh refining for the perforated block ties and fastened on surface is shown in **Figure 4-12**.

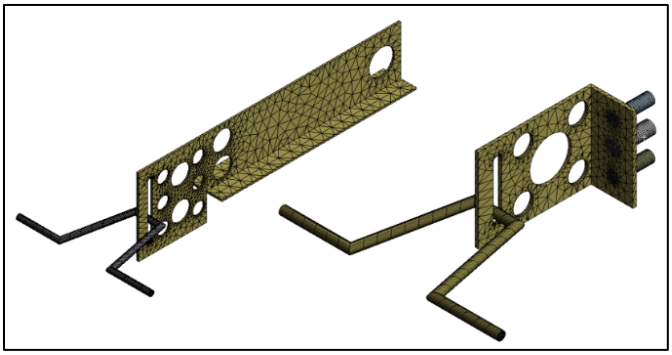

Figure 4-12: Perforated block tie and fastened on blocks surface tie meshing, respectively.

The temperature distribution for one of the studied models for Type A and B are shown in **Figure 4-13** and **Figure 4-14**, respectively.

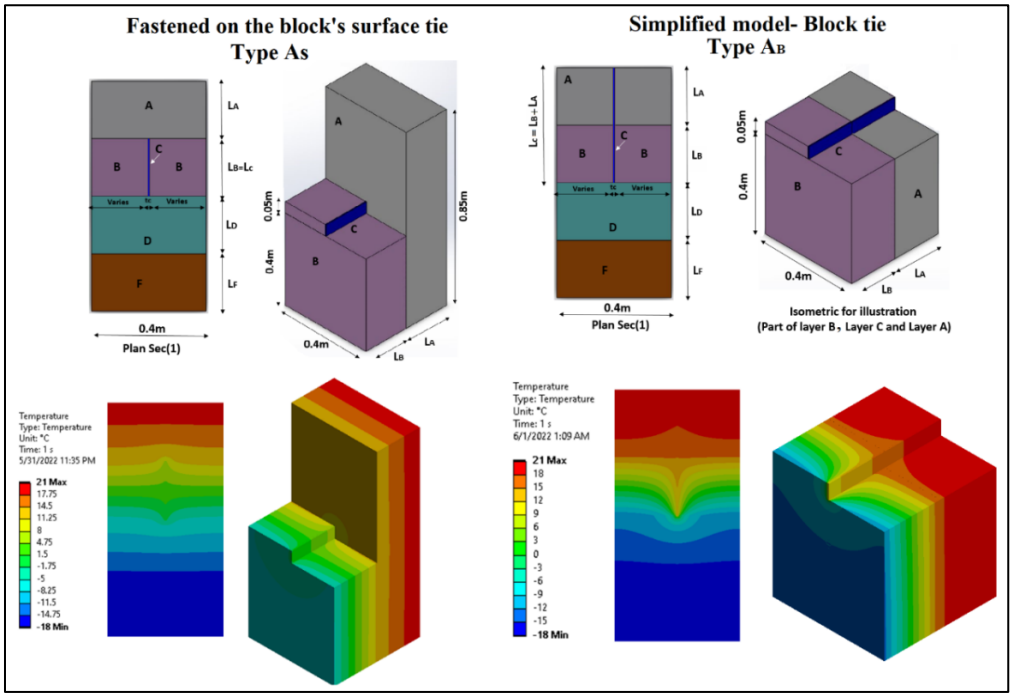

Figure 4-13: Temperature distribution (Type A)

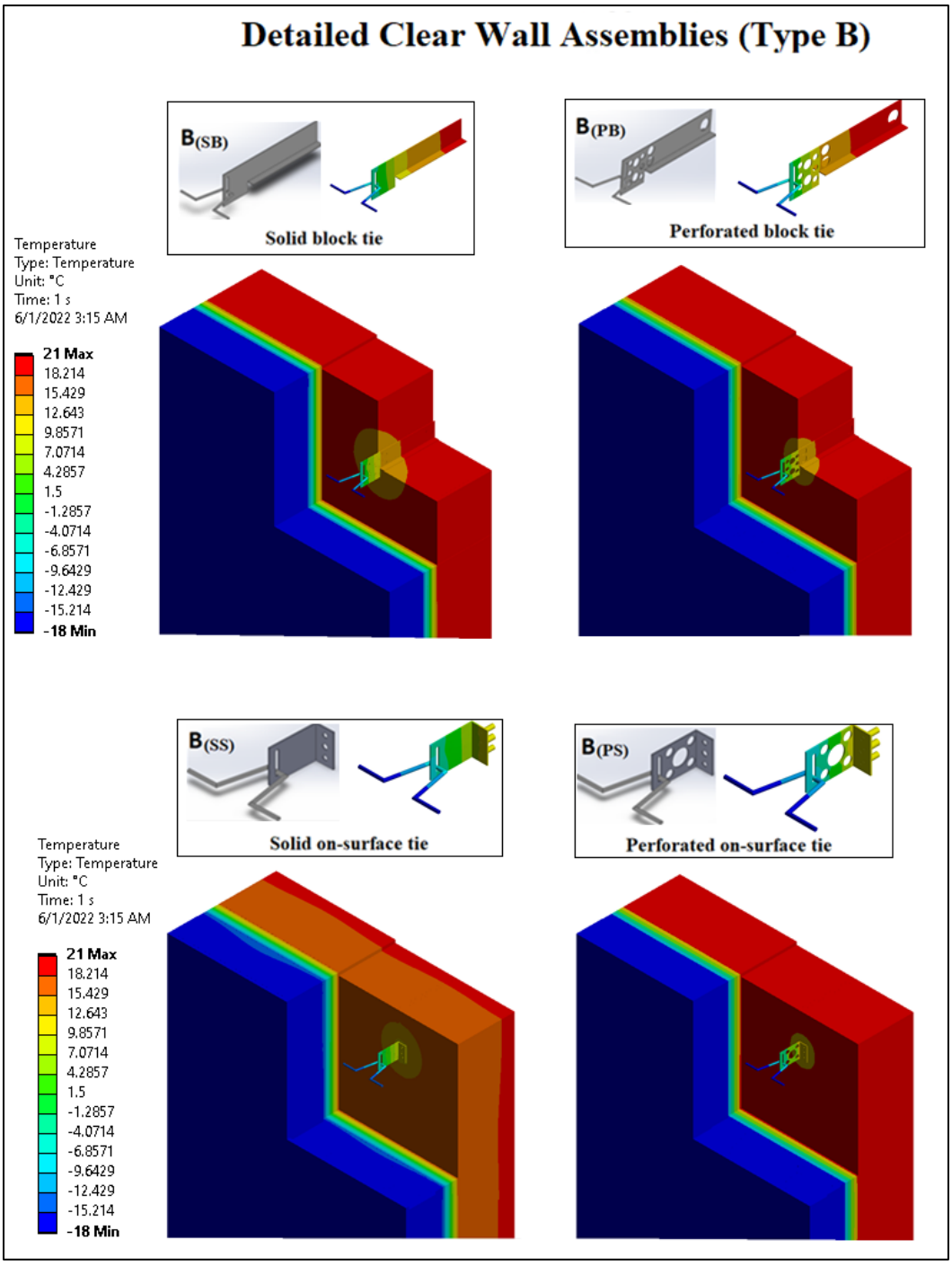

Figure 4-14: Temperature distribution and the heat flux distribution (Type B)

5. Adjustments of Existing Methods for Estimating the Thermal Resistance of Masonry Walls with Intermediate Floor Intersections

5.1. Introduction

Energy codes continue to drive the building construction industry toward more stringent thermal performance standards. Evaluation of exterior insulation in above-grade wall assemblies is becoming essential for a reliable assessment of the thermal behaviour and energy efficiency of buildings. Exterior insulation can be effective for achieving walls with higher thermal resistance values. Masonry veneer claddings are typically supported by the building structure using intermittent anchors and shelf angle bearing supports. However, elements with high thermal conductivity, such as floor intersections and cladding attachment systems, often penetrate the insulation and cause thermal bridging that leads to a significant degradation in the insulation's thermal performance. Therefore, in addition to structural and durability criteria, designers need to assess masonry veneer walls for thermal bridging. Therefore, there is an increasing need for more accurate evaluations of the thermal performance of masonry walls to satisfy the energy code requirements. This chapter discusses computer-based three-dimensional thermal modelling of four types of shelf angle support (directly attached, bracket, knife plate and HSS). This chapter is considered as an upgrade to the adjustments presented in chapter (4). It aims to suggest an adjustment of current thermal resistance estimation methods (i.e., the isothermal plane method) to include the effect of the thermal bridge resulting from veneer ties and linear slab intersections in the R-value estimations. Therefore, the presented suggested adjustments in this chapter are applied to estimate the effective R-value of the whole assembly including intermediate slab intersection. The analytical R- values obtained from the suggested adjustments were compared with numerical simulations using a 3D steady-state finite element method (FEM) in addition to experimental validation obtained from the literature. The results showed an average difference of 3.6% between the studied finite element simulations (ANSYS) and the R-value obtained using the suggested adjustments.

With the rapid change and higher standards of thermal requirements for building envelopes, masonry construction needs viable design improvements to meet stringent building energy codes as the minimum effective thermal resistance (R-value) has increased over time. In the 2017

National Energy Code of Canada for Buildings (NECB, 2017a), R-values have been increased by an average of 25% for some elements compared to its previous edition. This increase is expected to improve the overall energy performance of buildings by 10% to 15% in comparison to previous versions of the code (NECB, 2011 ; NECB, 2015).

The thermal properties of materials have a critical influence on the building's thermal performance. Due to their significant thermal energy storage capacity (i.e., thermal mass), masonry buildings can often provide superior thermal performance compared to light-frame buildings with similar thermal insulation values (ACI, 2002; Huberman and Pearlmutter, 2004; Huberman and Pearlmutter, 2008). One of the challenges in the assembly configuration is thermal bridging. Thermal bridging occurs when highly conductive structural components penetrate the insulation plane (CCMP, 2013). Thermal bridging should be minimized in designs and carefully calculated as it is considered the main source of thermal performance deficiency in masonry walls.

The exterior masonry wall consists of a clear wall and interface details. A "clear wall" is defined as a planar area with regularly spaced structural components that are free of windows, doors, and other irregularities (Barnes et al., 2013). Clear wall assemblies can contain thermal bridges from uniformly distributed secondary structural components, which is necessary to withstand loads. These thermal bridges do not include the ones related to intersections of the primary structure. The changes in construction or geometry that disrupt the uniformity of clear field assemblies are known as interface details. These details include slab edges, wall transitions, parapets, corners, and wall penetrations. Determining the impact of heat flow through clear field assemblies and interface details is necessary to accurately assess the thermal resistance of building envelope assemblies (ASHRAE, 2017c). This chapter focuses on estimating the impact of heat flow through interface details with slab intersections.

The typical components of concrete masonry are: concrete blocks, mortar, insulation boards, veneer ties, shelf angles, and air gaps in the case of brick veneer masonry walls. **Figure 5-1** shows the main masonry wall components addressed in this chapter. Shelf angles are anchored to structural backup using fasteners. Recently, intermittent structural support for shelf angles, which offset shelf angles from backing systems and reduce the cross-sectional area penetrating the insulation, thus minimizing thermal conductance, has been introduced to the market to reduce the

thermal bridging effect, such as knife plates (i.e., I-shape steel) and hollow structural section (HSS) tubes. **Figure 5-2** shows the common shelf angle types used in the market.

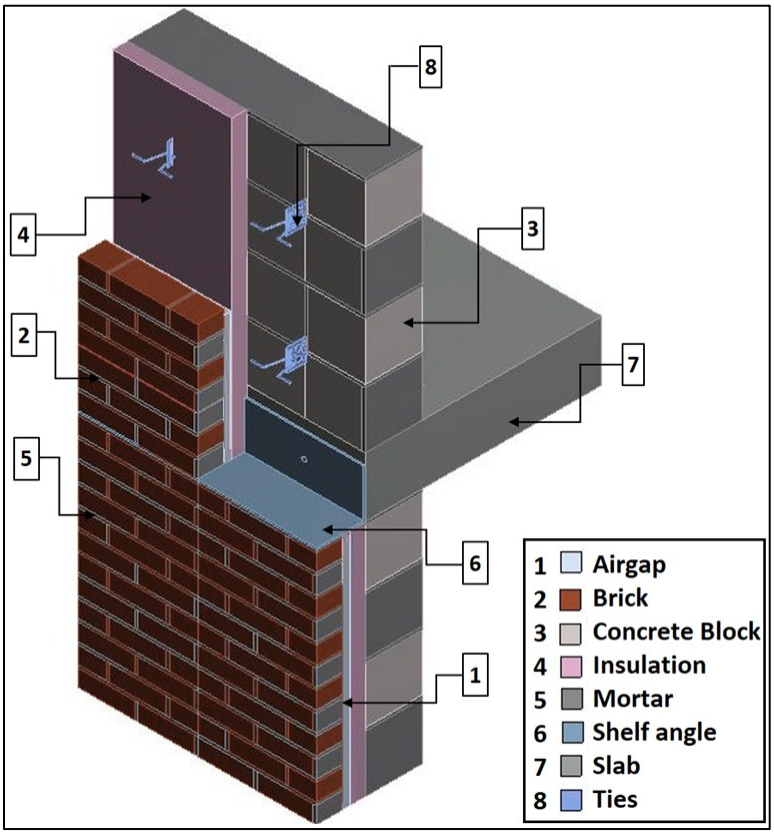

Figure 5-1: Components of masonry cavity walls with intermediate slab intersection

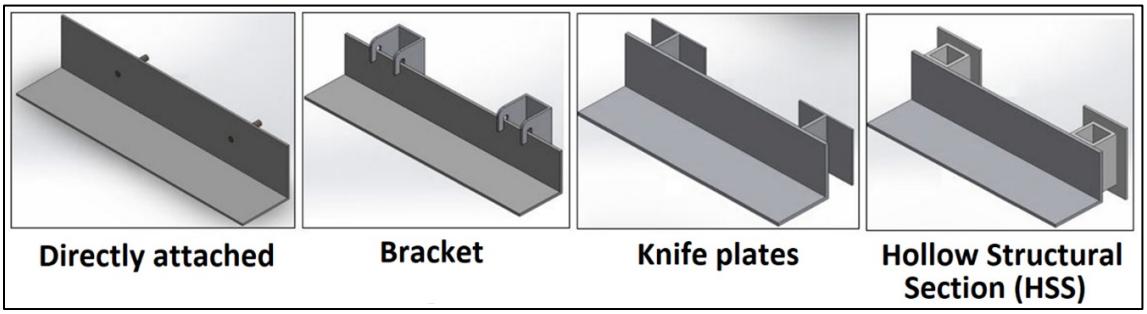

Figure 5-2 : Common shelf angles types

Thermal bridging should be minimized in the design and calculated carefully as it is considered the main reason for thermal performance deficiency in masonry walls. To comply with continuously evolving energy code requirements, the masonry and construction industries are developing new building techniques and are in search of an effective approach to calculate thermal resistance. Therefore, there is a need to review and improve the method for the

estimation of R-values. To serve the aforementioned purposes, this chapter aims to suggest adjustments to current thermal resistance estimation methods (i.e., isothermal plane method) to be applied on exterior masonry veneer walls considering the effect of the thermal bridge caused by the veneer ties, shelf angle and floor intersection slab. The significance of such work would help designers to estimate the thermal bridging effect caused by the veneer ties and shelf angles. In addition, accurate estimations of R-values will help with reliable estimation of energy needs for the buildings, with improvements to the thermal envelope and in the calculation of required heating ventilation and air conditioning (HVAC) equipment. This chapter is structured as follows, after the introduction section, a literature review describing the commonly used analytical methods and tools available in the previous studies for estimating the effective R-value is presented. Then, a description of the finite element models used in this study. This is followed by the development of the adjustment factors. Then, a detailed application of the suggested adjustments along with a comparison with the finite element simulation results is presented. Finally, the results and main concluding remarks are discussed.

5.2. The Point and Linear Transmittance method

In addition to the simplified analytical methods used to estimate the thermal resistance or transmittance of building elements discussed in chapter **(4)** section **(4.2)**. The Point and Linear Transmittance method is widely used in interface details (e.g., slab intersections). In this approach, the thermal transmittance introduced by thermal bridging components additional to that of the clear wall is called the point or linear transmittance, depending on the geometry of the thermal bridges. The linear transmittance Ψ (W/ (m K) due to linear thermal bridges (e.g., slab edges, shelf angles) can be calculated as follows:

$$\Psi = \frac{Q_A - Q_B}{L} \quad \textbf{(31)}$$

Where Q_B is the heat flow of the clear field of an assembly (W/K); Q_A is the heat flow of the assembly with a portion of the clear field replaced with intersections (W/K); and L is the assembly width (m), which represents the linear length of the intersection.

The point transmittance is similar to the linear transmittance but for point anomalies, such as beam end penetrations and intersections between linear details. The point transmittance χ (W/K) is a single additive of the amount of heat, as shown in Equation **(32**)

$$\chi = Q_1 - Q_2 \quad \textbf{(32)}$$

where, Q_1 is the heat flow of the whole assembly unit with intersections (W/K), and Q_2 is the heat flow of the assembly with no intersections (W/K).

In calculating the overall thermal transmittance of an entire building or wall, all thermal transmittances are categorized into three groups: clear field transmittance **(U_o),** linear transmittance (Ψ**),** and point transmittance *(χ)* (Hydro, 2016b). The overall U-value (W/m^2·K) is calculated as follows:

$$U_T = \frac{\sum(\Psi \times L) + \sum \chi}{A_{Total}} + U_O \quad \textbf{(33)}$$

Where U_o is the clear field thermal transmittance (W/m^2·K), A_{total} is the total opaque wall area (m^2), ψ is the point transmittance heat flow from the linear thermal bridge (W/(m K)), L is the length of the linear thermal bridge (m), and χ is the heat flow from the point thermal bridge (W/K).

The overall U-value for a wall can only be determined using Point and Linear Transmittances approach when the thermal performance values for the clear field (U_o), linear **(Ψ),** and point **(χ)** transmittances are known, which requires computer simulations or experimental testing.

5.3. Methodology

This chapter investigates the thermal resistance of masonry wall assemblies with floor intersections. The objective of this chapter is to develop an adjustment of current thermal resistance estimation methods, the isothermal plane method, to include the effect of the thermal bridge resulting from different types of veneer ties, in addition to the shelf angle and the slab penetration on the total R-value estimations.

5.3.1. Finite Element Analysis Simulations

Experimental measurements of an element's thermal behaviour can be expensive, especially for large-sized specimens. Computational numerical simulation is considered a practical alternative, as this method is cost-effective and accurate. Many thermal analysis programs are designed to simulate thermal problems in two dimensions, such as THERM, HEAT2, Energy2D (Xie, 2012),

and three dimensions, such as ANSYS, ABAQUS, HEAT3, and SIEMENS. Several studies on masonry walls have been conducted to improve and validate the simulation approaches with experimental data (del Coz Diaz et al., 2006; Norris et al., 2012a; Desjarlais and McGowan, 1997). Those studies showed good agreement between the numerical simulation and experiment results. Validated simulation approaches were then used to simulate the thermal performance of other wall configurations. If a physical test is not possible, computer simulation provides the next most accurate results. Computer simulation can also provide information on surface temperature distribution, which may be important for evaluating condensation-related problems. The results should be within ±5% of the test result (McGowan and Desjarlais, 1995).

ANSYS Workbench (ANSYS, 2019) was used to perform steady-state finite element thermal analysis simulations of typical brick veneer cavity wall assemblies. Simulations were conducted to calculate the overall R-value for different wall configurations (discussed in section **5.3.2**). There are some modelling assumptions considered in this study; all models were analyzed at a steady-state thermal analysis and air leakage was not considered. The models were evaluated at -18C°, which is the exterior temperature, and 21 C°, which is the interior. Contact resistance was not considered in the simulations. All the material properties were considered from the ASHRAE Handbook (ASHRAE, 2019b). The air gap between the wall backup and the brick veneer thermal properties were obtained from the literature (Hershfield, 2016b; Roppel et al., 2011; Hydro, 2016a). The element used to simulate the wall components in the ANSYS modelling is SOLID70 based on its properties which complies well with the assemblies required to be investigated. SOLID70 has a three-dimensional thermal conduction capability. The element has eight nodes with a single degree of freedom, temperature, at each node. The element can be applied to a three-dimensional, steady-state or transient thermal analysis. Meshing was done by using ANSYS's advanced sizing feature. A mesh was generated that is relatively fine for specific parts of the model (such as the ties). A sequence of mesh convergence tests had been conducted for a suitable balance between the accuracy and computational time of the addressed models. The convergence study on the mesh size was carried out by evaluating the variation of the heat flux versus the number of mesh nodes. It was found that the mesh size of 10 mm (which corresponds to 2,670,876 nodes for the intermediate floor assemblies) is appropriate for the accuracy and model running time for all studied cases. **Figure 5-3** shows the convergence of the heat flux versus the number of nodes used in the mesh.

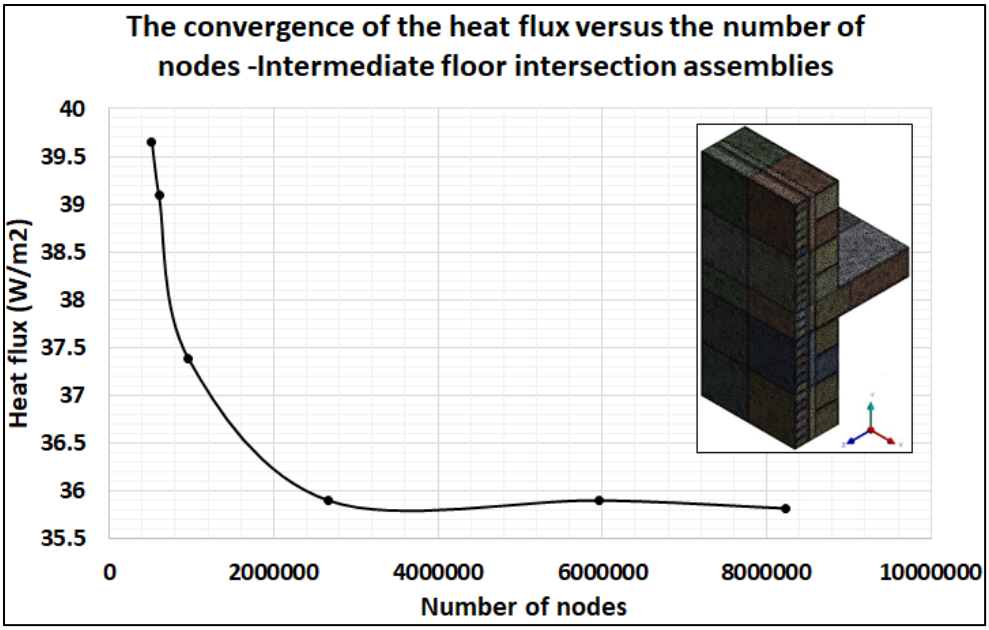

Figure 5-3: Convergence of the heat flux versus the number of nodes used in the mesh for intermediate floor intersection assemblies

The general heat conduction equation in rectangular coordinates in the case of constant thermal conductivity is simplified to consider the steady-state condition with no heat generation (Laplace equation) (ASHRAE, 2021a):

$$\frac{\partial}{\partial x}\left(k_x \frac{\partial t}{\partial x}\right) + \frac{\partial}{\partial y}\left(k_y \frac{\partial t}{\partial y}\right) + \frac{\partial}{\partial z}\left(k_z \frac{\partial t}{\partial z}\right) = 0 \quad \textbf{(34)}$$

where: $k_x, k_y, k_z =$ thermal conductivity in direction of x, y and z axes, (W/m.K), and $\frac{\partial t}{\partial x}, \frac{\partial t}{\partial y}\ and\ \frac{\partial t}{\partial z}$ are the gradient of temperature (change in temperature per unit length perpendicular to isothermal surfaces) along x, y and z axis, respectively (K/m).

If the steady-state heat flux is only in one direction (e.g., perpendicular to the building envelope) and materials are assumed to be isotropic, heat transfer by conduction in a solid is governed by Fourier's law and can be simplified for each material layer within the building envelope as follows (ASHRAE, 2021a):

$$q = -k_m \frac{\Delta t}{\Delta x} = -U\,\Delta t = -\frac{1}{R}\,\Delta t \quad \textbf{(35)}$$

where: Δt is the temperature difference between two interfaces of one material layer (K), Δx is the layer thickness (m), k_m is the mean thermal conductivity of the material layer with a thickness Δx (W/m K), U is the thermal conductance of layer with a thickness Δx (W/ m^2 K), and R is the thermal resistance of layer with a thickness Δx (m^2 K /W).

For verification purposes, models were constructed and simulated to compare the simulation results with data from the literature. Results presented in the literature were obtained from three-dimensional finite element analysis and were compared with experimental results obtained from guarded hotbox measurements and data provided in ISO Standard 10211 (ISO, 2017c). The validation models addressed were five clear wall models with galvanized steel solid block ties using different insulation R-values (R-5, R-10, R-15, R-20, and R-25). While the intermediate intersection was a directly attached galvanized steel shelf angle, and the ties used were also solid galvanized block ties. Five intermediate intersection assemblies were addressed using insulation R-values of R-5, R-10, R-15, R-20. and R-25. The validation models were obtained from detail number 7.2.14 building envelope thermal envelope guide version 1.4 Appendix B Catalogue Thermal Data Sheets (Hershfield, 2020) . **Figure** 5-4 shows a comparison between the results obtained from the validation modelling and literature. The comparison showed an average difference of 7.13% in the case of intermediate floor intersection assemblies. While 6.8% in the case of the clear wall assemblies.

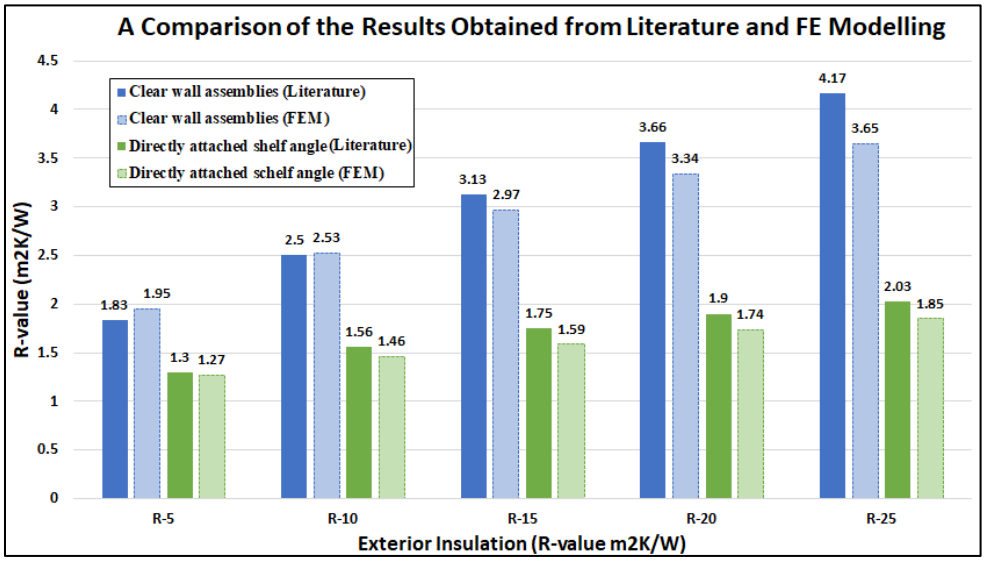

Figure 5-4: A comparison between the results obtained from the validation modelling and literature

5.3.2. Models Description

Assemblies shown in **Figure** 5-5 represent intermediate floor intersections (i.e., floor slabs). All assemblies were addressed using solid block ties only. Besides, four shelf angles were considered: directly attached large shelf angle, bracket shelf angle, knife plate, and hollow structural section (HSS) tubes.

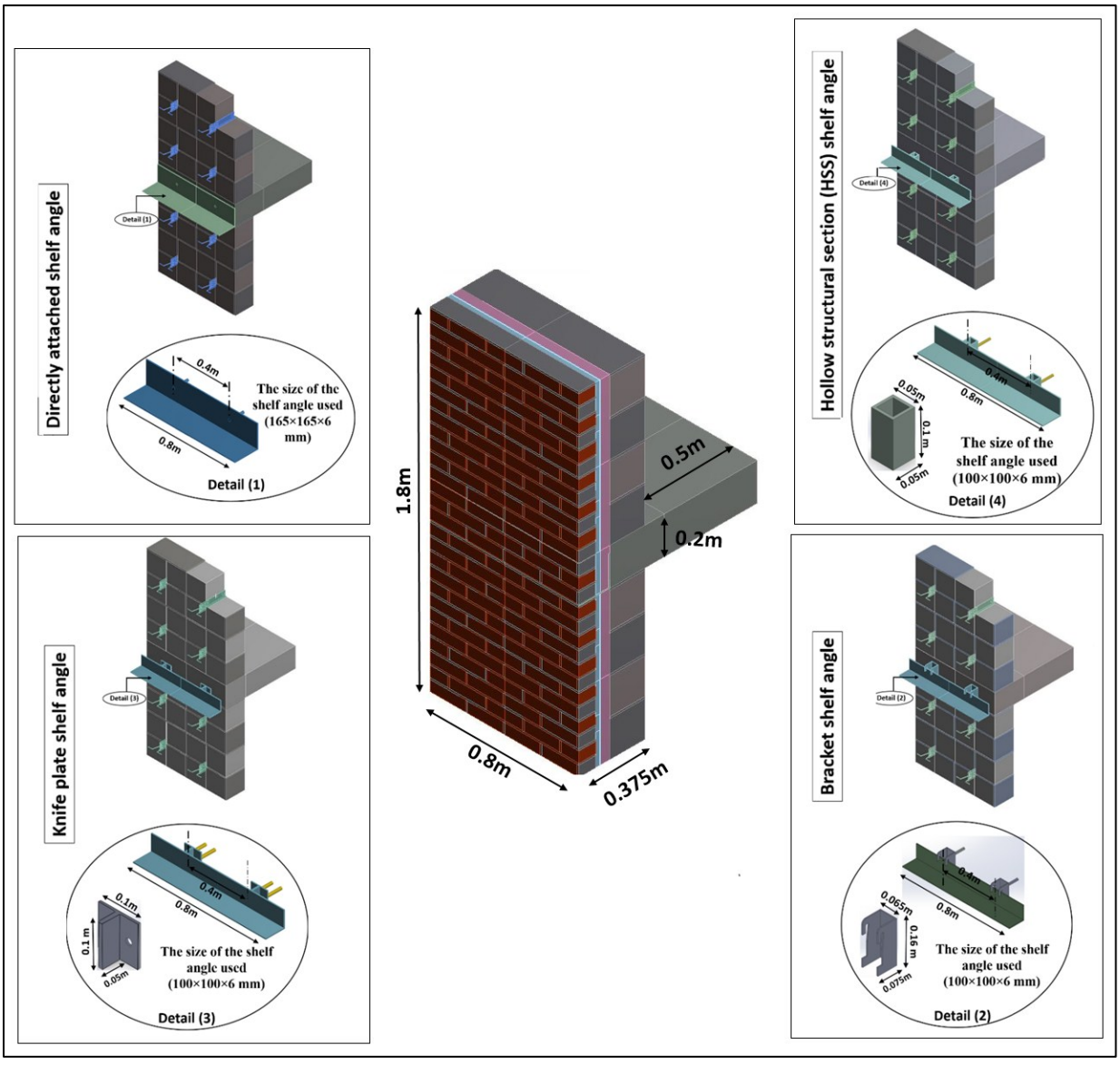

Figure 5-5: Type and dimensions of the 3D studied intermediate floor intersections finite element assemblies

Table 5-1 presents the fixed material properties for all the studied assemblies. All models with an interior and exterior air film were considered in the analysis with a nominal resistance of 0.11 and 0.03 m^2K/W, respectively. All the material properties (shown in **Table 5-2**) were considered from the ASHRAE Handbook (ASHRAE, 2019b). The air gap between the wall back-up and the brick veneer thermal properties were obtained from the literature (Hershfield, 2016b; Roppel et al., 2011; Hydro, 2016b). The slab extension of 0.5 m (**Figure** 5-5**)** showed a uniform temperature distribution and heat flux, indicating that a sufficient slab extension length is considered for representing the effective thermal bridging zone. 240 models were considered in this study (4 types of shelf angles x 2 shelf angle materials x 3 insulation R-value x 2 grout conditions x 5 block density = 240). Variables were considered in the simulated assemblies to address the suggested adjustment factors and validate the suggested calculation method for complex geometries and different conditions. The data was randomly split into training (80% = 192 configurations) and validation (20% = 48 configurations) subsets, enabling validation (Berrar, 2019). While the training subset was used for adjustment factors estimation, the validation subset was used to test the performance of the suggested factors on new data (validation data subset).

Table 5-1: Common material thickness and properties used in the studied scheme

Component	**Thickness (mm)**	**Conductivity (W/m K)**
Standard concrete Block Size Block 390X190X190 mm (Size block no.20) (Sturgeon et al., 2013a; Sturgeon et al., 2013b)	190	Varies
Concrete slab	200	1.8
Brick veneer	90	0.81
Air Gap (assumed vented)	25	0.3571
Cement Mortar	10	1.2
Masonry ties (400mm on center)	14 gauge	Varies
Insulation	50	Varies

Table 5-2: The variables considered in each studied scheme

Schemes	**Variables considered**
General variables considered for each assembly	insulation R-value, concrete block density, concrete blocks' type, shelf angle material, shelf angle type
Thermal insulation values in R, BTU/($ft^2 \cdot °F \cdot hr$) and in (m^2K/W)	R-15 (2.64), R-20 (3.52), R-25(4.40)
Block Density (kg/m^3) and	Hollowed: 2100(k=1.17), 1800(k=0.87), 1550(k=0.66), 1380 (k=0.6),

corresponding conductivity (k=W/m K)	1150(k=0.35) Fully grouted: 2100(k=1.9), 1800(k=1.13), 1550(k=0.78) , 1380(k=0.6), 1150(k=0.36)
Block Density (kg/m^3) and corresponding compressive strength (f_m') in MPa	For the grouted hollow units: 2100 and 1800 (f_m'=13.5),1550 (f_m'=10),1380 (f_m'=7.5) and 1150 (f_m'=5) For the un-grouted hollow units 2100 and 1800 (f_m'=17.5),1550 (f_m'=13),1380 (f_m'=10) and 1150 (f_m'=6.5)
Grout conditions	Hollow block wall, Fully grouted wall
Tie type	Block solid tie
Tie thermal conductivity (k=W/m K)	Galvanized steel (k=50)
Shelf angle type	Directly attached shelf angle, Bracket shelf angle, Knife plate, HSS shelf angle (Shown in Figure 5-5)
Shelf angle materials (k=W/m K)	Galvanized steel(k=50), Stainless steel (k=17)

5.3.3. Adjustment Description

All addressed assemblies were divided into two parts; the clear wall and the shelf angle. All assemblies have similar clear wall parts, e.g. dimensions, number of ties, and ties type, and material. The assemblies have four different shelf angle parts representing the directly attached shelf angle, bracket, knife plate and HSS. Equivalent isothermal thermal circuits were developed for the clear wall part and for the different shelf angle parts, as shown in **Figure 5-6**, and **Figure 5-7,** respectively.

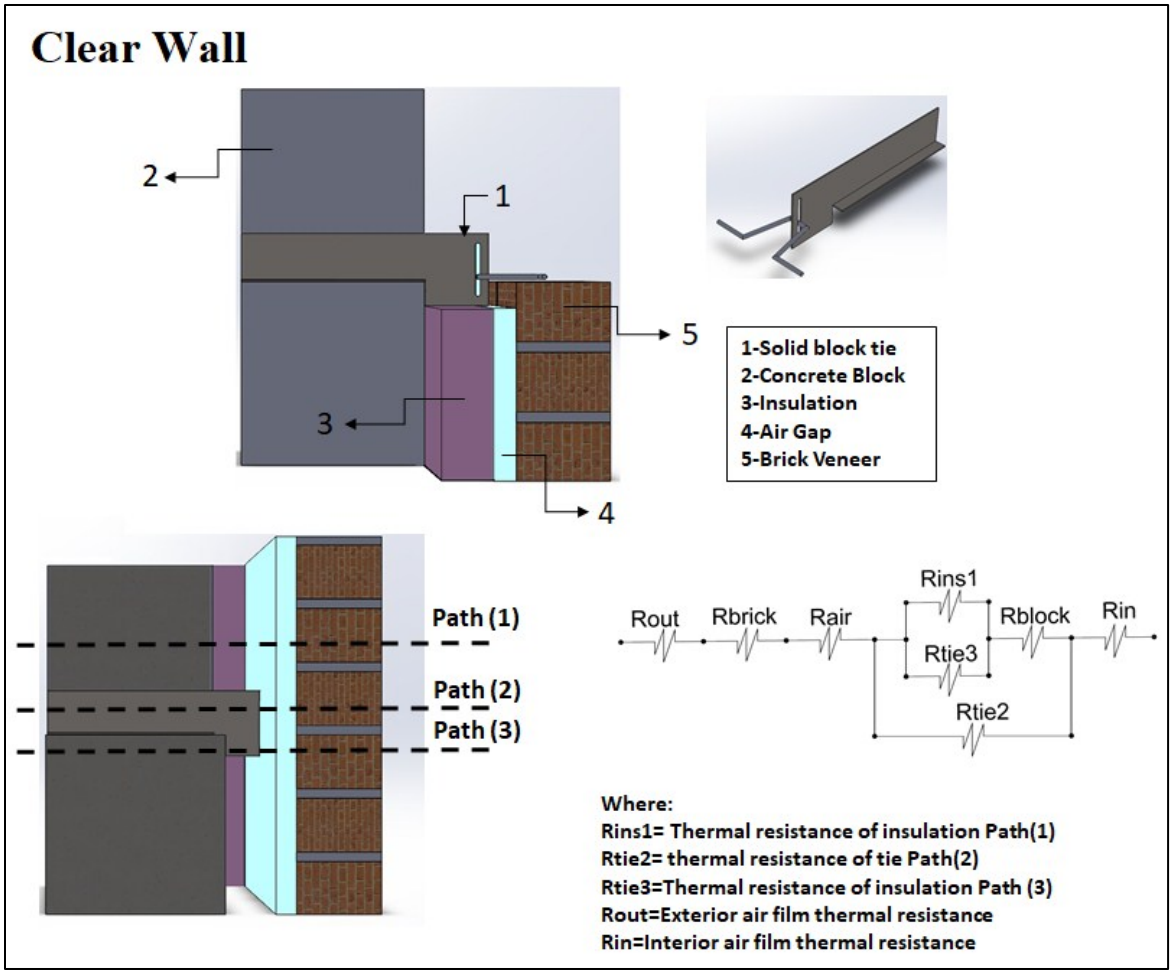

Figure 5-6: Equivalent isothermal circuits for clear wall part (all shown images are side view)

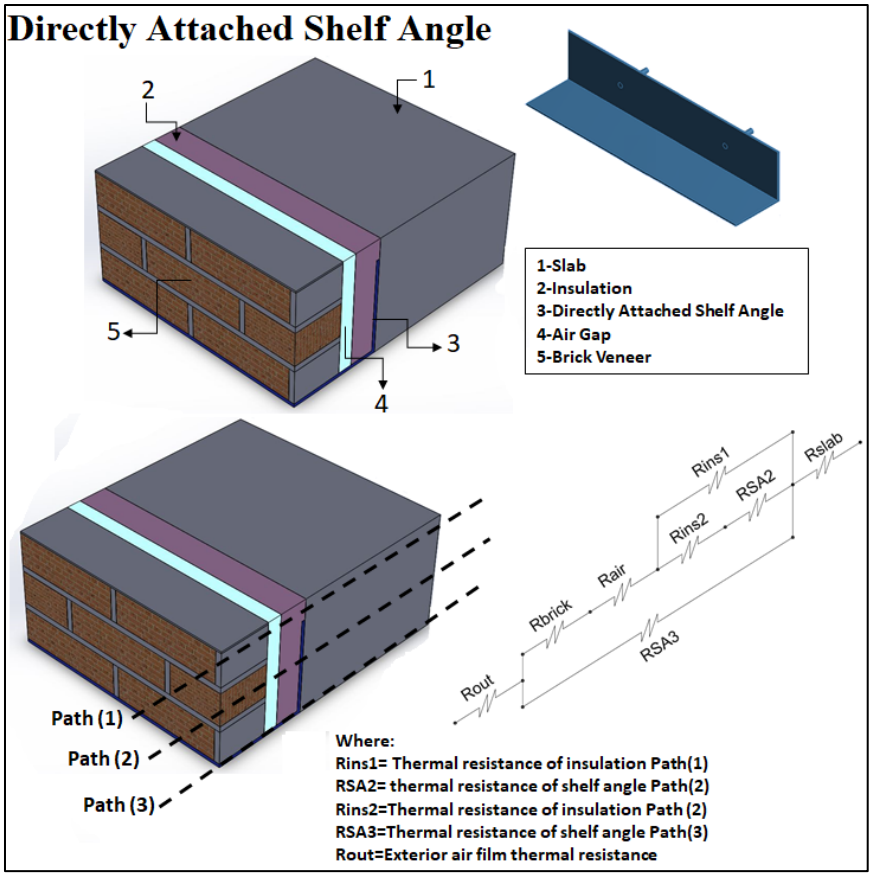
Directly Attached Shelf Angle
1
2
3
4
5
1-Slab
2-Insulation
3-Directly Attached Shelf Angle
4-Air Gap
5-Brick Veneer
Path (1)
Path (2)
Path (3)
Rins1
RSA2
Rslab
Rins2
Rair
Rbrick
RSA3
Rout
Where:
Rins1= Thermal resistance of insulation Path(1)
RSA2= thermal resistance of shelf angle Path(2)
Rins2=Thermal resistance of insulation Path (2)
RSA3=Thermal resistance of shelf angle Path(3)
Rout=Exterior air film thermal resistance

(a)

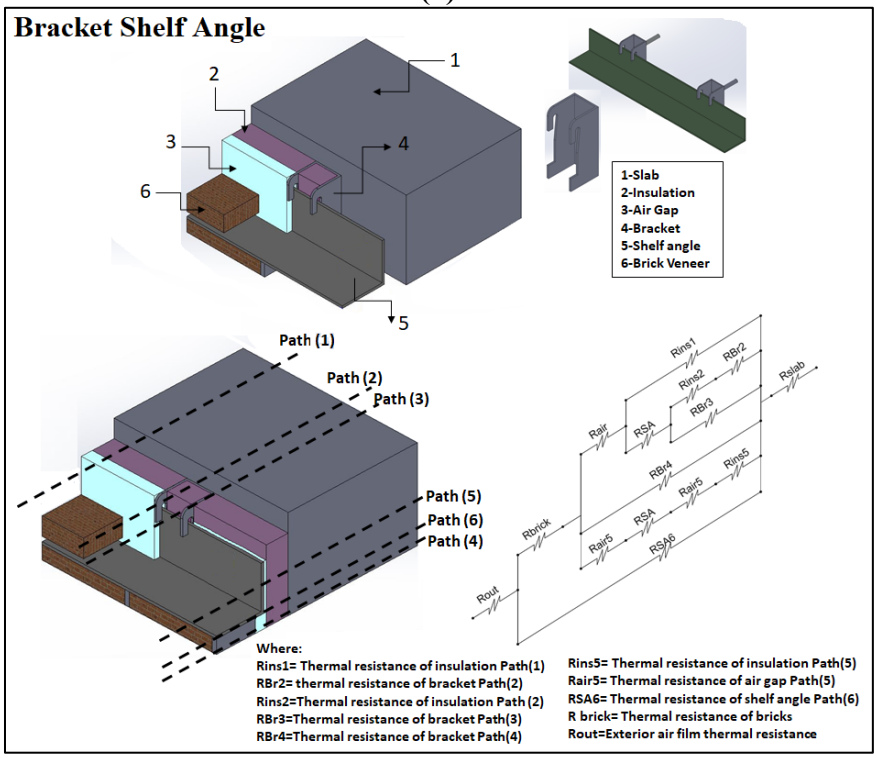
Bracket Shelf Angle
1
2
3
4
5
6
1-Slab
2-Insulation
3-Air Gap
4-Bracket
5-Shelf angle
6-Brick Veneer
Path (1)
Path (2)
Path (3)
Path (5)
Path (6)
Path (4)
Rins1
RBr2
Rins2
Rslab
RBr3
Rair
RSA
RBr4
Rins5
Rair5
Rbrick
RSA
Rair5
RSA6
Rout
Where:
Rins1= Thermal resistance of insulation Path(1)
RBr2= thermal resistance of bracket Path(2)
Rins2=Thermal resistance of insulation Path (2)
RBr3=Thermal resistance of bracket Path(3)
RBr4=Thermal resistance of bracket Path(4)
Rins5= Thermal resistance of insulation Path(5)
Rair5= Thermal resistance of air gap Path(5)
RSA6= Thermal resistance of shelf angle Path(6)
R brick= Thermal resistance of bricks
Rout=Exterior air film thermal resistance

(b)

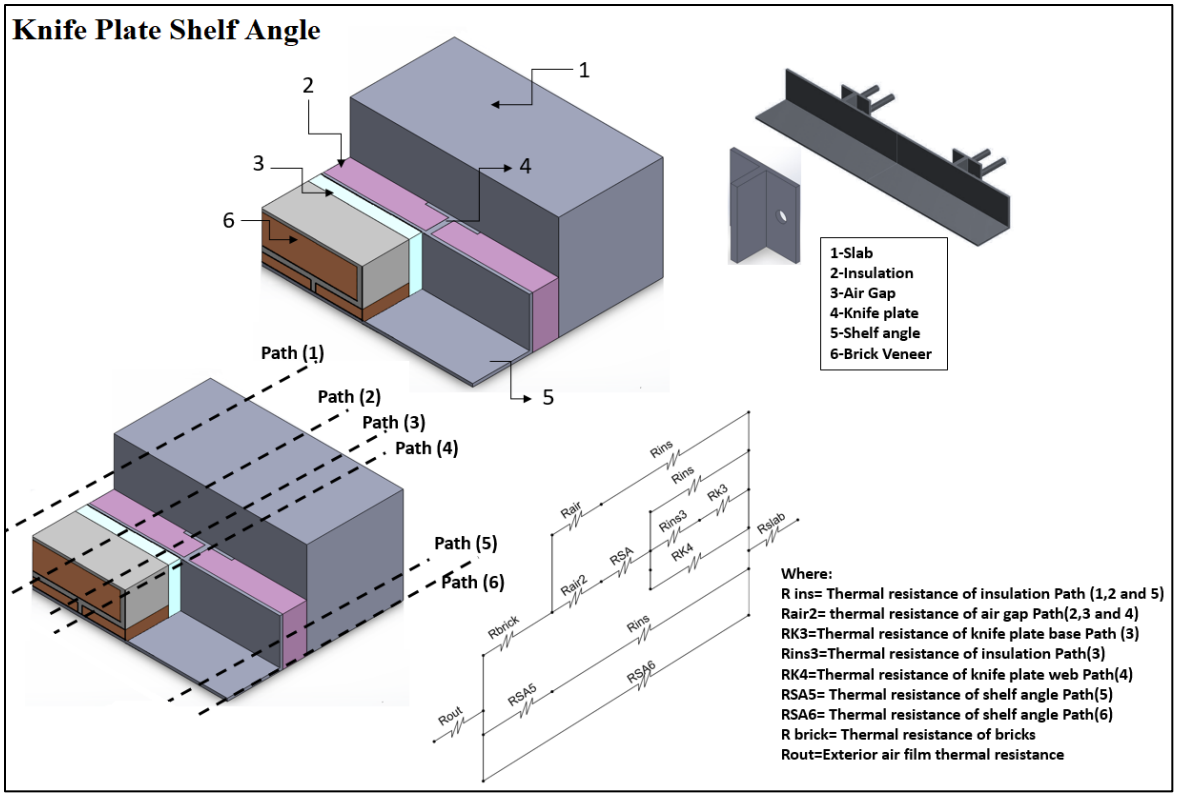

(c)

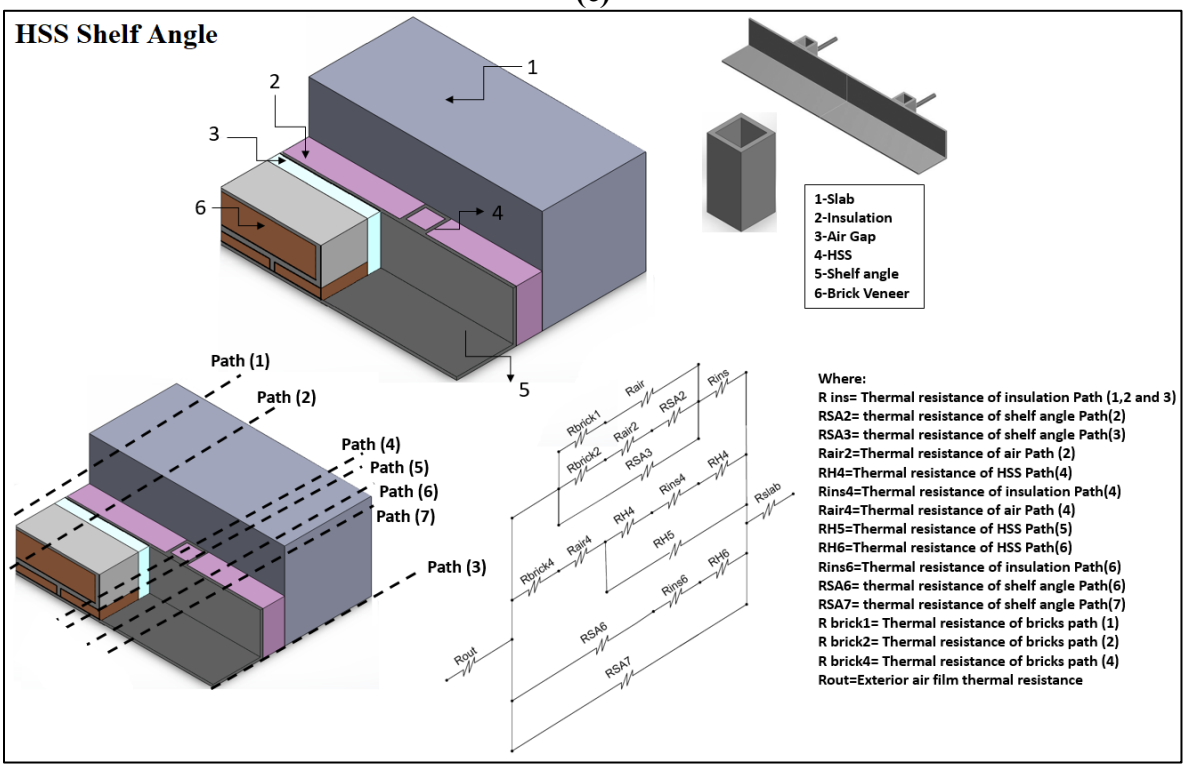

(d)

Figure 5-7: Equivalent isothermal circuits for shelf angle parts, (a) directly attached, (b) Brackets, (c) Knife plate and (d)HSS respectively

The final R-value was estimated by determining the R-value obtained from the clear wall and the shelf angle part as shown below;

$$R_{effective} = \frac{1}{U_{effective}} = \frac{1}{\%Clear\ wall/R_{clear\ wall} + \%Shelf\ angle/R_{shelfangle}}$$

(36)

where; $R_{effective}$ is the total R-value of the assembly ($m^2 \cdot K/W$), $U_{effective}$ is the total thermal transmittance of the assembly ($W/m^2 \cdot K$, % clear wall and % shelf angle are the area percentage of the clear wall and the shelf angle parts respectively. $R_{clear\ wall}$ is the thermal resistance ($m^2 \cdot K/W$) of the clear wall part obtained by using the isothermal plane method as shown in **Figure 5-6**. $R_{shelfangle}$ is the thermal resistance ($m^2 \cdot K/W$) of the shelf angle part obtained by using the isothermal plane method as shown in **Figure 5-7**.

5.4. Results

Using FEM results, adjustment factors were deduced by a procedure that is executed iteratively by comparing various solutions until a satisfactory solution is achieved. The unconstrained optimization technique was used in this study based on setting the design objective to minimize the resulting difference between the values obtained by using a suggested adjustment and the actual values obtained by the FEM simulations. The optimization objective was the minimization of the residual sum of squares (the sum of squared errors of prediction). The residual sum of squares essentially measures the variation of modelling errors. Generally, a lower residual sum of squares indicates that the model (with suggested factors) can better explain the data, while a higher residual sum of squares indicates that the model poorly explains the data. Therefore, the residual sum of squares is the objective function that is required to be minimized. A solver was used to find an optimal (minimum) value for the objective function. The solver works with a group of variables, called decision variables or simply variable numbers, that are used in computing the formulas for the objective function and constraint. The solver adjusts the values in the decision variable (adjustment factors) to produce the required result for the objective function (the minimization of the residual sum of squares). The GRG (Generalized Reduced Gradient)

algorithm was chosen to be the solving method. This solver method focuses on the gradient or slope of the objective function as the decision variable changes and determines that it has reached an optimum solution when the partial derivatives equal zero. The adjustment factors were categorized based on the shelf angle material type (thermal conductivity) and the shelf angle shape as shown in **Table 5-3.** The results showed a smooth trend. Therefore, further data categorization (to achieve better accuracy) using the ratio presented in chapter (4)- equation (28) was not needed. One adjustment factor was suggested for each case and categorizing the assemblies based on the shelf angle, material type, and shape was sufficient to achieve an acceptable accuracy as shown in **Table 5-3.**

Table 5-3: Adjustment factors

Shelf angle Material / Shelf angle type	Galvanized steel (K=50 W/m k)	Stainless steel (K=17 W/m k)	% Difference between FE and adjustment results (Galvanized steel)	% Difference between FE and adjustment results (Stainless steel)	% Difference between FE and adjustment results (Average)
Directly attached Shelf	0.85	0.9	5.3	3.6	4.5
HSS	0.8	0.9	1.5	0.78	1.18
Knife Plate	0.85	1	1.7	1.4	1.5
Bracket	1	1	4.2	2.8	3.5

A comparison of the suggested adjustments with respect to the finite element modelling R-value results for the four-shelf angles addressed is shown in **Figure 5-8**. A comparison of the suggested adjustments with respect to the FEM simulation results is shown in **Figure 5-9**. A ccomparison between different walls showing the thermal distribution and the heat flux for cases with an insulation value of R-20 insulation, fully grouted blocks and concrete blocks' density of 1550 Kg/m^3 is shown in **Figure 5-10** and **Figure 5-11 .** The accuracy of the presented R-value multipliers was investigated by computing the coefficient of determination R^2 for the studied assemblies, which is equal to 0.95, and the average error percentage between the ANSYS results and the suggested results was 3.1%.

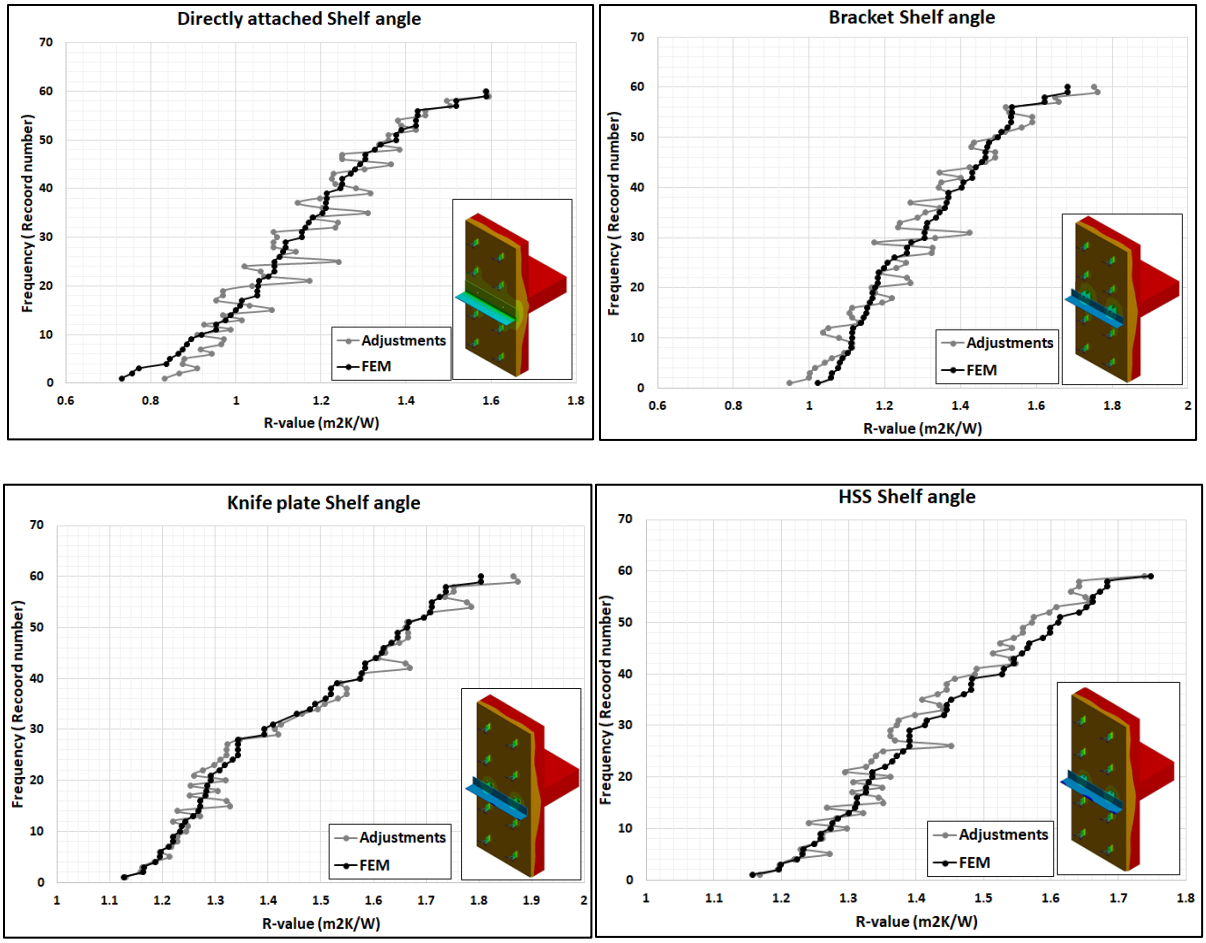

Figure 5-8: Adjusted method with respect to the finite element modelling results

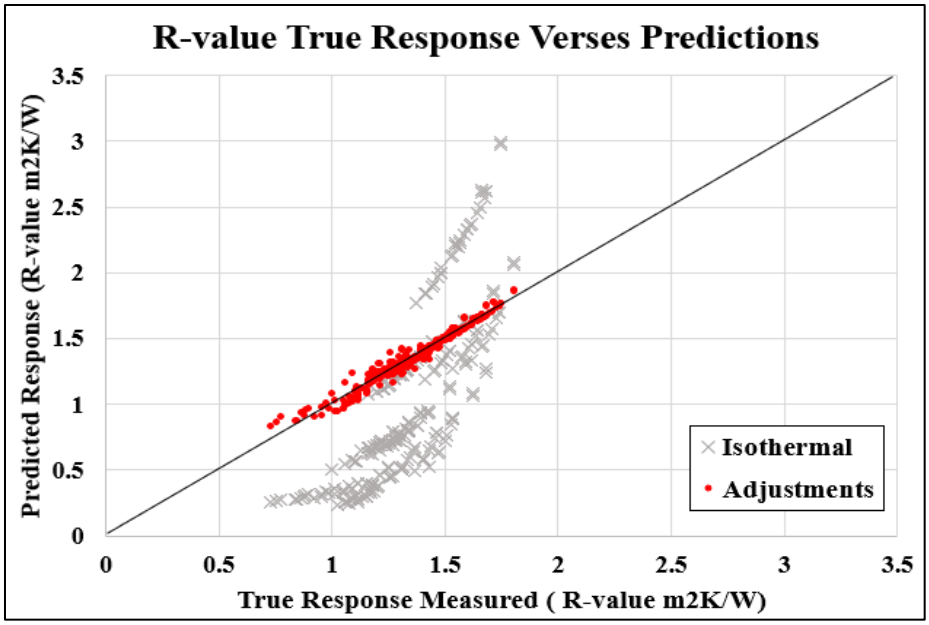

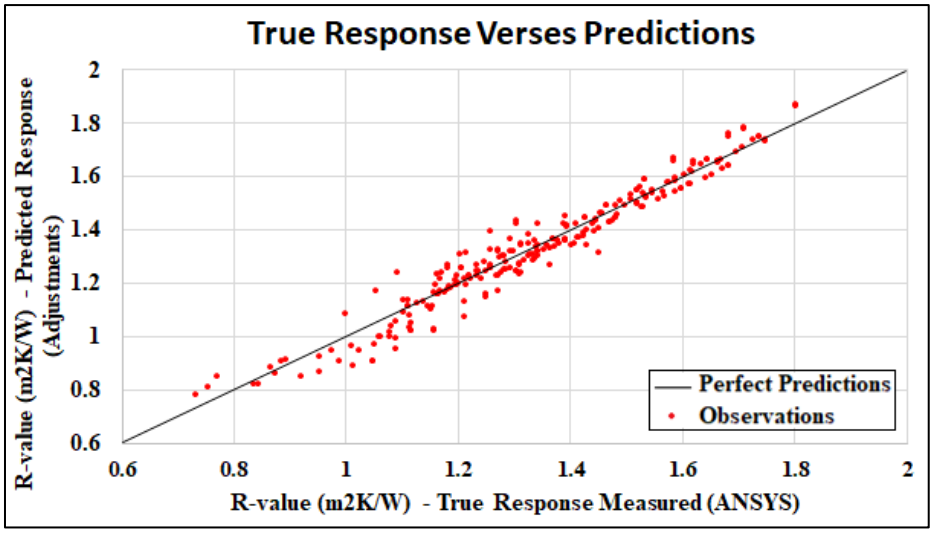

Figure 5-9: Adjusted method with respect to the Finite Element modelling results for all intermediate floor assemblies

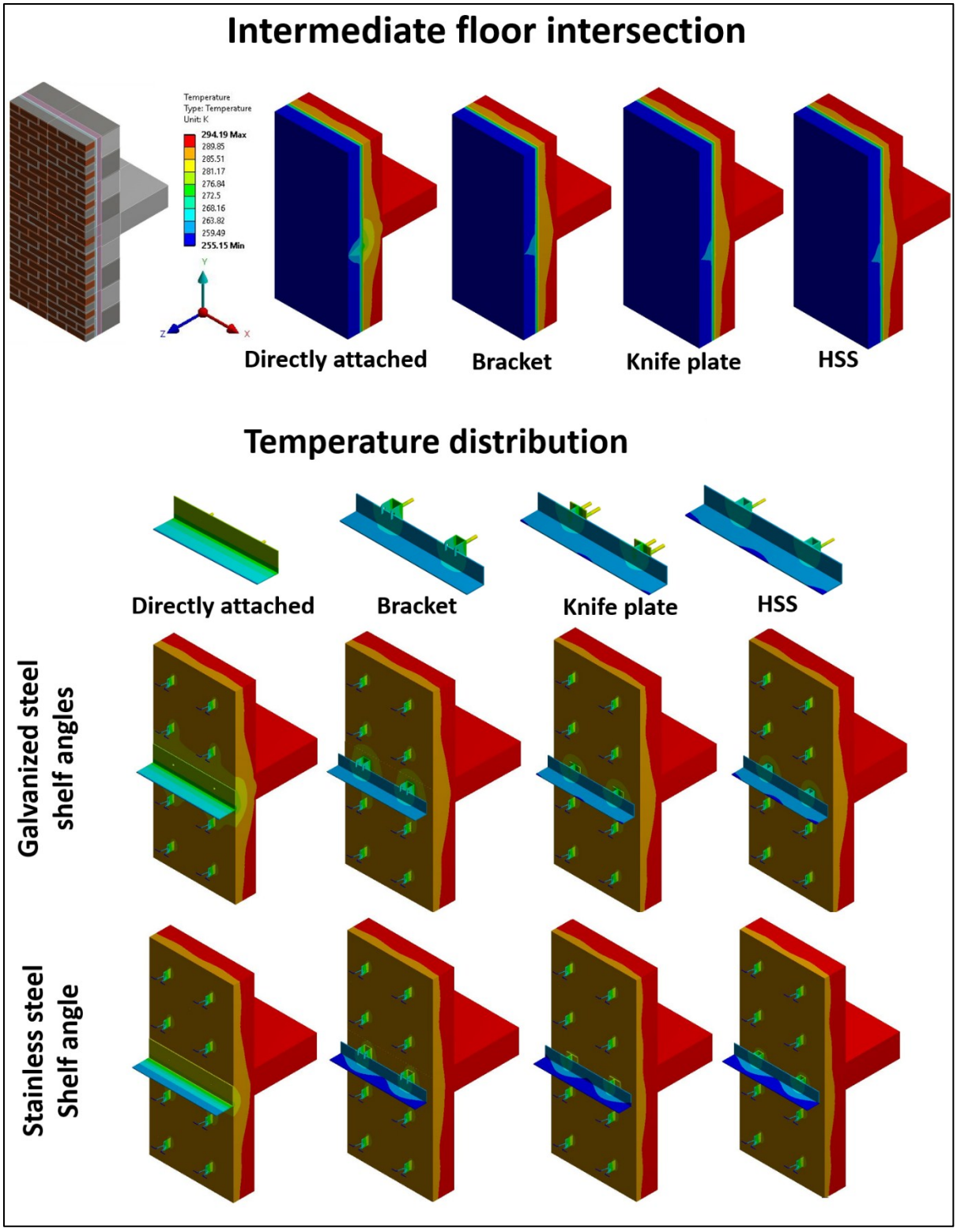

Figure 5-10: Thermal distribution for intermediate floor intersections using insulation R-20 and concrete block density of 2100 kg/m^3

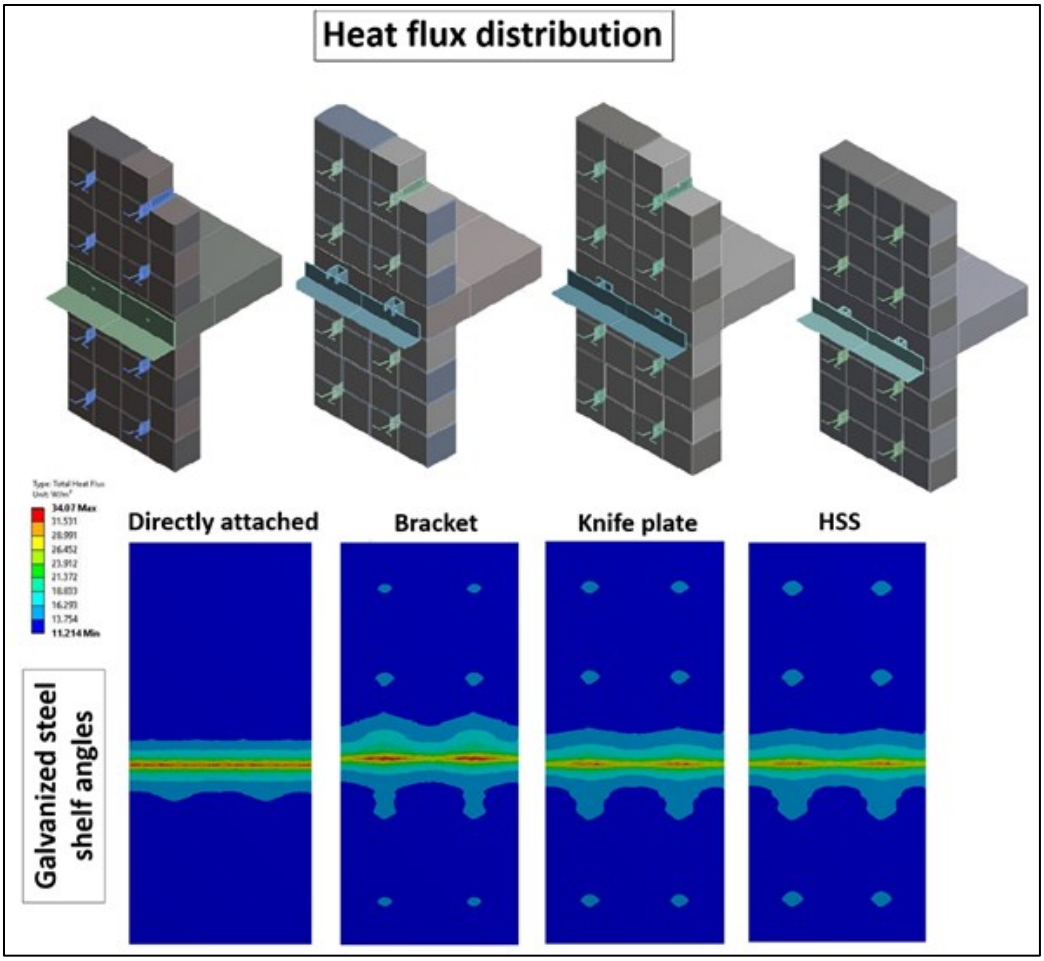

Figure 5-11: The heat flux (on the brick veneer surface) for intermediate floor intersections using insulation R-20 and concrete block density of 2100 kg/m^3

5.5. Conclusion

Results showed that by applying adjustments to the isothermal plane method, the estimation of the effective R-value of masonry veneer walls, including intersections of the primary structure, can be estimated with good accuracy (3.1%). The effect of the thermal bridging sources (e.g., veneer ties and shelf angles) can be estimated by applying the suggested adjustment factors to the isothermal plane method results. The factors outlined above show good agreement with FEM results.

6. Conclusions

This research provided a critical literature review on numerical calculations, computer simulations, and experimental investigations on the evaluation of the thermal resistance of masonry veneer walls. It was indicated that a material's thermal properties are among the largest contributing factors to the thermal performance of masonry walls. Recommendations for the thermal design of masonry wall improvements, thus reducing the energy consumption of buildings, were provided.

An efficient approach for estimating the R-values of common masonry cavity wall configurations in the form of simple design charts and R-value multipliers was presented. The approach simultaneously provides the mechanical (the masonry compressive strength, fm′) and thermal (R-value) properties of different cavity wall configurations, allowing designers to obtain appropriate structural and thermal properties during a preliminary design phase. The suggested R-value multipliers are applicable to predict the effect of changing the key parameters (i.e., thermal conductivity and shapes of ties and shelf angles) on the R-values of many common masonry wall configurations. By comparing the clear wall configurations and results, it was concluded that the lowest thermal resistance values were for the galvanized steel solid block ties (reference group). The clear wall reference group was compared to other groups using galvanized steel but with different tie types (slotted block tie, solid and slotted fastened on surface tie). The thermal resistance values of the groups using different tie types were higher than the reference group by 7.75%, 16.37%, and 25.13%, respectively. Stainless steel was also compared to the galvanized steel solid block ties group. A significant improvement in the R-values was observed. On average, the R-value exceeds the reference group by 20.59%, 28.79%, 33.70%, and 42.68% for a block solid ties block slotted ties, fastened on surface solid and slotted ties, respectively in the case of using stainless steel ties. Glass fibre reinforced polymer (GFRP) materials were studied in clear wall configurations and showed a remarkable increase in the R-value when compared to the reference group. The R-values increased by 60% in the case of block ties and by 64% in the case of fastened on-surface ties. The presence of holes did not show any significant effect on the R-values in the case of GFRP ties due to their low conductivity.

The intermediate floor configurations were also presented. Four types of shelf angles were studied (directly attached large angle, bracket, knife plate, and hollow section tube HSS), and two shelf angles' materials were considered; galvanized steel and stainless steel. Results showed that the galvanized steel for the directly attached shelf angle with solid galvanized steel block ties has the lowest R-value. The stainless steel directly attached large shelf angle has a higher average R-values by 30%, and the bracket galvanized and stainless-steel shelf angles, which have higher average R-values by 18% and 47% respectively. The knife plate galvanized and stainless-steel shelf angles have higher overall average R-values of 28% and 63% respectively. While the hollow section tube HSS galvanized and stainless-steel shelf angles have higher overall average R-values of 32% and 58%, respectively, if compared to the directly attached large galvanized steel shelf angle.

For both intermediate floor intersection configurations and the clear wall, the configurations with the highest insulation board R-values (R-25) showed the maximum improvements in R-values percentages compared to the reference group for each type. Therefore, it was concluded that the shape and material of the ties and shelf angles are more effective in configurations with higher insulation R-values. In addition, using solid ties is more sensitive to the block's density reduction than using perforated (slotted) ties. The fastened on-surface ties also showed more sensitivity to the density reduction if compared to the block tie. Therefore, the maximum thermal insulation benefit in the case of using lightweight concrete blocks could be achieved in the case of using solid ties, fastened on the block's surface and with a high thermal conductivity value.

On average, the reduction of the concrete blocks' density by 10% showed an improvement in the effective R-value by 3.5%. In addition, configurations with expected lower effective thermal resistance are more sensitive to the concrete blocks' density. Using a directly attached galvanized steel shelf angle showed the highest R-value improvement of 7% in the case of reducing the concrete block's density by 10%. The lowest R-value improvement was noticed for the stainless-steel knife plate configurations by 1.75%. It is concluded that the concrete block's density is one of the dominant factors in the effective thermal resistance of masonry cavity walls and should be carefully considered.

Adjustments of the current thermal resistance estimation methods (e.g. isothermal plane method and parallel path method) were suggested to be applied on exterior masonry veneer walls

considering the effect of the thermal bridge resulting caused by the veneer ties, shelf angle and floor intersection slab. The estimated thermal bridging effect caused by the veneer ties and shelf angles could be estimated using these adjustments without using computer simulations or experimental investigations. The clear wall results show that the ratio between the summation of thermal conductivities of layers penetrated by the thermal bridging source and the thermal conductivity of the thermal bridging source is a useful basis for estimating R-values for masonry walls with steel veneer ties. It was concluded that in the case of having a low conductive element penetrating the insulation layer, the results will be the same regardless of using the parallel path method or the isothermal plan method. In addition, the finite element simulation results were closer to the average of the isothermal and the parallel path methods in the case of the ratio between the summation of thermal conductivities of layers penetrated by the thermal bridging source and the thermal conductivity of the thermal bridging source being greater than 0.1. Moreover, results showed that by applying adjustments to the isothermal plane method, the estimation of the effective R-value of masonry veneer walls, including intersections of the primary structure, can be estimated with good accuracy (3.1%). The effect of the thermal bridging sources (e.g., veneer ties and shelf angles) can be estimated by applying the suggested adjustment factors to the isothermal plane method results.

This study presents two approaches to estimate the effective thermal resistance of exterior masonry walls. The design charts approach presented in chapter 3 is applicable in the case of addressing the effect of changing a parameter such as the tie or the shelf angle material and/or type on an existing assembly with a known effective R-value, regardless of the *assembly's* dimensions or the other components material properties. While the second approach, the adjustments of existing methods presented in chapters 4 and 5 apply to any masonry clear wall or intermediate floor assembly even if there are no preliminary estimations or any information available about the effective R-values of masonry assemblies. Moreover, there is no limitation on the material properties or dimensions used in this approach. Both approaches focus on the masonry assemblies due to the need for an accurate and simple estimation approaches of the effective thermal resistance of masonry components and the effect of the thermal bridging with sufficient precision due to the complexity of masonry construction. Both methods could be modified and applied to other building envelope types (e.g., wood and steel frame constructions) in future research.

7. Research Contribution and Future Recommendation

The outcomes of this research and its significance are summarised as follows:

- Literature review, on numerical calculations, computer simulations, and experimental investigations on the evaluation of the thermal resistance of masonry veneer walls.
- Analysis and discussion of the impact of different components (ties, shelf, angles, slabs, air cavity, grout, etc.) on the thermal behaviour of masonry walls.
- Efficient method for estimating the R-values of common concrete-block masonry walls and facilitating their structural and thermal design. Design charts and R-value multipliers are presented to relate the key parameters (e.g., concrete block density and the shape and thermal properties of thermal bridging components) to the R-values of different masonry wall configurations.
- Adjustments of the current thermal resistance estimation methods (e.g., isothermal plane method, and parallel path method) were suggested to be applied on exterior masonry veneer walls considering the effect of the thermal bridge resulting caused by the veneer ties, shelf angle, and floor intersection slab. The estimated thermal bridging effect caused by the veneer ties and shelf angles could be estimated using these adjustments without using computer simulations or experimental investigations. An accuracy of 3.1% was shown for using the suggested adjustments compared to the FE results.

The outcomes of this research aim to provide guidelines and relations for the construction industry and designers to be able to predict the R-value of masonry walls with different conditions such as different blocks' schemes, materials, dimensions, and properties. Besides, it would help designers predict the R-value of masonry walls under different conditions and address the effect of thermal bridging on the overall thermal performance. The significance of such work would contribute to having a reliable estimation of energy needs for the buildings and will be a guideline for improving the thermal envelope and calculating the HAVC equipment required without experimental investigations or computer simulations.

A research gap was found on topics that have a significant effect on the thermal performance of masonry walls and buildings (e.g., the insulation ageing effects and the effect of building components on the whole building thermal analysis rather than one element (e.g., walls). Further

research is required to address these factors and topics. Moreover, simple and accurate estimation techniques for computing the effective R-value of masonry assemblies, including corners and parapets, are required to be addressed further. Also, few researches address the thermal mass of masonry walls. Unlike thermal insulation, which can be characterized by thermal resistance, thermal mass is difficult to quantify as a single parameter. Different indicators to characterize thermal mass have been used over the years. Thus, coefficients like thermal diffusivity or the effective heat capacity per unit area are widely used. This property also has a significant effect on the effective thermal resistance between the interior and the exterior; besides, the thermal mass causes a link between the maximum external temperature and the maximum instantaneous heat flux transmitted to the interior. Both effects can be used to reduce the energy consumption of the HVAC equipment. Further research is required to address these factors and topics.

Additionally, a time interval numerical model (transient modelling) is required to be investigated further to analyze the building's dynamic thermo physical processes, while relevant professional software, such as EnergyPlus, is not compatible with different time intervals. Few researches address the transient thermal modelling of masonry walls. However, further research is required to improve the knowledge of the thermo physical characterization of opaque walls by determining and comparing the thermo physical properties of an experimental massive wall and by performing transient finite element modelling.

References

(2014) CSA Committee, C., CSA S304-14: Design of Masonry Structures. Mississauga, ON, Canada: CSA Group.

Ã–zisik MN, Özışık MN and Özısık MN (1993) *Heat conduction.* John Wiley & Sons.

Abdou OA and Hamid AA (1993) Thermal energy performance of load-bearing concrete masonry in residential buildings in hot, dry climates. *Energy sources* 15(1): 159-170.

Abdou OA and Murali KS (1994) The effect of air cells and mortar joints on the thermal resistance of concrete masonry walls. *Energy and buildings* 21(2): 111-119.

ACI (2002) 122R-02 Guide to thermal properties of concrete and masonry systems. . Reportno. Report Number|, Date. Place Published|: Institution|.

Adam Di Placido P, Chong D and Schumacher C (2019a) Thermal evaluation of masonry shelf angle supports for exterior-insulated walls. *ASHRAE Topical Conference Proceedings.* American Society of Heating, Refrigeration and Air Conditioning Engineers, Inc., 309-317.

Adam Di Placido P, Chong PD and Schumacher C (2019b) Thermal Evaluation of Masonry Shelf Angle Supports for Exterior-Insulated Walls.

Al-Jabri KS, Hago A, Al-Nuaimi A, et al. (2005) Concrete blocks for thermal insulation in hot climate. *Cement and Concrete Research* 35(8): 1472-1479.

Alshatshati SF, Hallinan KP, Arlobaian A, et al. (2017) Data Mining Approach for Estimating Residential Attic Thermal Resistance From Aerial Thermal Imagery, Utility Data, and Housing Data. *Energy Sustainability.* American Society of Mechanical Engineers, V001T009A001.

ANSYS (2019) *https://www.ansys.com/products/platform*.

ASHRAE (1993a) ASHRAE Handbook-Fundamentals, chapter 22. Atlanta. Ga.: American Society of Heating, Refrigerating and Air-Conditioning Engineers, Inc.

ASHRAE (2017a) 25.2.1.3 Heat Flow across an Air Space. *2017 ASHRAE® Handbook - Fundamentals (SI Edition)*. American Society of Heating, Refrigerating and Air-Conditioning Engineers, Inc. (ASHRAE), pp.6.

ASHRAE (2017b) 25.2.1.7 Series and Parallel Heat Flow Paths. *2017 ASHRAE® Handbook - Fundamentals (SI Edition)*. American Society of Heating, Refrigerating and Air-Conditioning Engineers, Inc. (ASHRAE), pp.7.

ASHRAE (2017c) 27.1.2.3 constructions containing metal. *2017 ASHRAE® Handbook - Fundamentals (SI Edition)*. American Society of Heating, Refrigerating and Air-Conditioning Engineers, Inc. (ASHRAE).

ASHRAE (2017d) 27.1.2.3 constructions containing metal. 2017 ASHRAE® handbook - fundamentals (SI edition) (pp. 27.4) American Society of Heating, Refrigerating and Air-Conditioning Engineers, Inc. (ASHRAE). Retrieved from https://app.knovel.com/hotlink/pdf/id:kt011GGSX1/ashrae-handbook-fundamentals/constructions-containing.

ASHRAE (2017e) Heat, Air, and Moisture Control in Building Assemblies - Fundamentals. *ASHRAE Handbook* Fundamentals. 2017.

ASHRAE (2019a) ASHRAE 90.1- energy standard for buildings except low-rise residential buildings. Reportno. Report Number|, Date. Place Published|: Institution|.

ASHRAE (2019b) ASHRAE 90.1- Energy Standard for Buildings except Low-Rise Residential Buildings. Vol. Vol. 90 ASHRAE.

ASHRAE (2021a) 25.2.1 Steady-State Thermal Response. *2021 ASHRAE® Handbook - Fundamentals (I-P Edition)*. American Society of Heating, Refrigerating and Air-Conditioning Engineers, Inc. (ASHRAE).

ASHRAE (2021b) 25.2.1.7 Series and Parallel Heat Flow Paths. *2021 ASHRAE® Handbook - Fundamentals (I-P Edition)*. American Society of Heating, Refrigerating and Air-Conditioning Engineers, Inc. (ASHRAE).

ASHRAE (2021c) 27.1.2.3 constructions containing metal. 2021 ASHRAE® handbook - fundamentals (SI edition) (pp. 27.4) American Society of Heating, Refrigerating and Air-Conditioning Engineers, Inc. (ASHRAE). Retrieved from https://app.knovel.com/hotlink/pdf/id:kt011GGSX1/ashrae-handbook-fundamentals/constructions-containing.

ASHRAE (2021d) 27.1.2.5 Modified Zone Method for Metal Stud Walls with Insulated Cavities. *2021 ASHRAE® Handbook - Fundamentals (I-P Edition)*. American Society of Heating, Refrigerating and Air-Conditioning Engineers, Inc. (ASHRAE).

ASHRAE (2021e) Energy Standard for Buildings except Low-Rise Residential Buildings. Vol. 90 ASHRAE.

Association CCMP (2013) Thermal Properties & Design Details. Reportno. Report Number|, Date. Place Published|: Institution|.

ASTM (2011) C1363-11: Standard test method for thermal performance of building materials and envelope assemblies by means of a hot box apparatus. American Society for Testing and Materials West Conshohocken, PA. .

ASTM (2013) C1155 -95: Standard practice for determining thermal resistance of building envelope components from the in-situ data. ASTM International West Conshohocken, United States.

ASTM (2015a) C518: standard test method for steady-state thermal transmission properties by means of the heat flow meter apparatus. Annual Book of ASTM Standards, : ASTM.

ASTM (2015b) C1060-11a: Standard practice for thermographic inspection of insulation installations in envelope cavities of frame buildings. ASTM International West Conshohocken, United States.

Bai G-l, Du N-j, Xu Y-z, et al. (2017) Study on the thermal properties of hollow shale blocks as self-insulating wall materials. *Advances in Materials Science and Engineering* 2017.

Baldwin S, Bindewald G, Brown A, et al. (2015) Quadrennial technology review: An assessment of energy technologies and research Opportunities. Reportno. Report Number|, Date. Place Published|: Institution|.

Barbour E, Goodrow J, Kosny J, et al. (1994) Thermal performance of steel-framed walls. Final report. Reportno. Report Number|, Date. Place Published|: Institution|.

Barnes BP, Pagán-Vázquez A, Heffron AP, et al. (2013) Analysis techniques, materials, and methods for treatment of thermal bridges in building envelopes.

Basiricò T, Cottone A and Enea D (2020) Analytical Mathematical Modeling of the Thermal Bridge between Reinforced Concrete Wall and Inter-Floor Slab. *Sustainability* 12(23): 9964.

Bažant ZP, Kaplan MF and Bazant ZP (1996) Concrete at high temperatures: material properties and mathematical models.

Belanger D and Berardi U (2018) The Impact of Aging on the Effective Thermal Conductivity of Foam Insulation: A Simulation Investigation Using Laboratory Characterization Data.

Berardi U (2017) The impact of temperature dependency of the building insulation thermal conductivity in the Canadian climate. *Energy Procedia* 132: 237-242.

Berardi U (2019) The impact of aging and environmental conditions on the effective thermal conductivity of several foam materials. *Energy* 182: 777-794.

Berardi U, Tronchin L, Manfren M, et al. (2018) On the effects of variation of thermal conductivity in buildings in the Italian construction sector. *Energies* 11(4): 872.

Berrar D (2019) Cross-Validation.

Bradfield M (2011) The effectiveness of effective R-value. *The Masonry Edge/the StoryPole Pursuit of Excellence*, 15-18.

Bradfield M and Szoke S (2010) Insulating masonry walls. *ASHRAE*.

Brown W and Stephenson D (1993a) Guarded Hot Box Measurements of the Dynamic Heat Transmission Characteristics of Seven Wall Specimens: Part II (RP-515). *TRANSACTIONS-AMERICAN SOCIETY OF HEATING REFRIGERATING AND AIR CONDITIONING ENGINEERS* 99: 643-643.

Brown W and Stephenson D (1993b) Guarded hot box procedure for determining the dynamic response of full-scale wall specimens- Part I. *the 1993 Winter Meeting of ASHRAE Transactions. Part 1.* 632-642.

Callejas IJA, Durante LC and Oliveira ASd (2017) Thermal resistance and conductivity of recycled construction and demolition waste (RCDW) concrete blocks. *REM-International Engineering Journal* 70(2): 167-173.

Canadian Commission on B and Fire C. DOI: 10.4224/rr3q-hm83.(2022) National Energy Code of Canada for Buildings: 2020.

Cao X, Dai X and Liu J (2016) Building energy-consumption status worldwide and the state-of-the-art technologies for zero-energy buildings during the past decade. *Energy and buildings* 128: 198-213.

CCMP (2013) METRIC TECHNICAL MANUAL.thermal properties & design details. Reportno. Report Number|, Date. Place Published|: Institution|.

CCMPA (2013) Canadian Concrete Masonry Producers' Association-Thermal Properties & Design Details. *Technical Notes- Retrieved from:* https://ccmpa.ca/download/metric-technical-manual/6-thermprop/.

CIANFRINI M, CORCIONE M, DE LIETO VOLLARO R, et al. (2015) Thermal inertia of hollow wall blocks: actual behavior and myths. *Proceedings of International Conference CISBAT 2015 Future Buildings and Districts Sustainability from Nano to Urban Scale.* LESO-PB, EPFL, 149-154.

Concrete SL (2007) Durability/Service Life of Structural Lightweight Concrete.

Conway P (2016) Ventilated masonry cavity walls. RCI's Interface In: *Building Envelope Technology Symposium*, pp.23-32.

Corporation F (2016) *https://www.arrowco.ca/fero-corporation/*.

Cui H, Hu F, Zhang Y, et al. (2019) Heat spreading path optimization of IGBT thermal network model. *Microelectronics reliability* 103: 113511.

D'Aloisio J, Anderson J, DeLong D, et al. (2012) Thermal bridging solutions: Minimizing structural steel's impact on building envelope energy transfer. *Modern steel construction. Chicago: AISC*.

de Souza RP, Pacheco F, Prager GL, et al. (2019) Verification of the influence of loading and mortar coating thickness on resistance to high temperatures due to fire on load-bearing masonries with clay tiles. *Materials* 12(22): 3669.

Deb K (2012) *Optimization for engineering design: Algorithms and examples.* PHI Learning Pvt. Ltd.

Deconinck A-H and Roels S (2016) Comparison of characterisation methods determining the thermal resistance of building components from onsite measurements. *Energy and buildings* 130: 309-320.

del Coz Diaz J, Nieto PG, Rodriguez AM, et al. (2006) Non-linear thermal analysis of light concrete hollow brick walls by the finite element method and experimental validation. *Applied Thermal Engineering* 26(8-9): 777-786.

Desjarlais AO and McGowan AG (1997) Comparison of experimental and analytical methods to evaluate thermal bridges in wall systems. *Insulation Materials: Testing and Applications, 3rd Volume*. ASTM International.

Energy UDo (2015) Increasing efficiency of building systems and technologies. Department of Energy, 145-182.

ESCSI (2007) Durability/Service Life of Structural Lightweight Concrete. *Expanded Shale, Clay & Slate Institute.*

Eurima EIMA (2008) Energy efficiency in buildings. . Retrieved from https://www. eurima.org/energy-efficiency-in-buildings.html (accessed 19 February 2020).
Evola G, Marletta L, Natarajan S, et al. (2017) Thermal inertia of heavyweight traditional buildings: Experimental measurements and simulated scenarios. *Energy procedia* 133: 42-52.
Excel M (2021) *https://support.microsoft.com/en-us/office/define-and-solve-a-problem-by-using-solver-5d1a388f-079d-43ac-a7eb-f63e45925040#:~:text=Solver%20is%20a%20Microsoft%20Excel,formula%20cells%20on%20a%20worksheet*.
Finch G and Higgins J (2017) Cladding attachment solutions. *ROCKWOOL Group.* 2-5.
Finch G, Wilson M and Higgins J (2013a) Thermal bridging of masonry veneer claddings & energy code compliance. *ASTM International: Philadelphia, PA, USA*.
Finch G, Wilson M and Higgins J (2013b) Thermal Bridging of Masonry Veneer Claddings & Energy Code Compliance. *12th Canadian Masonry Symposium, Vancouver, BC, June.* 2-5.
Fiorato A (1979) Laboratory tests of thermal performance of exterior walls. *Proceedings.* 221-236.
Gould N (2006) An introduction to algorithms for continuous optimization. Oxford University Computing Laboratory Notes.
Harmathy T and Allen L (1973) Thermal properties of selected masonry unit concretes. *Journal Proceedings.* 132-142.
Helwig NE (2017) Data, Covariance, and Correlation Matrix. *University of Minnesota (Twin Cities)*.
Hershfield M (2016a) Building Envelope Thermal Bridging Guide, version 1.1. Vancouver: BC Hydro Power Smart.
Hershfield M (2016b) Building Envelope Thermal Bridging Guide, version 1.1. Hydro Power Smart. Vancouver, Canada.
Hershfield M (2020) BUILDING ENVELOPE THERMAL BRIDGING GUIDE v1.4. *ASHRAE 1365-RP* B.7.28.
Hershfield M (2022a) Building Envelope Thermal Bridging Guide, version 1.6. Hydro Power Smart. Vancouver, Canada.
Hershfield M (2022b) Thermal performance of building envelope details for mid- and high-rise buildings. ASHRAE Research Project RP-1365, Report.
Huberman N and Pearlmutter D (2004) Life cycle energy performance of building materials: alternatives for a desert environment. *Plea2004-The 21th Conference on Passive and Low Energy Architecture.*
Huberman N and Pearlmutter D (2008) A life-cycle energy analysis of building materials in the Negev desert. *Energy and buildings* 40(5): 837-848.
Hydro B (2016a) Commercial new construction. building envelope thermal bridging guide
Hydro B (2016b) Commercial new construction. Building envelope thermal bridging guide available at http://www. bchydro. com/powersmart/builders_developers/high_performance_building_program. html. *WT. mc_id= rd_construction*.
IECC (2012) International energy conservation code 2012. C403, 2.
Ismaiel M, Chen Y, Cruz-Noguez C, et al. (2021) Thermal resistance of masonry walls: a literature review on influence factors, evaluation, and improvement. *Journal of Building Physics*. 17442591211009549.
ISO (1999) 834: Fire resistance tests-elements of building construction. . *International Organization for Standardization, Geneva, Switzerland,* .
ISO (2017a) 6946: Building components and building elements. Thermal Resistance and Thermal Transmittance.Calculation Methods. (Polish Version PN-EN ISO 6946: 2017).Available Online: Https://Www.Iso.Org/Standard/65708.Html (Accessed on 20 December 2018), .

ISO (2017b) 6946: Building components and building elements. Thermal Resistance and Thermal Transmittance.Calculation Methods. (Polish Version PN-EN ISO 6946: 2017). Available Online: Https://Www.Iso.Org/Standard/65708.Html (Accessed on 20 December 2018).
ISO (2017c) 10211:2017 (E) Thermal bridges in building construction - Heat flows and surface temperatures - Detailed calculations. In: International Organization for Standardization (ISO).
ISO (2017d) International Standard ISO/DIS 6946-1, EN ISO 6946:2017: Thermal resistance and thermal transmittance of building components and building elements. Geneva: International Organization for Standardization.
Kodur V and Sultan M (2003) Effect of temperature on thermal properties of high-strength concrete. *Journal of materials in civil engineering* 15(2): 101-107.
Koester JH (2006) Moisture drainage product, wall system incorporating such product and method therefore. Google Patents.
Kontoleon K, Theodosiou TG and Tsikaloudaki K (2013) The influence of concrete density and conductivity on walls' thermal inertia parameters under a variety of masonry and insulation placements. *Applied energy* 112: 325-337.
Kosny J (1995) Thermal performance of concrete masonry unit wall systems. Reportno. Report Number|, Date. Place Published|: Institution|.
Kosny J and Christian JE (1995) Reducing the uncertainties associated with using the ASHRAE zone method for R-value calculations of metal frame walls. Reportno. Report Number|, Date. Place Published|: Institution|.
Kosny J and Christian JE (2001) Whole wall thermal performance. *Oak Ridge, TN: Oak Ridge National Laboratory. Accessed November* 9: 2015.
Kumar A, Buddhi D and Chauhan D (2012) Indexing of building materials with embodied, operational energy and environmental sustainability with reference to green buildings. *Journal of Pure and Applied Science & Technology* 2(1): 11-22.
Lawton M, Roppel P, Fookes D, et al. (2010) Real R-value of exterior insulated wall assemblies. *All are with Morrison Hershfield Ltd., Vancouver, BC, Canada*.
Lie T and Kodur V (1996) Thermal and mechanical properties of steel-fibre-reinforced concrete at elevated temperatures. *Canadian Journal of Civil Engineering* 23(2): 511-517.
Lindsey K (1993) DEVELOPMENT OF A REVISED COOLING AND HEATING LOAD CALCULATION MANUAL.
Liu C (2019) The Convergence of Standard 90.1, 62.1 and 55: Examples of Energy Efficiency Measures. *ASHRAE Transactions* 125.
Loghmanpour S (2014) Framing with Steel Versus Wood Heat Transfer Issues and Analysis. *California Energy Commission. Retrieved*.
Love A (2011) *Material impacts on operational energy usage*. Massachusetts Institute of Technology.
Lstiburek J (2008) BSI-001: The Perfect Wall. *Retrieved October* 2: 2011.
Malik M, Bhattacharyya S and Barai SV (2020) Thermal and mechanical properties of concrete and its constituents at elevated temperatures: A review. *Construction and Building Materials*. 121398.
McCall CW (1985) Thermal properties of sandwich panels. *Concrete International* 7(1): 35-41.
McGowan A and Desjarlais A (1995) A comparison of thermal bridging calculation methods. *Thermal Performance of the Exterior Envelopes of Buildings VI. Clearwater Beach FL.* 241-246.
Mohebbi F and Sellier M (2016) Estimation of thermal conductivity, heat transfer coefficient, and heat flux using a three dimensional inverse analysis. *International Journal of Thermal Sciences* 99: 258-270.
Nadjai A, O'garra M and Ali F (2003) Finite element modelling of compartment masonry walls in fire. *Computers & structures* 81(18-19): 1923-1930.
NCMA (2010) Tek6-11a- insulating concrete masonry walls. Reportno. Report Number|, Date. Place Published|: Institution|.

NCMA (2012) Thermal catalog of concrete masonry assemblies. Reportno. Report Number|, Date. Place Published|: Institution|.
NCMA (2013) R-values of single-wythe concrete masonry walls. . Reportno. Report Number|, Date. Place Published|: Institution|.
NECB (2011) The national energy code of canada for buildings. Reportno. Report Number|, Date. Place Published|: Institution|.
NECB (2015) The national energy code of canada for buildings. Reportno. Report Number|, Date. Place Published|: Institution|.
NECB (2017a) The national energy code of canada for buildings. Reportno. Report Number|, Date. Place Published|: Institution|.
NECB (2017b) The national energy code of canada for buildings.
Norris N, Lawton M and Roppel P (2012a) The concept of linear and point transmittance and its value in dealing with thermal bridges in building enclosures. *Building enclosure science & technology conference.*
Norris N, Lawton M and Roppel P (2012b) The concept of linear and point transmittance and its value in dealing with thermal bridges in building enclosures. *Building enclosure science & technology conference.* 1-10.
Omar E (2002) Impact of columns and beams on the thermal resistance of the building envelope.
Ono R (2007) Parâmetros para garantia da qualidade do projeto de segurança contra incêndio em edifícios altos. *Ambiente construído* 7(1): 97-113.
Phan LT and Phan L (1996) *Fire performance of high-strength concrete: A report of the state-of-the art.* US Department of Commerce, Technology Administration, National Institute of ….
Pierzchlewicz J (1996) Modern concrete wall-units with improved thermal resistance for housing in hot climate. *Sci. Technol* 1: 69-80.
Rasooli A and Itard L (2018) In-situ characterization of walls' thermal resistance: An extension to the ISO 9869 standard method. *Energy and buildings* 179: 374-383.
Rigão AO (2012) Comportamento de pequenas paredes de alvenaria estrutural frente a altas temperaturas.
Roppel P, Hershfield M, Marif W, et al. (2011) Research Project Report RP-1365: Thermal Performance of Buildings Envelope Details for Mid and High-Rise Buildings. *ASHRAE Inc.* Report No. 5085243.01.
Roppel P, Lawton M and Norris N (2012) Thermal Performance of Building Envelope Details for Mid-and High-Rise Buildings. *ASHRAE Transactions* 118(2).
Rowley FB and Algren AB (1937) Thermal conductivity of building materials.
Schulenburg (2000) Masonry weep hole insert. United States Patent, 6,112,476. Reportno. Report Number|, Date. Place Published|: Institution|.
Schumacher C, Straube J, Ober D, et al. (2013) Development of a new hot box apparatus to measure building enclosure thermal performance. *Proceedings of Buildings XII*. 1-19.
Shin K-Y, Kim S-B, Kim J-H, et al. (2002) Thermo-physical properties and transient heat transfer of concrete at elevated temperatures. *Nuclear Engineering and Design* 212(1-3): 233-241.
Soares N, Martins C, Gonçalves M, et al. (2019) Laboratory and in-situ non-destructive methods to evaluate the thermal transmittance and behavior of walls, windows, and construction elements with innovative materials: A review. *Energy and buildings* 182: 88-110.
Sourlis T (1993) Mortar and debris collection device and system. Google Patents.
Sourlis T (2000) Combination flashing and mortar and debris collection device and system. Google Patents.

Stovall TK and Karagiozis A (2004) Airflow in the ventilation space behind a rain screen wall. *Performance of Exterior Envelopes of Whole Buildings IX International Conference, Clearwater, Florida, USA.*

Straube J (2017) Meeting and exceeding building code thermal performance requirements. *Canadian Precast/Prestressed Concrete Institute*.

Strobel H (1989) Strang, g., introduction to applied mathematics. wellesley, mass. wellesley-cambridge press 1986. ix, 758 pp. isbn 0-9614088-0-4. *Zeitschrift Angewandte Mathematik und Mechanik* 69(9): 311-312.

Sturgeon G, Eng B and Eng P (2013a) Coursing Tables, Metric Shapes and Sizes.

Sturgeon G, Eng B and Eng P (2013b) Physical Properties. Retrieved from Canadian Concrete Masonry Producers Association: Metric ….

Su H, Wu D, Shen M, et al. (2019) Development and performance test including mechanical and thermal of new tenon composite block masonry walls. *Advances in Materials Science and Engineering* 2019.

Suter G, Borgal C and Blades K (2001) Overview of mortars for Canadian historic structures. *Proceedings of the 9th Canadian masonry symposium. University of New Brunswick, Canada.* 4-6.

Tawade S Comparative Analysis of Two-Dimensional Steady State Heat Flow Problem of a Rectangular Plate by Analytical and Numerical Approach.

Theodosiou T, Tsikaloudaki K, Kontoleon K, et al. (2021) Assessing the accuracy of predictive thermal bridge heat flow methodologies. *Renewable and Sustainable Energy Reviews* 136: 110437.

Urban B, Engelmann P, Kossecka E, et al. (2011a) Arranging insulation for better thermal resistance in concrete and masonry wall systems. *9th Nordic symposium on building physics, Finland.*

Urban B, Engelmann P, Kossecka E, et al. (2011b) Arranging insulation for better thermal resistance in concrete and masonry wall systems. *9th Nordic Symposium on Building Physics.*

Van Geem M, Fiorato A and Musser D (1982) Calibrated hot box tests of thermal performance of concrete walls. *Proceedings of the ASHRAE/DOE Conference on Thermal Performance of the Exterior Envelopes of Buildings II, Las Vegas, NV.*

Wang J, Zheng K, Cui N, et al. (2020) Green and Durable Lightweight Aggregate Concrete: The Role of Waste and Recycled Materials. *Materials* 13(13): 3041.

Wilson M, Finch, G., Higgins, J. (2013) Masonry Design Support Details: Thermal Bridging. *Proceedings from 12th Canadian Masonry Symposium.* Vancouver, BC, Canada.

Wilson M and Higgins J (2019) Fero rap tie and fast system

thermal analysis. American Journal of Hematology, 94, S3-S33. doi:10.1002/ajh.25639. *thermal analysis. American Journal of Hematology* 94.

Xhexhi KA, Maliqari A and Meunier PL (2020) Determination of Temperature-Moisture Relationship by Linear Regression Models on Masonry and Floor, Kruja, Albania. *European Journal of Engineering and Technology Research* 5(4): 421-428.

Xie C (2012) Interactive heat transfer simulations for everyone. *The Physics Teacher* 50(4): 237-240.

Zedan MF, Al-Sanea S, Al-Mujahid A, et al. (2016) Effect of thermal bridges in insulated walls on air-conditioning loads using whole building energy analysis. *Sustainability* 8(6): 560.

Zieukiewicz O and Taylor R (1991) The finite element method, 4-th Edition. *Ed. Me Graw Hill*.

Zorainy M, Ashour A and Galal K (2018) *Comparing Canadian and American Standards Requirements for Evaluating Masonry Compressive Strength.*